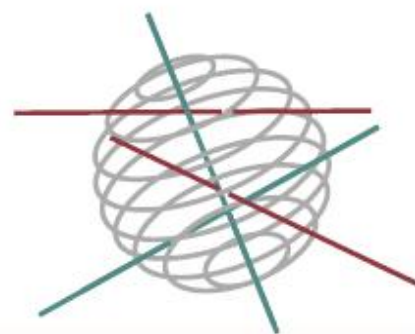


SSD

SCIENCE FOR A SUSTAINABLE DEVELOPMENT



“IMPACT OF BIOGENIC EMISSIONS ON ORGANIC AEROSOLS AND OXIDANTS IN THE TROPOSPHERE”

«IBOOT»

J.-F. MÜLLER, K. CEULEMANS, S. COMPERNOLLE, T. STAVRAKOU,
J. PEETERS, L. VEREECKEN, T.L. NGUYEN, R. WINTERHALTER,
G. MOORTGAT, B. KANAWATI, A. SADEZKY



ENERGY



TRANSPORT AND MOBILITY



AGRO-FOOD



HEALTH AND ENVIRONMENT



CLIMATE



BIODIVERSITY

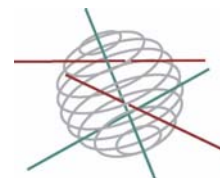


ATMOSPHERE AND TERRESTRIAL AND MARINE ECOSYSTEMS



TRANSVERSAL ACTIONS





Atmosphere

FINAL REPORT

**IMPACT OF BIOGENIC EMISSIONS ON ORGANIC AEROSOLS AND
OXIDANTS IN THE TROPOSPHERE
"IBOOT"**

SD/AT/03

Promotors

J.-F. Müller

Institut d'Aéronomie Spatiale de Belgique (IASB-BIRA)
Avenue Circulaire 3, B-1180 Bruxelles

Jozef Peeters, Luc Vereecken and Minh Tho Nguyen
Katholieke Universiteit Leuven

Geert Moortgat, Richard Winterhalter and Jos Lelieveld
Max Planck Institute for Chemistry (MPI, Mainz, Germany)

Authors

J.-F. Müller, Karl Ceulemans, Steven Compennolle, T. Stavrou
(IASB-BIRA)

Jozef Peeters, Luc Vereecken, Thanh Lam Nguyen
(Katholieke Universiteit Leuven)

Richard Winterhalter, Geert Moortgat, Basem Kanawati, Alexa Sadezky
(MPI-Mainz)





D/2011/1191/7

Published in 2011 by the Belgian Science Policy

Avenue Louise 231

Louizalaan 231

B-1050 Brussels

Belgium

Tel: + 32 (0)2 238 34 11 – Fax: + 32 (0)2 230 59 12

<http://www.belspo.be>

Contact person: Martine Vanderstraeten

+ 32 (0)2 238 36 10

Neither the Belgian Science Policy nor any person acting on behalf of the Belgian Science Policy is responsible for the use which might be made of the following information. The authors are responsible for the content.

No part of this publication may be reproduced, stored in a retrieval system, or transmitted in any form or by any means, electronic, mechanical, photocopying, recording, or otherwise, without indicating the reference :

J.-F. Müller, K. Ceulemans, S. Compernelle, T. Stavrakou, J. Peeters, T.L. Nguyen, L. Vereecken, R. Winterhalter, G. Moortgat, B. Kanawati, A. Sadezky. ***Impact of Biogenic emissions on Organic aerosols and Oxidants in the Troposphere***. Final Report. Brussels : Belgian Science Policy 2009 – 94 p. (Research Program Science for a Sustainable Development

TABLE OF CONTENT

SUMMARY	5
Context	5
Objectives.....	6
Science results.....	6
Contribution in a context of scientific support to a sustainable development policy ...	8
Keywords	9
I. INTRODUCTION	11
II. METHODOLOGY AND RESULTS.....	13
II.1 Laboratory investigations of mono- and sesquiterpenes ozonolysis.....	13
II.1.1 Products and reaction mechanism of the ozonolysis of β -caryophyllene and α -humulene	13
II.1.1.1 Methodology	13
II.1.1.2 Results: β -Caryophyllene	13
II.1.1.3 Results: α -Humulene	21
II.1.2 Determination of aerosol yields from sesquiterpene-ozonolysis.....	31
II.1.3 Identification and quantification of hydroperoxides from sesquiterpene ozonolysis	32
II.1.4 Formation of oligomers and polymers	33
II.1.5 Determination of CCN activity of sesquiterpene ozonolysis products	35
II.2 Development of predictive tools for mechanism construction	35
II.2.1 Alkoxy radical decomposition	35
II.2.2 Isomerization of alkoxy and alkylperoxy radicals by H-migration	38
II.2.3 H-abstraction from substituted hydrocarbons by OH-radicals	40
II.2.4 Site-specific addition of OH radicals on substituted (poly)alkenes.....	41
II.3 Development of oxidation mechanisms	42
II.3.1 OH-initiated oxidation of β -pinene.....	42
II.3.2 Specific pathways in the ozonolysis of α -pinene.....	43
II.3.3 O ₃ -initiated oxidation of β -pinene.....	44
II.3.4 O ₃ -initiated oxidation of β -caryophyllene	46
II.4 Model simulations of terpene oxidation experiments	48
II.4.1 Gas phase mechanism	48
II.4.2 Oligomerization reactions	49

II.4.3 Gas/particle partitioning model	50
II.4.3.1 General formulation.....	50
II.4.3.2 Activity coefficients.....	50
II.4.3.3 Vapor pressures	52
II.4.4 Model evaluation against smog chamber experiments	56
II.4.4.1 Photo-oxidation experiments	57
II.4.4.2 Dark ozonolysis experiments	58
II.4.4.3 Comparison with other box model studies	60
II. 5 Atmospheric oxidation of oxygenates.....	61
Isoprene oxidation and its impact on the oxidizing capacity of the atmosphere.....	61
II.5.1 Pressure and temperature dependence of reactions of oxygenates with OH	62
II.5.2 Reactions of carbonyl-bearing compounds with HO ₂ -radicals.....	63
II.5.3 HO _x radical regeneration in the oxidation of isoprene	65
II.6 Global Modeling.....	70
II.6.1 Development of reduced mechanism for the oxidation of terpenes	70
II.6.2 Development of SOA parameterization for use in a global model	71
II.6.2.1 General formulation.....	71
II.6.2.2 Parameterization for reversible SOA formation	72
II.6.2.3 Parameterization for irreversible SOA formation from dicarbonyls.....	73
II.6.3 Results: distribution and budget of organic aerosols (OA)	73
II.6.4 Validation by comparison with observations	76
II.6.4.1 Glyoxal and formaldehyde.....	76
II.6.4.2 Organic aerosol	76
III. POLICY SUPPORT.....	79
IV. DISSEMINATION AND VALORISATION.....	81
V. PUBLICATIONS.....	83
VI. ACKNOWLEDGEMENTS	87
VII. REFERENCES.....	89

SUMMARY

Context

Terrestrial vegetation releases vast quantities of volatile organic compounds (VOCs) to the atmosphere, of the order of 1000 millions of tons each year. Although of natural origin, biogenic VOCs (BVOCs) are central to our understanding of the role played by human activities (e.g. land use changes and anthropogenic emissions) in climate change and air quality issues. Most importantly

- they influence the oxidizing capacity of the atmosphere and therefore the abundance of many key gases, especially the greenhouse gas methane, but also air quality compounds (e.g. carcinogenic benzene) and chemicals contributing to stratospheric ozone depletion (e.g. HCFCs)
- in polluted areas, they participate to summertime “ozone smog” episodes, i.e. to the build-up of noxious pollutants, primarily ozone, due the catalytic action of nitrogen oxides of anthropogenic origin
- they are a source of Secondary Organic Aerosol (SOA) which makes up a substantial fraction of fine aerosols (i.e. particulate matter or PM).

Aerosols play a central role in climate through direct radiative effects and through their influence on clouds. Along with ground-level ozone, fine aerosols are also a major component of smog over polluted regions. They have acute adverse effects on human health, in particular on the respiratory and cardiovascular systems; over Europe, PM pollution has been estimated to cause ~200,000 premature deaths per year.

Regulation measures in the United States and Europe are tightening as a growing body of scientific evidence suggests that there is no safe level of exposure to ozone or PM. Although anthropogenic emissions of ozone precursors have generally decreased in Europe since the 1990s, exposure to ground-level ozone has failed to decline substantially, and the number of premature deaths due to ground level ozone worldwide is expected to quadruple by 2030. This global pollution trend has also negative consequences for crop yields and for natural ecosystems and their ability to take up atmospheric carbon dioxide.

Although crucial to these issues, the effects of BVOCs remain poorly quantified, as illustrated by the failure of state-of-the-art models to reproduce field measurements of OH radicals over forests. A better understanding of the chemical and physical

transformations affecting the BVOCs and their oxidation products is required in order to assess

- the role of the biosphere, and its evolution in response to climate and composition changes induced by anthropogenic emissions and land-use changes,
- the effect of regulatory measures aiming at the mitigation of air pollution and climate change, in particular at the European level (for air quality compounds) and in the framework of global climate negotiations

Objectives

The objectives of the IBOOT project were a better understanding and quantification of the role of BVOCs, in particular with respect to the formation of oxidants and aerosols, by means of laboratory, theoretical and modeling investigations of the chemical degradation and aerosol formation potential of important BVOCs.

Science results

Laboratory studies (MPI-Mainz)

The reaction with ozone of two specific BVOCs (the sesquiterpenes β -caryophyllene and α -humulene) has been studied in the laboratory. This detailed investigation provided key insights on the degradation mechanism. In addition, the reaction rates and the yields of SOA, OH-radical and hydrogen peroxide were determined. Long-chain hydroperoxides were also detected.

In the case of β -caryophyllene, a dozen products could be identified in the particulate phase. The respective contributions of the hydroperoxide channel, the ester channel and collisional stabilisation of the Criegee Intermediates (CI) were estimated to 10%, 5-10% and $> 80\%$. The stabilized CI can undergo ring closure to produce internal secondary ozonides (SOZ).

In the case of α -humulene, 37 compounds in the aerosol phase and 5 products in the gas phase were assigned. The initial ozonolysis of α -humulene leads to 6 different CI's. Subsequent reaction with ozone leads to a wide range of products. The primary ozonide is found to decompose rapidly, and a large fraction of the excited CI is stabilized to form stable SOZ, while the hydroperoxide channel is a minor process.

Oligomers were observed in the SOA formed from ozonolysis of simple alkenes. They possess the basic structure of a linear oligoperoxide, $-\text{[CH(R)-O-O]}_n-$, with the repeated chain unit having the same elementary composition as the main CI in these ozonolysis reactions. This process represents a new pathway for SOA formation and is valid for a wide range of alkenes.

Theoretical development of BVOC oxidation mechanisms (KULeuven)

Tools (Structure-Activity Relationships) necessary for the construction of VOC oxidation mechanisms were developed or extended, in particular for OH-reactions and for reactions of alkoxy radicals. The OH-initiated degradation mechanism of α -pinene has been updated by inclusion of novel radical pathways. The OH-initiated degradation mechanism of β -pinene is being finalized. The ozonolysis of three important BVOCs was also investigated; the results, including the very fast primary ozonide formation and internal SOZ formation for β -caryophyllene, are confirmed by experimental data (see above).

The atmospheric oxidation of oxygenates (KULeuven)

Detailed theoretical analyses of reactions of oxygenated compounds with OH radicals were conducted and verified by experimental data. Reactions of HO₂ with oxygenated compounds and with HOCH₂OO were investigated; in the latter case, the unexpected OH regeneration observed experimentally is confirmed by our calculations, but with co-products different from the proposed ones.

The oxidation of isoprene (KULeuven and BIRA-IASB)

Prompted by recent observations of unexpectedly high OH radical concentrations above forests (*Lelieveld et al., 2008*), we investigated the OH-initiated oxidation of isoprene using the highest levels of theory applicable, in order to rationalize the efficient HOx radical regeneration that clearly occurs, contrary to all current model predictions. In a first paper (*Peeters et al., 2009*), we showed that much of the peroxy radicals react in new ways that directly and by subsequent processes give rise to ample HOx regeneration. The new chemistry, with its impact on the global oxidizing capacity of the atmosphere, has been further addressed in a joint modeling effort of the KULeuven and BIRA teams.

Modeling α -pinene degradation and aerosol formation

The α -pinene oxidation and aerosol formation model BOREAM (Biogenic Oxidation and Related Aerosol formation Model) has been extended. A parameterization has been developed to account for non-ideality of the aerosol. Non-ideality is found to have a moderate effect in dry conditions, and to reduce SOA yields in humid conditions, due to repulsion between water and organics. Our vapor pressure estimation method has been refined. The set of experimental data has been enlarged considerably, and the method now includes neighbor effects between functional groups, and treats the effect of multiple hydrogen bonding groups.

BOREAM has been tested against more than 130 smog chamber experiments. The model generally reproduces the measured SOA yields within a factor of 2-3, in contrast

with large underestimations found in previous modeling studies. Specific particle-phase oligomerization reactions have been tested but found to have only a moderate impact on SOA yields.

Based on BOREAM, a parameterization for SOA formation from α -pinene has been developed and implemented in a global model. The parameterization accounts for water uptake and for the NO_x-dependence of SOA. Highest yields are achieved in the OH-initiated oxidation at low NO_x. The resulting model distribution of organic aerosol agrees fairly well with measurements in the Eastern US, providing support to the large SOA source inferred by the model (~100 Teragrams/year globally).

Contribution in a context of scientific support to a sustainable development policy

Environmental policy should be based on accurate information regarding the respective roles of natural and anthropogenic emissions on the abundance of air pollutants. IBOOT has contributed to answer the following questions:

Do BVOCs deplete the oxidizing capacity of the atmosphere?

BVOCs were previously believed to deplete hydroxyl radical (OH) concentrations and to reduce the oxidizing capacity of the atmosphere. However, recent observations have indicated that the oxidation of isoprene, the single-most important BVOC, regenerates OH radicals in remote areas, and that the overall effect of isoprene emissions on the oxidizing capacity of the atmosphere is weak. The theoretical work performed within IBOOT provides a first detailed explanation as to how this regeneration takes place. This finding is essential for policy-making, since it will strongly impact the model estimates of how anthropogenic activities (i.e. pollutants emissions and land-use changes) influence the abundance of key pollutants like ozone and the climate gas methane. A recent global modeling study has demonstrated the impact of the new chemistry on the expected future evolution of the oxidizing capacity of the atmosphere.

How much do BVOCs contribute to atmospheric aerosol concentrations?

Secondary organic aerosol (SOA) is a major component of fine aerosols over continents. Work within IBOOT provided new insights allowing improved estimations for the role of BVOCs as a source of secondary organic aerosols. Our model calculations show that biogenic SOA is by far the largest component of organic aerosol, although a large fraction of it is due to poorly characterized oligomerization processes in clouds and in aerosols. The presence of nitrogen oxides appears to partially inhibit the formation of SOA from α -pinene, in agreement with experimental data.

In conclusion, our work shows that BVOC emissions have only little impact on the oxidizing capacity, in particular at remote locations (e.g. rainforests). It appears therefore that, contrary to previous model estimations, deforestation is not expected to increase the self-cleansing property of the atmosphere and to mitigate pollutant build-up. However, BVOCs are a substantial source of organic aerosol having far-reaching effects on climate and air quality. The complex interaction of these emissions with anthropogenic emissions (e.g. NO_x and sulfur compounds) warrants further investigation.

Keywords

Biogenic volatile organic compounds (BVOC); air quality; climate change; oxidizing capacity of the atmosphere; secondary organic aerosols (SOA); tropospheric ozone; hydroxyl radical; smog

I. INTRODUCTION

Context

The biosphere releases large amounts of reactive gases having a profound impact on our environment. In particular, the non-methane volatile organic compounds (NMVOCs) are overwhelmingly biogenic (BVOCs). Secondary pollutants resulting from their oxidation in the air include ozone and aerosols, which are key actors in air quality and climate change. Their emissions also influence the oxidizing capacity of the atmosphere, mainly through their impact on the hydroxyl radical (OH). Although the general lines of their oxidation mechanisms are believed to be well-known, recent findings suggest that the current models are incomplete.

Smog chamber experiments provide essential constraints to the chemical oxidation mechanisms and parameterizations used in models to estimate the formation of Secondary Organic Aerosol (SOA). However, as illustrated by recent work on the degradation of pinenes by OH (Peeters *et al.*, 2001; Capouet *et al.*, 2004), important differences exist between product yields in laboratory conditions and in the atmosphere, due in part to the existence of unexpected reaction sequences. Detailed mechanisms are still lacking for important BVOC classes, like the monoterpenes (C₁₀H₁₆) and sesquiterpenes (C₁₅H₂₄). The degradation mechanism of sesquiterpenes is essentially unknown, in spite of its relevance for new particle formation and SOA growth. Even the oxidation of the most prominent BVOC, isoprene, appears poorly understood, since current models underestimate the observed OH-radical concentrations by up to an order of magnitude over forested environments such as Amazonia (e.g. Lelieveld *et al.*, 2008).

Furthermore, current models of SOA formation are unable to match the aerosol yields from laboratory experiments (Jenkin, 2004; Xia *et al.*, 2008). Possible causes include, among others (i) simplifications in the chemical mechanism used in the models, (ii) uncertainties in the estimation of saturation vapor pressures of the semi-volatile compounds, and (iii) unaccounted processes such as polymer and oligomer formation. In spite of their probable high relevance in the troposphere, heterogeneous and particle-phase reactions are still poorly characterized, although they are believed to generate low-volatility oligomers and enhance SOA formation.

Objectives

Our primary objective is to better quantify the role of biogenic hydrocarbons, in particular with respect to the formation of ozone and aerosols and the oxidation capacity of the atmosphere, by means of

- experimental determination of the composition and yields of the organic aerosol formed in the ozonolysis of the sesquiterpenes β -caryophyllene and α -humulene in atmospheric conditions, including the influence of Criegee-Intermediate scavengers (H_2O , HCOOH and HCHO) and of an OH-scavenger (MPI-Mainz),
- development of predictive tools for mechanism building, based on advanced theoretical calculations (KULeuven). These tools are needed to estimate the reaction parameters in a given reaction class from the available data for individual compounds,
- gas-phase mechanism development for important mono- and sesquiterpenes, based on advanced theoretical tools and Structure Activity Relationships (SARs) (KULeuven)
- validation of oxidation mechanism against laboratory results obtained under various conditions (IASB-BIRA),
- gas/particle partitioning model development (IASB-BIRA), including the determination of the vapor pressures and activity coefficients of the products, and evaluation against smog chamber experiments,
- study of reactions of oxygenated compounds with OH and/or HO_2 in the conditions of the upper troposphere, and of OH/ HO_2 regeneration by reactions of particular oxygenated radicals and intermediate compounds in the oxidation of isoprene (KULeuven),
- assessment of the global impact of BVOCs on the budget of oxidants and aerosols, using a global Chemical Transport Model (CTM) (IASB-BIRA), and validation against field measurements.

II. METHODOLOGY AND RESULTS

II.1 Laboratory investigations of mono- and sesquiterpenes ozonolysis

II.1.1 Products and reaction mechanism of the ozonolysis of β -caryophyllene and α -humulene

II.1.1.1 Methodology

Investigations were conducted in a 570 L glass reactor at atmospheric conditions (*Winterhalter et al.*, 2000). Ozone was produced by a mercury lamp inside the reactor, prior to the addition of the sesquiterpene. Gas-phase products (e.g. CO, CO₂, HCOOH and HCHO) were analyzed on-line with Fourier Transform Infrared (FTIR) spectroscopy. The aerosol concentration and size distribution was monitored with a scanning mobility particle sizer (SMPS). Particulate products were sampled on Teflon filters and extracted in methanol (HPLC grade). The methanolic sample was analyzed by liquid chromatography coupled to mass spectrometry (LC-MS-MS-TOF QSTAR MDS-Sciex). Two different ionization sources were used in the mass spectrometer. ElectroSpray ionization was used in negative mode (ESI-) and Atmospheric Pressure Chemical Ionization was used in positive mode (APCI+). Collisional induced dissociation (CID) experiments of isolated positively and negatively charged parent ions were done to gain structural information of the resolved components.

The reaction of Criegee-Intermediates (CI), which are formed by decomposition of the primary ozonide, with scavengers like HCOOH and HCHO are performed in order to clarify the reaction mechanism. Since OH-radicals are formed in course of the ozonolysis, different OH-radical scavengers (cyclohexane, butanol) are added and their influence on the product formation investigated. In these experiments PTR-MS was used to gain insight of the OH radical yields (*Wisthaler et al.*, 2001).

II.1.1.2 Results: β -Caryophyllene

The reactive β -caryophyllene contains two double bonds (DB) with different reactivity. After oxidation of the first very reactive DB the first-generation products are still reactive and their further oxidation has not been studied so far. Therefore experiments with varying ratios of ozone and β -caryophyllene can help to determine the kinetics of the ozone reaction, the OH-radical formation yield and products of the first-generation products.

FTIR Spectroscopy of the ozonolysis of β -caryophyllene

FTIR-spectroscopy was used to monitor ozone, β -caryophyllene and small gaseous molecules such as CO, CO₂, HCHO and HCOOH. The measured yields of only a few ppb have therefore a large uncertainty of a factor of 2. The yields of the gaseous products have been calculated for the first DB versus reacted β -caryophyllene and for the second DB (from first-generation products) versus additionally reacted ozone. The observed yields for CO range from 1-6 % for the first DB with an average yield $\pm 1\sigma$ of (2.0 ± 1.8) % and from 2-13 % for the second DB, average (5.5 ± 4.8) %. For CO₂ the observed yields vary between 1 and 7 % for the first DB, average (3.8 ± 2.8) %, and between 5 and 11 % for the second DB, average (8.2 ± 2.8) %.

HCHO was determined at its characteristic absorption at 1740 cm⁻¹ and in the range from 2700 to 2800 cm⁻¹. The observed yield for the first DB ranges from 2-15 %, with an average of (7.7 ± 4.0) %. Only one study reports so far a yield of 8 % HCHO for the first DB (*Grosjean et al.*, 1993), which is in agreement with the obtained yield in this study. The yield of HCHO from the second DB ranges from 50 to 63 % with an average of (60 ± 6) %.

Interestingly formic acid, possessing a sharp absorption at 1105 cm⁻¹, is not detected in any of the product spectra. In the experiment with HCOOH as Cl-scavenger it was observed that a large fraction of HCOOH was consumed corresponding to 60 % of the reacted ozone. Therefore it can be concluded that the formation yield of HCOOH is either very low or that all formed HCOOH reacts efficiently with the stabilized Criegee intermediates (CI).

The analysis of the residual FTIR-spectra revealed the formation of an internal secondary ozonide (SOZ) of β -caryophyllene (Figure 1 A). The strong absorption in the residual spectrum at 1104 cm⁻¹ originates from secondary ozonides (SOZ). Typical FTIR-absorptions of SOZ from simple alkenes (*Neeb et al.*, 1996; *Bariseviciute et al.*, 2006) and β -pinene (*Winterhalter et al.*, 2000) are in the range from 1050 to 1150 cm⁻¹. In Figure 1 also the effect of excess ozone can be seen. The top spectrum (A) shows the absorption in the residual spectrum, when only the first DB is oxidized. The peak at 1116 cm⁻¹ is in the range of C-O stretching vibration. A similar peak, with maximum at 1116 cm⁻¹ has been reported from liquid phase ozonolysis of β -caryophyllene using CCl₄ as solvent (*Dallwigk et al.*, 1952). In liquid phase ozonolysis with non-participating solvents SOZ are the main products. From the similarity of the liquid phase and gas-phase spectra it was concluded that the SOZ of β -caryophyllene is also formed in the gas-phase. Further addition of ozone leads to ozonolysis of the second less reactive DB. The corresponding residual spectrum is shown at the bottom of Figure 1. A change in the region 1100-1150 cm⁻¹ is observed as well as an increased absorption in the region

of the C=O absorption ($1650\text{--}1750\text{ cm}^{-1}$). This change in the spectrum can be attributed to a SOZ, whose external DB bond has been oxidized by ozone to yield a carbonyl functional group.

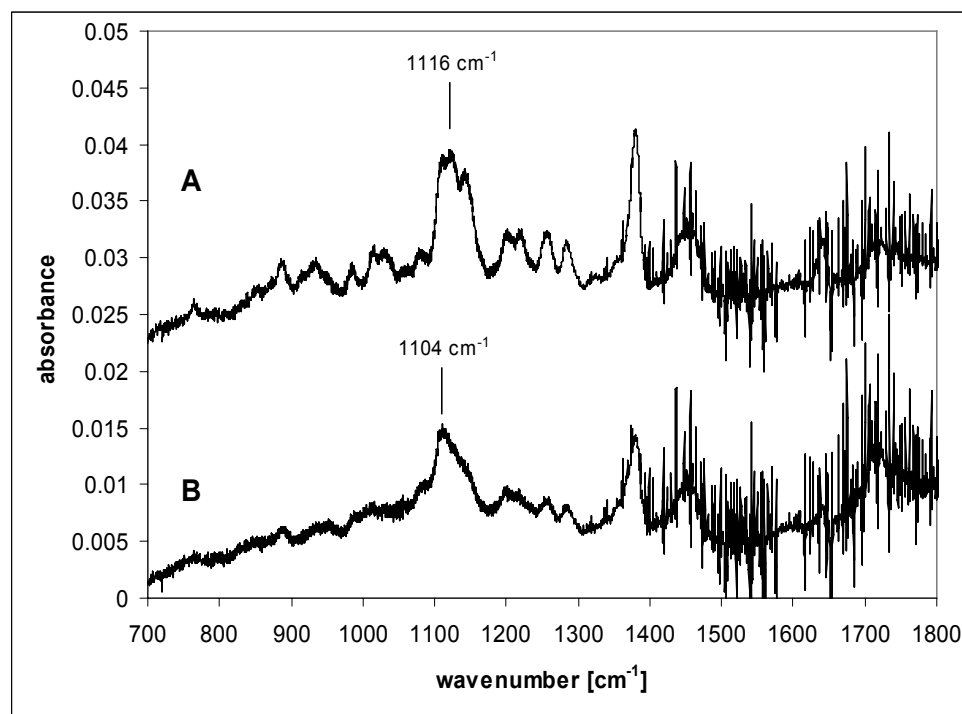


Figure 1: Residual FTIR spectra from experiment BC1107. A: obtained under conditions with excess β -caryophyllene (only internal DB oxidized); B: after further ozonolysis of the second DB.

Product analysis of organic aerosol particles in the ozonolysis of β -caryophyllene

The components of the organic aerosol compounds formed in the gas-phase ozonolysis of β -caryophyllene were characterized and published by *Kanawati et al.* (2008) using HPLC coupled to a triple quadrupole and a time-of-flight analyzer using two different ionisation sources (ESI- and ACPI+). A large number of multifunctional oxidation products were detected in the aerosol samples, and structures have been deduced from collision-induced dissociation (CID) fragmentation pathways of pseudo-molecular ions. For example, an oxocarboxylic acid believed to be formed from the ester channel of a Criegee-Intermediate generated in the first steps of the mechanism has been identified unequivocally. Moreover, the identification of several isomers with e.g. molecular weight 252 was accomplished with this method and confirmed by theoretical investigations of the fragmentation pathways. An Electrospray method was developed to ionize not only organic acids but also aldehydes in the negative mode, extending widely the range of oxidation products that can be detected in one analysis step.

Structures of the most prominent identified products were optimized by the use of quantum mechanical DFT calculations and the site dependent deprotonation potentials from different acidic positions in each product were calculated (Kanawati *et al.*, 2008), to determine the identity of the most probable parent anion for further CID studies.

Figure 2a (A) shows the chromatogram of anions with $m/z = 253$. The fragmentation pattern of one parent anion $[M-H]^-$ that is generated from this neutral species is shown in Figure 2a (B) as an example and reveals the existence of two distinct fragmentation pathways:

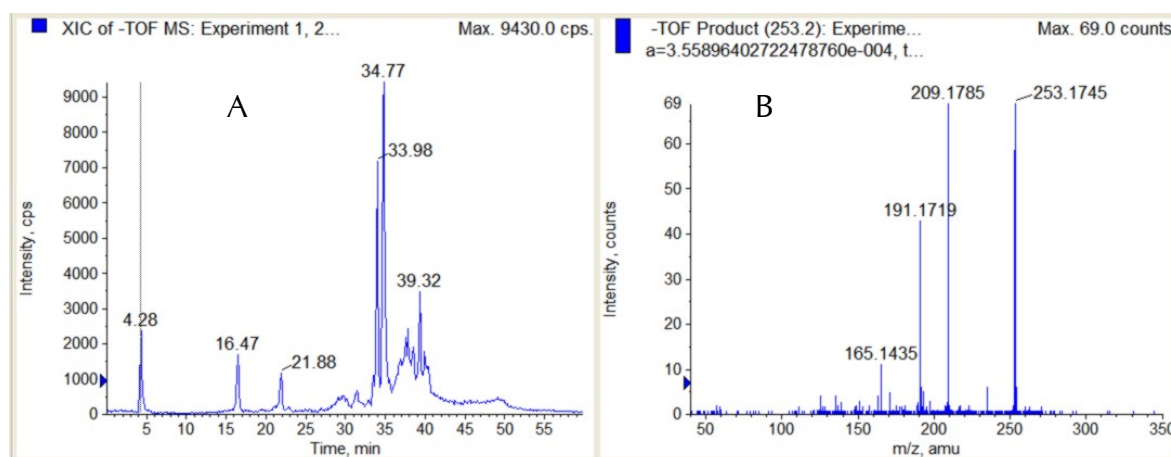
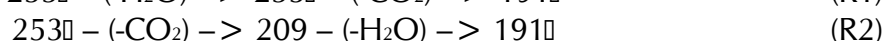
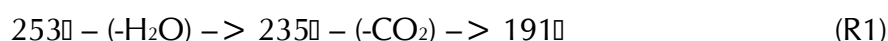


Figure 2a: A: Extracted ion chromatogram of m/z 253. B: CID spectrum of the peak at retention time 4.28 min.

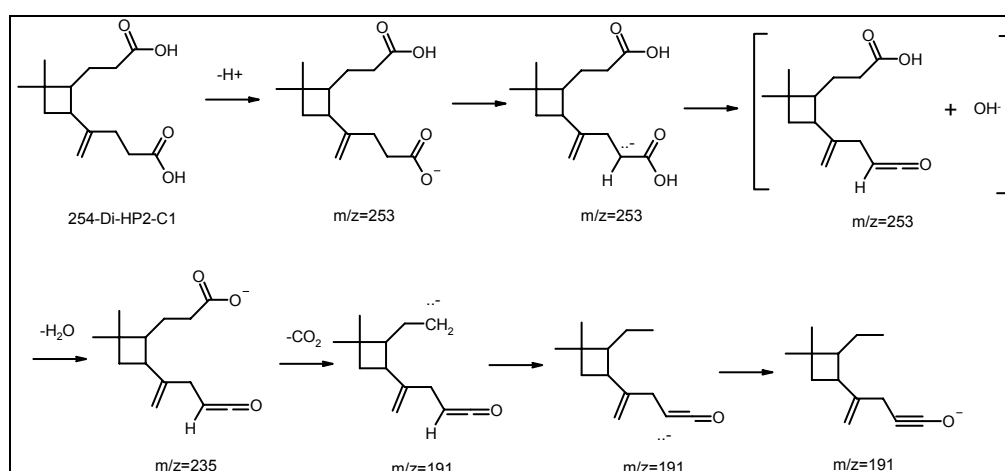


Figure 2b: Fragmentation mechanism in agreement with the pathway shown in reaction (R1).

Identified products in ozonolysis of β -caryophyllene

The oxidation products observed by mass spectrometry (using ESI and APCI ionization sources) from aerosol samples of β -caryophyllene ozonolysis with reactant ratio β -caryophyllene to ozone of 1.5 to 1 are shown in Figure 3. Under this condition only the more reactive internal double bond is oxidized.

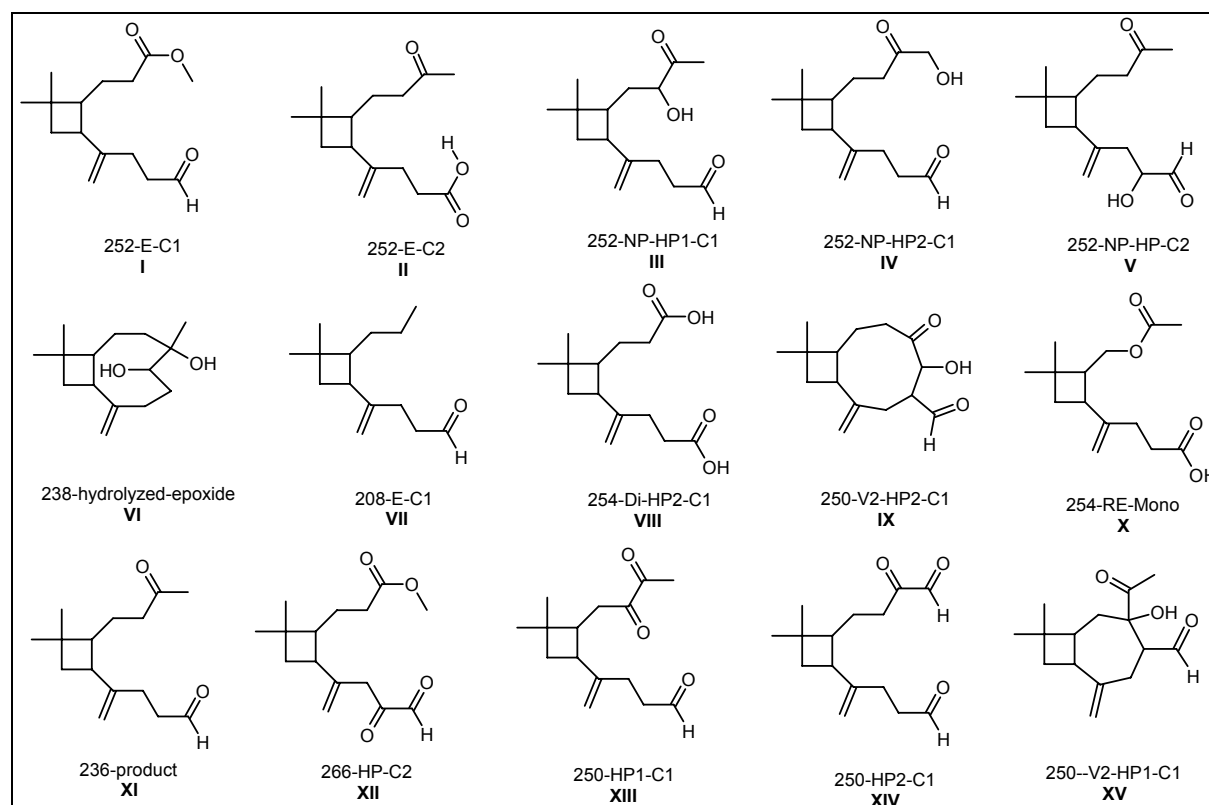


Figure 3: Oxidation products from β -caryophyllene ozonolysis with excess β -caryophyllene.

Many of the observed products can be assigned to pathways generally accepted for the ozonolysis of simple alkenes, such as the hydroperoxide and ester channels (*Calvert et al.*, 2000). Table I and Figure 4 present the main observed products (**P1** to **P11**), which are thought to be formed by these channels. Some of the products have also been identified by *Calogirou et al.* (1997) and *Jaoui et al.* (2003).

Table I. Ozonolysis products of β -caryophyllene.

Product ID used in text	M_w	Product ID <i>(Jaoui et al., 2003)</i>	Product ID <i>(Calogirou et al., 1997)</i>	Terpene nomenclature <i>(Larsen et al., 1998)</i>
P1	236	IV	1	β -caryophyllone-aldehyde
P2	252	-	-	ester-type product
P3	208	-	-	not considered
P4	252	VIII	7	β -caryophyllonic acid
P5	252	XIII	-	β -14-hydroxy caryophyllone aldehyde
P6	250	-	-	β -14-oxo caryophyllone aldehyde
P7	250	-	-	β -8-oxo caryophyllone aldehyde
P8	252	-	-	β -8-hydroxy caryophyllone aldehyde
P9	252	-	-	β -5-hydroxy caryophyllone aldehyde
P10	254	VI	-	β -caryophyllinic acid
P11	222	V	4	β -norcaryophyllone-aldehyde

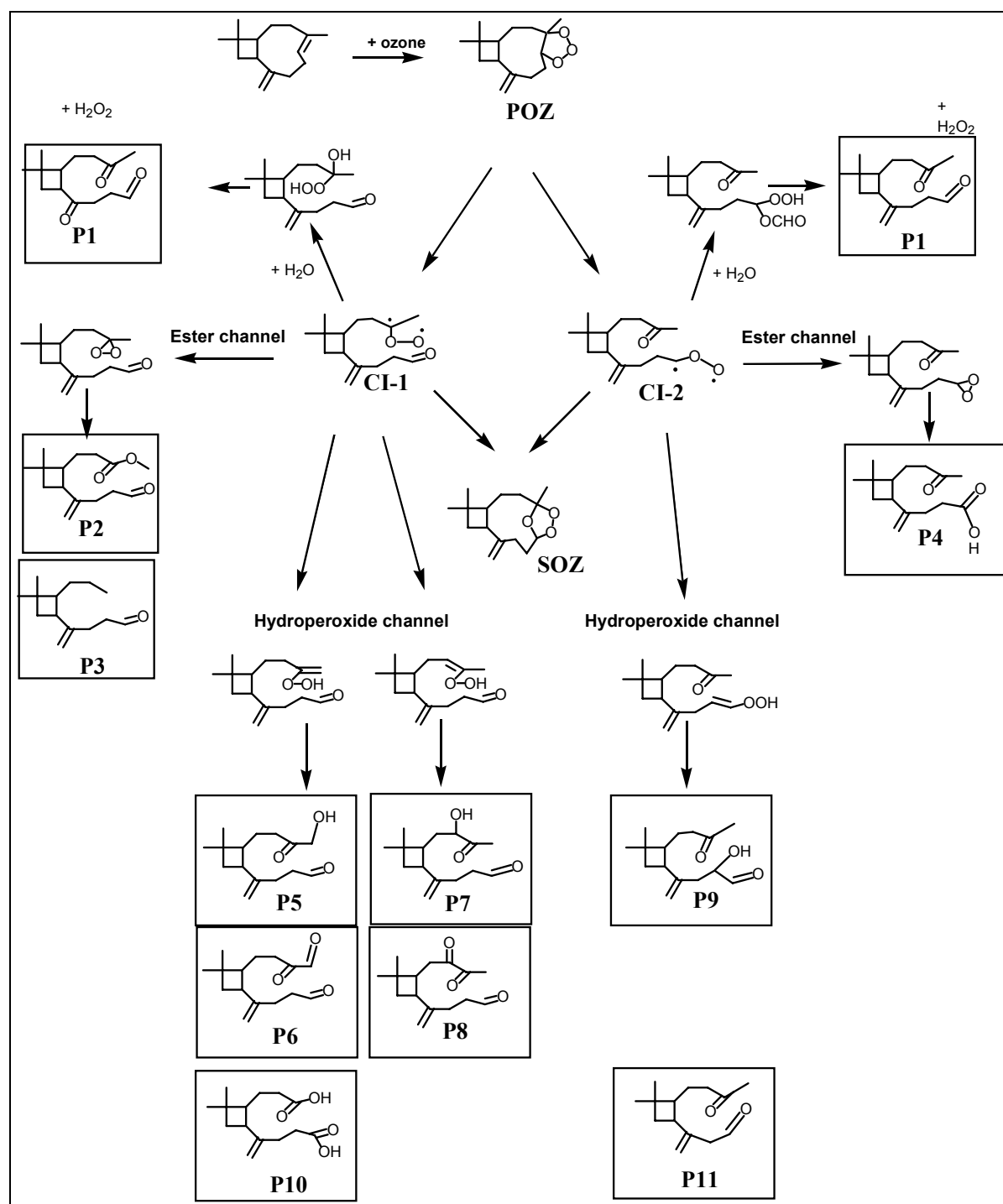


Figure 4: Reaction channels leading to identified first-generation products from β -caryophyllene ozonolysis (see Table I).

Final mechanism of the β -caryophyllene + ozone reaction

β -Caryophyllene contains two double bonds (DB) (Figure 5), of which the reactivity toward O_3 is different. The rate constant (R1a) of the internal (endocyclic) double bond (1) is nearly 100 times larger than of the external (exocyclic) DB (2). The internal DB (1) will therefore react first with O_3 , producing a primary ozonide (POZ). Ozone attack at

the exocyclic DB (R1b) is much slower and only contributes less than 5% according to theoretical calculations (Nguyen *et al.*, 2009b) to the initial ozone consumption.

The POZ decomposes into 2 different Criegee intermediates CI-1 and CI-2 both in the *syn* and *anti* configuration. The POZ exists in two conformations (POZ-1 and POZ-2, see Section II.3.4 and the theoretical paper by Nguyen *et al.*, 2009b), which can rapidly interconvert, as shown in Figure 5. The theoretical calculations predict a stabilization fraction of 64.5% for the POZ. The stabilized POZ should yield mainly thermalized CI, and in atmospheric conditions the major stabilized CI is expected to yield SOZ faster than reacting with H₂O. The remainder decomposes into the four Criegee-Intermediates. The theoretical calculations predict a yield of 6.6% for CI-1a (*syn*), 17.6% for CI-2a (*anti*), 0.3% for CI-2b (*syn*) and 11% for CI-1b (*anti*).

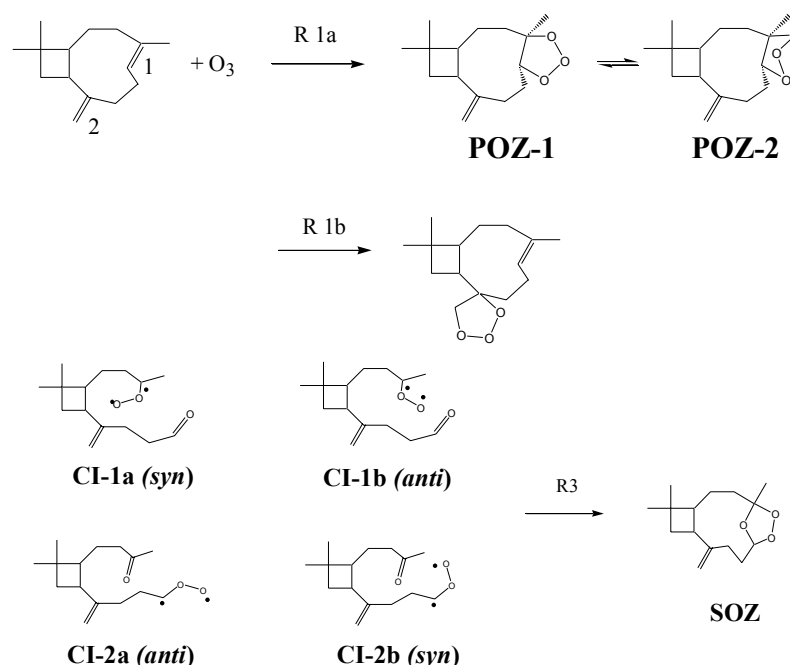


Figure 5. Formation of primary ozonides POZ (and its conformers POZ-1 and POZ-2) and the Criegee intermediates CI (*syn* and *anti*) after decomposition of the POZ (R2, not shown). Reaction R3 displays the intramolecular ring closure to produce the secondary ozonide SOZ.

The excited Criegee Intermediates CI-1 and CI-2 can rearrange via the ester and hydroperoxide channel or become collisionally stabilized and may then react further with hydroxylic or carbonyl compounds (such as H₂O, HCOOH or HCHO) in accordance with the general mechanism of ozonolysis of alkenes. Figure 4 shows the structure of the 3 resolved isomers with a neutral nominal mass of 252 formed via the hydroperoxide channel. After OH elimination and reaction with O₂, a series of hydroxyketone-(P5, P7, P9) and diketone- (P6 and P8) type products are generated. The diacid β-caryophyllinic acid (P10) is also generated after several rearrangement steps via

the hydroperoxide channel from CI-1, whereas the dicarbonyl P11 is generated from CI-2. Two isomers with mass 252 are believed to be formed from the ester channel via a dioxirane intermediate: the products P2 and P4 (β -caryophyllonic acid) have been identified unequivocally. The dioxirane intermediate can eliminate CO_2 (see FTIR results) to produce the aldehyde P3.

The extent of collisional stabilization of the POZ and/or the CI-1 and CI-2 can be estimated by the consumed HCOOH (60% of the ozone consumption) in experiments with added HCOOH (FTIR results) due to reaction of CI-1 and CI-2 with HCOOH . Theoretical calculations predict 74% stabilized intermediates (POZ and CI) for the first-generation products (Nguyen *et al.*, 2009b). A large fraction of the POZ and CI could therefore form a SOZ by intramolecular rearrangement. β -caryophyllone-aldehyde (P1) is a main product of the reaction of CI-1 and CI-2 with H_2O . All experimental and mechanistic details have been published by Winterhalter *et al.* (2009).

II.1.1.3 Results: α -Humulene

The reaction was investigated under several experimental conditions in order to gain insight into the complex reaction mechanism caused by the presence of three reactive double bonds in α -humulene. The experimental conditions are summarized in Table II. Using different ratios of ozone and α -humulene, the experiments enable to distinguish between primary reactions (only one DB oxidized) and consecutive reaction of the primary products, still containing two DB and reaction of the secondary products (still containing one DB). Further mechanistic insight can be obtained using OH-radical and CI-scavenger.

Table II. Number of experiments at various selected conditions in the ozonolysis of α -humulene.

added scavenger	ratio ozone / α -humulene		
	1-1.5	1.5-2.5	2.5 and higher
none	4	2	2
acetic acid	1	2	2
formic acid	2	3	3
cyclohexane	3	2	1
cyclohexane + formic acid	2	2	1
formic acid + acetic acid	1	1	1
water	3	4	4
water + cyclohexane	3	4	5

Aerosol phase products from ozonolysis of α -humulene

Aerosol phase products were analyzed using HPLC-MS-MS and gas phase products by FTIR analogue to the methods already described in the study of β -caryophyllene. Selected examples of CID spectra for a range of products are displayed in Figures 6 and 7.

The CID spectrum of ion with m/z 171 (Figure 6a) shows several fragment ions which are due to loss of CO_2 and CO from the pseudo-molecular ion 171 and consecutive losses of either CO or CO_2 and the loss of H_2O . The reconstructed structure and fragmentation mechanism is given in Figure 6b. The multifunctional (with OH and carbonyl group) unsaturated acid with 8 carbon atoms and 1 DB is named product Q3a (see Table III). The reaction mechanism which accounts for the formation of this acid is shown in Figure 6c.

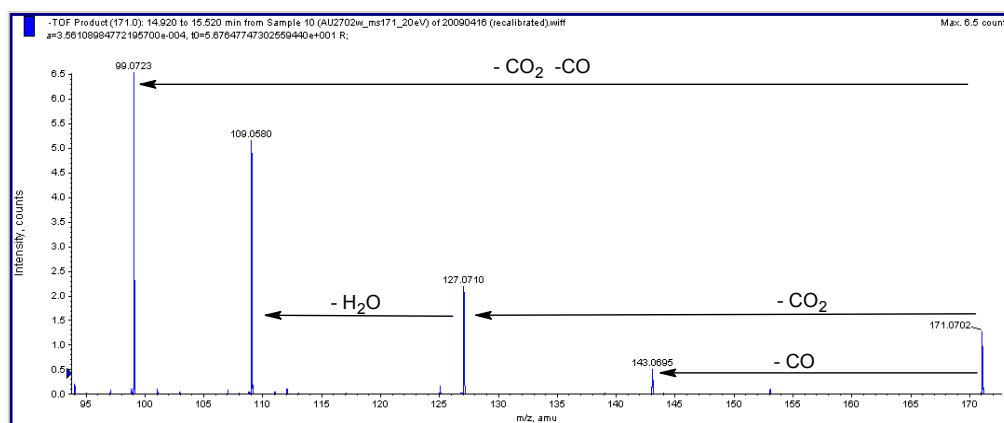


Figure 6a. Collision induced dissociation (CID) of ion with m/z 171.

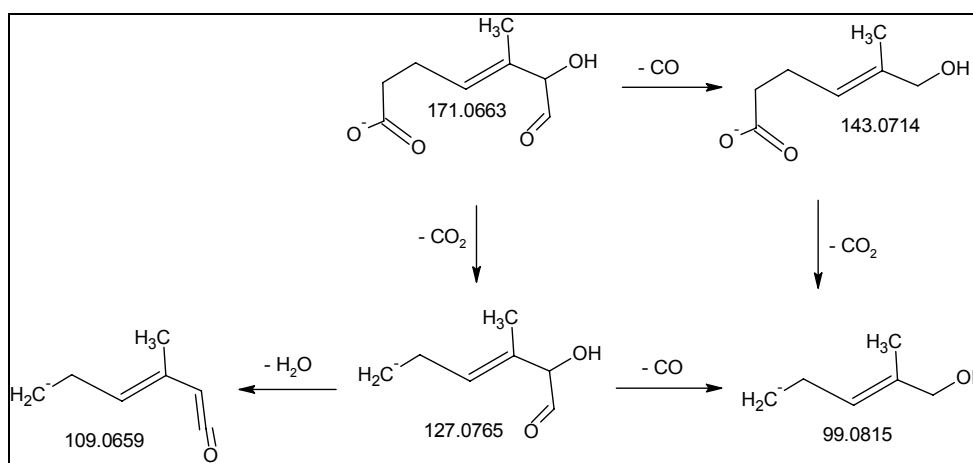


Figure 6b. Fragmentation pathway of ion with m/z 171 (Q3a).

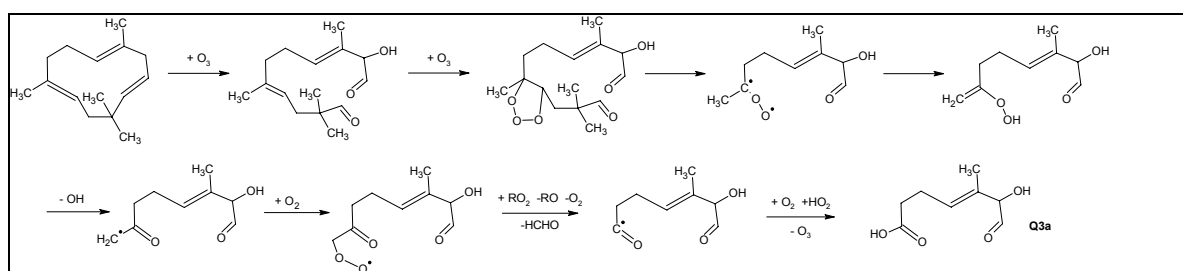


Figure 6c. Possible formation pathway of the product Q3a

A product which still contains two DB's is presented in Figure 7a. The pseudo-molecular ion 239 fragments upon loss of CO_2 and H_2O or by loss of $\text{C}_7\text{H}_{10}\text{O}_2$, yielding an unsaturated acid with MW 114 (ion 113 in Figure 7b). The formation of this product (Q9a) can be rationalized by ozone attack at DB 1 (see Figure 11 for numbering of the DB's in α -humulene), decomposition of the CI via the hydroperoxide channel and reactions analogue as in the case of β -caryophyllene lead to the dicarboxylic acid (Q9a) with 9 C-atoms and two DB's (Figure 7c).

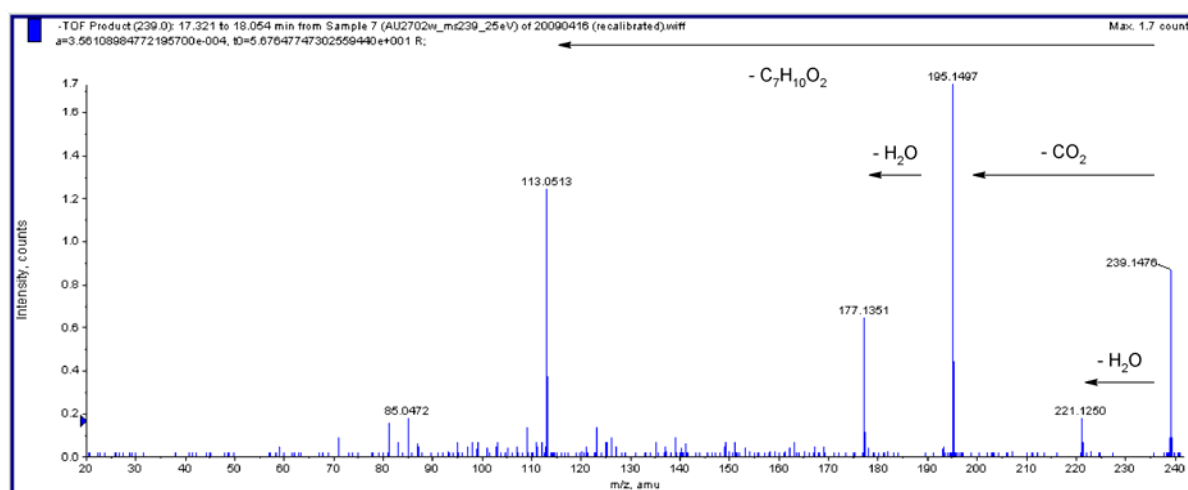


Figure 7a. Collision induced dissociation (CID) of ion with m/z 239 (Q9a)

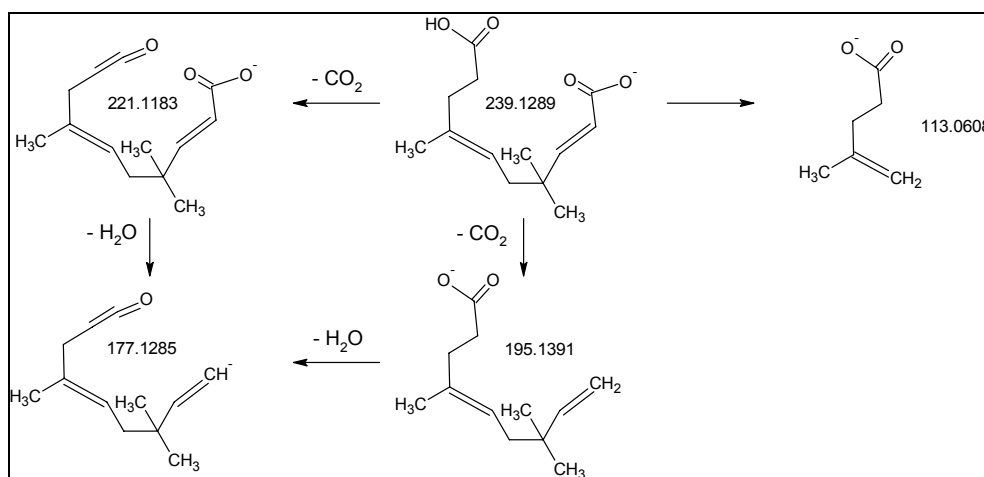


Figure 7b. Fragmentation pathway of Q9a

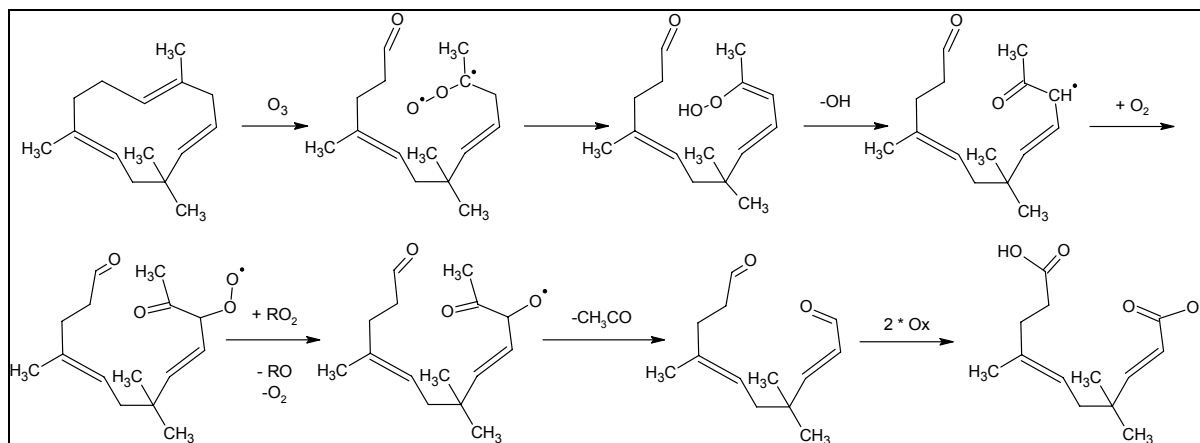
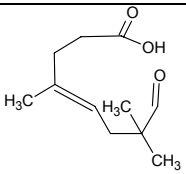
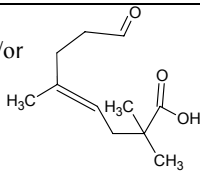
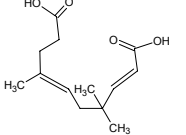
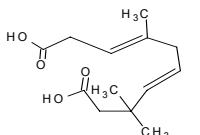
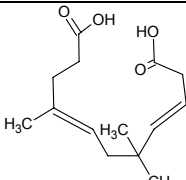
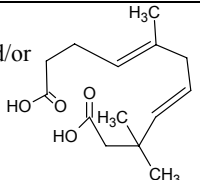
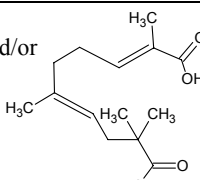
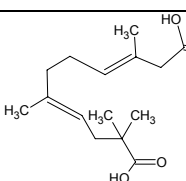


Figure 7c. Possible formation pathway of the product Q9a

Using the above method, a range of products (Q1 to Q11 in Table III) from the oxidation of one, two and all three DB's could be tentatively assigned based on the fragmentation in MS-MS experiments (Beck, 2009). A summary of identified products is presented in Table III. About twenty multifunctional products could be tentatively identified by their fragmentation patterns. The classification of the assigned products with respect to the number of remaining double bonds according to the extent of ozonolysis is shown in Table IV.

Table III. Structure of the assigned products in the ozonolysis of α -humulene

m/z 145 main peak C6	 Q1 Mw=146 class A	m/z 129 main peak	 Q2a Mw=130 class B	and/or Q2b Mw=130 class B
m/z 171 main peak C9	 Q3a Mw=172 class B	and/OR Q3b Mw=172 class B		
m/z 183 early main peak C10	 Q4 Mw=184 class B	m/z 183 late main peak	 Q5a Mw=184 class C	and/or Q5b Mw=184 class C
m/z 185 + 207 ^a early main	 Q6	m/z 185 late main peak	 Q7a	and/or Q7b

peak C9	Mw=186 class B		Mw=186 class C	Mw=186 class C	
m/z 197 main peak C11	 Q8a Mw=198 class B	and/or	 Q8b Mw=198 class B		
m/z 239 + 261 ^a main peak C13	 Q9a Mw=239 class B	and/or	 Q9b Mw=239 class B		
m/z 253 + 275 ^a 3 peak C14	 Q10a Mw=254 class B	and/or	 Q10b Mw=254 class B	and/or	 Q10c Mw=254 class B
m/z 267 + 289 ^a 1 peak C15	 Q11 Mw=268 class B				

^a Na-adduct

class A: positively identified product

class B: tentatively identified (with and without isomeric structures)

class C: identification uncertain

Table IV. Classification of assigned products with various double bonds according to the extent of ozonolysis

α -humulene products with:	3 double bonds	2 double bonds	1 double bond	no double bond
Carbon skeleton	α -humulene	C15, C14, C13	C11, C10, C9, C8	C6, C5, C4
Assigned products*		Q9a, Q9b, Q10a, Q10b, Q10c, Q11	Q3a, Q3b, Q4, Q5a, Q5b, Q6, Q7a, Q7b, Q8a,	Q1, Q2a, Q2b

* The structure of assigned products is shown in Table III

Possible formation pathways of the smallest (i.e. most oxidized) products Q1, Q2a and Q2b are shown in Figure 8. After oxidation of the first two DB's, an unsaturated aldehyde (or unsaturated CI) remains. This can further react to yield organic acids with an additional carbonyl group (Q2a and Q2b). The dicarboxylic acid Q1 could then be formed by OH or ozone oxidation of the carbonyl group of Q2a and Q2b. The relative yield of the final product Q1 versus the ratio ozone/ α -humulene increases linearly with increasing excess of ozone (Figure 9) in accordance with the proposed mechanism. Also shown in Figure 9 is the relative yield of the unsaturated product Q4. In this case a maximum in the yield is observed since product Q4 is formed after oxidation of two DB's from α -humulene. The remaining DB in Q4 on the other hand leads to further oxidation with excess ozone and lower yields are observed with higher ozone/ α -humulene ratios.

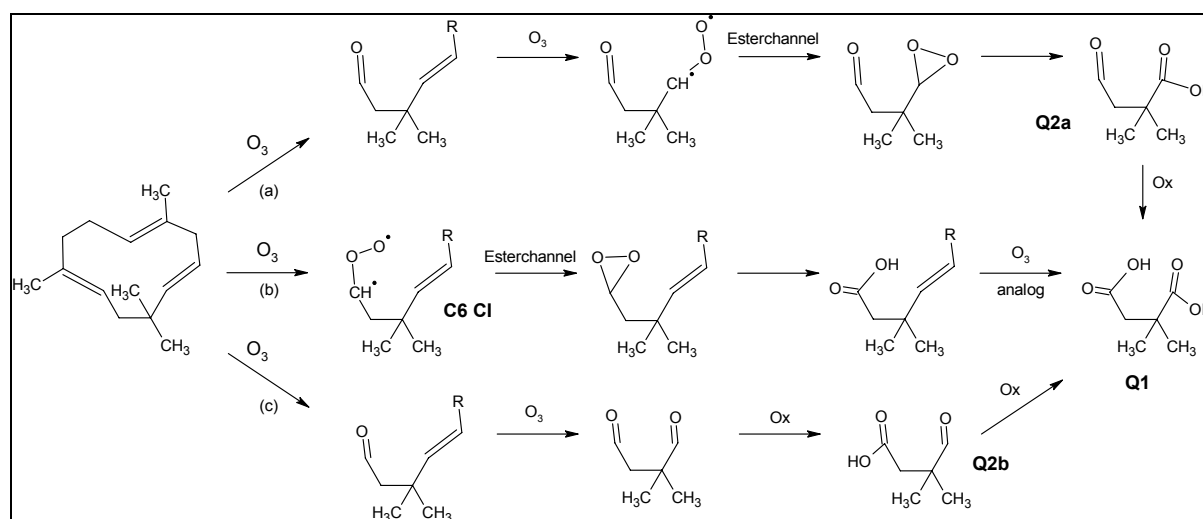


Figure 8. Possible formation pathways of the products Q1, Q2a and Q2b.

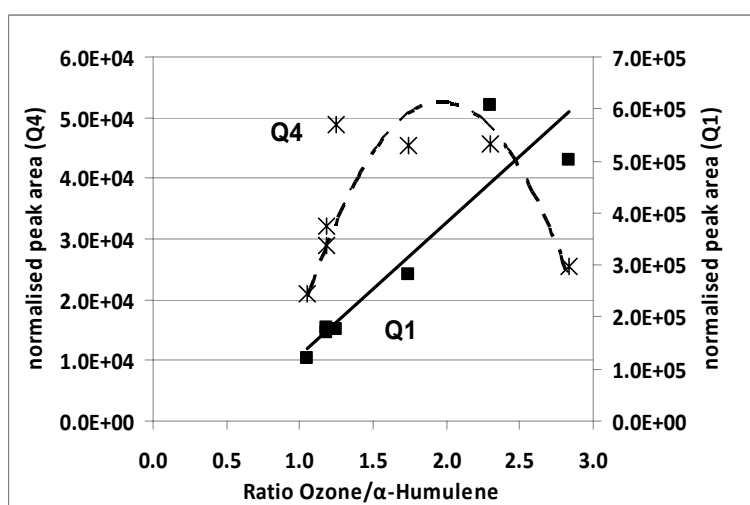


Figure 9. Relative yield of the formation of the products Q1 and Q4.

Formation of SOZ was observed by FTIR spectroscopy

Characteristic absorptions in the gas-phase FTIR-spectrum of α -humulene products (upper spectrum in Figure 10) at 970 cm^{-1} and between 1100 and 1150 cm^{-1} indicate the formation of secondary ozonides (SOZ) as described for β -caryophyllene. Ozonolysis of the different DB could lead to several SOZ and the three peaks at 1100 and 1150 cm^{-1} might be due to the fact that not only one SOZ is favorably formed. These SOZ are not measurable with the mass spectrometric method applied for aerosol analysis, but it can be expected that SOZ collected with the aerosol phase are not very stable upon sample extraction and HPLC.

An interesting finding is that the formation of SOZ is not suppressed in the presence of Cl-scavenger (lower spectrum in Figure 10), which is the case for e.g. β -pinene (Winterhalter *et al.*, 2000). The intramolecular SOZ formation is so fast that even HCOOH and H_2O as Cl-scavenger in large excess cannot compete with the intramolecular SOZ formation. This is also in agreement with the low hydrogen peroxide yields observed in presence of water (see below).

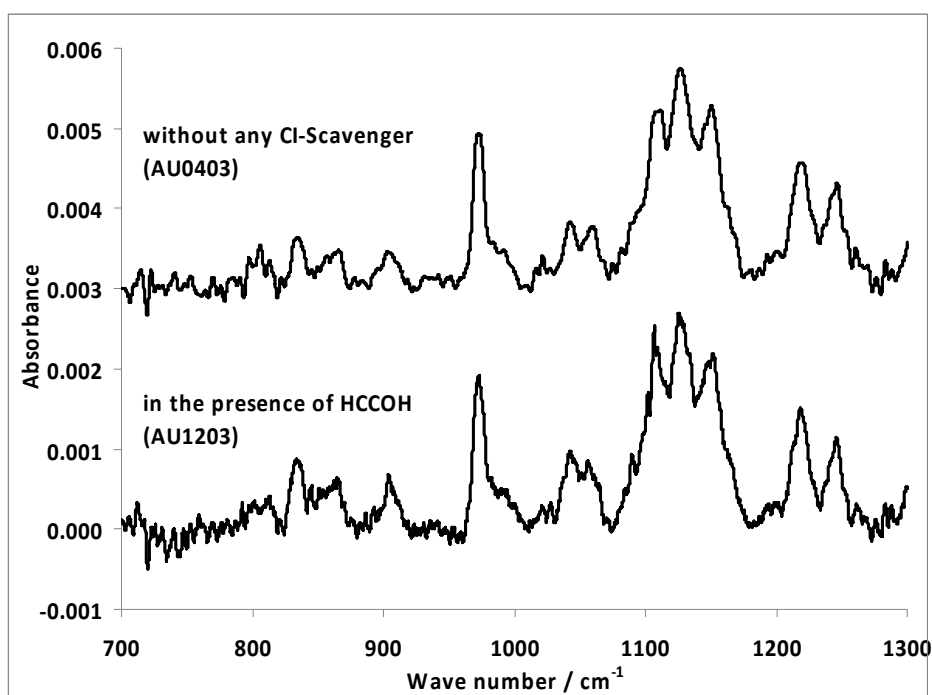


Figure 10: FTIR-spectra from experiments with Cl-scavenger (HCOOH) and in the absence of Cl-scavenger. The typical SOZ-absorption (see e.g. β -caryophyllene SOZ) are at 970 cm^{-1} and 1100 to 1150 cm^{-1} . The formation of SOZ from α -humulene is not affected by Cl-scavenger.

Reaction mechanism of the α -humulene + ozone reaction

From the three DB 's of α -humulene (Figure 11) two have three alkyl substituents (DB 1 and 2) and are expected to have similar reactivities, whereas the DB 3 with only two alkyl substituents is expected to be less reactive. Ozone addition at DB 1 and DB 2 leads to the two primary ozonides (POZ 1 and POZ 2), whereas the less reactive DB yields POZ 3. Each POZ decomposes then to two Criegee Intermediates CI 1a and CI 1b and CI 2a and CI 2b, CI 3a and CI 3b, respectively (with syn and anti conformation a total of 12 CI). Their consecutive reactions are in analogy to the reactions already discussed for β -caryophyllene (Nguyen *et al.*, 2009b, Winterhalter *et al.*, 2009) and only the SOZ formation as a main pathway is shown in Figure 11.

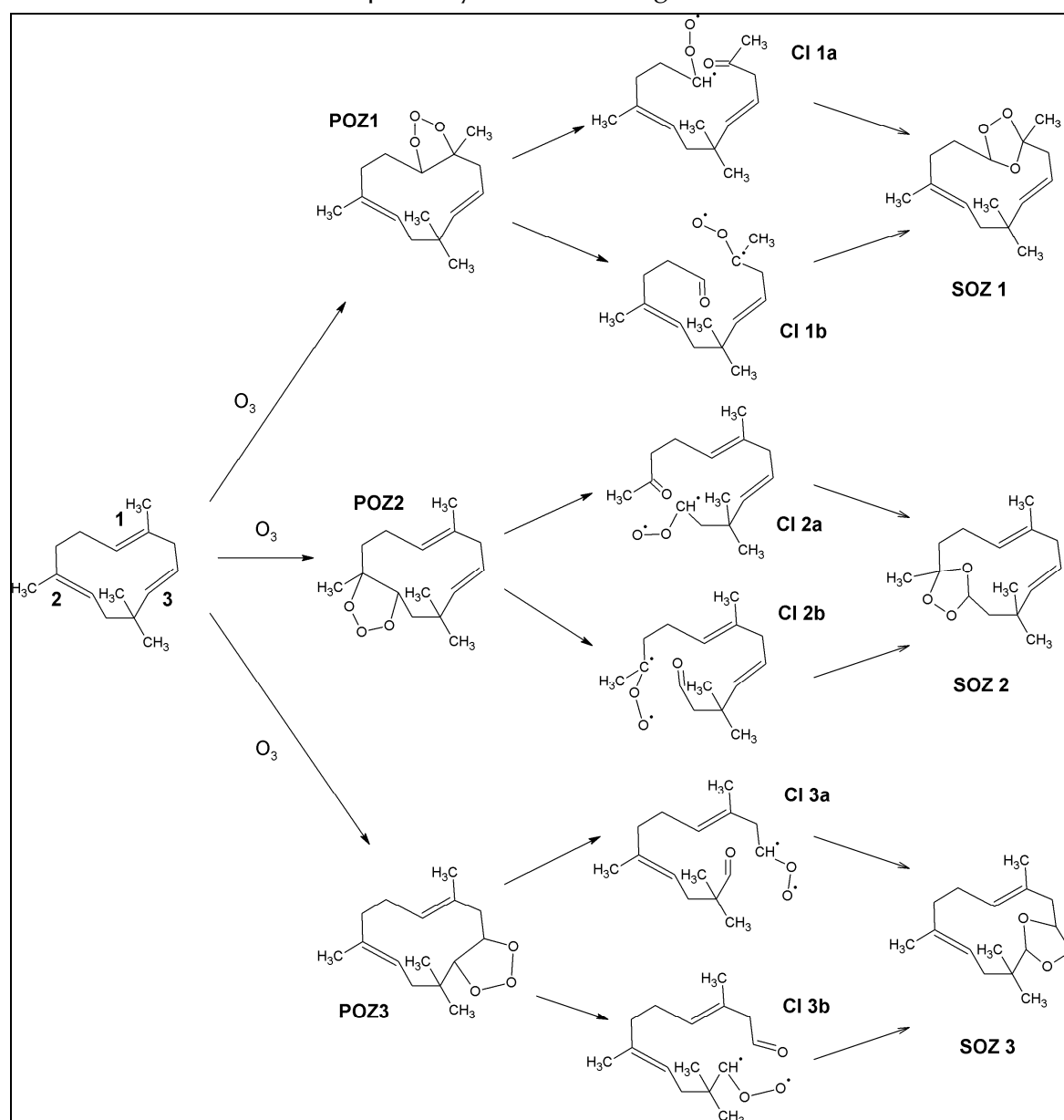


Figure 11: Initial reactions of α -humulene ozonolysis. Formation and decomposition of the main primary ozonides POZ into six Criegee Intermediates CI. Also shown are the formation pathways of the observed secondary ozonides SOZ.

Final mechanism of the α -humulene + ozone reaction

In contrast to β -caryophyllene, where one DB is much less reactive than the other, the presence of three DB's in α -humulene, with similar reactivity, gives rise to a manifold of products with two or one DB, which again react with ozone and OH. Complete oxidation yields small compounds with 4, 5 or 6 carbon-atoms. Products of all three product generations could be tentatively identified: those of the first-generation contained 13 to 15 carbon atoms, these of the second-generation 8 to 11 and those of the third-generation 4 to 6. Because of the unavailability of reference substances only the C6-dicarboxylic acid **Q1** (2,2-dimethyl-succinic acid) could be positively identified by comparison with an authentic standard; the corresponding oxocarboxylic acids **Q2a+b** only tentatively.

Only compounds with a carboxylic acid group could be detected. The C11- and C9-dicarboxylic acids **Q7a+b**, were tentatively identified. For the C11-compound both structural corresponding oxocarboxylic acids (**Q8a+b**) were also observed. A C10-dicarboxylic acid could not be identified, although the C10-oxocarboxylic acid **Q4** is structurally very similar to the corresponding C11-compound **Q8a**. The other tentatively identified C10-oxocarboxylic acid **Q5a** contained another remaining double bond (DB3). Three compounds in this generation are hydroxy-oxocarboxylic acids, two contained 8 carbon atoms (**Q3a+b**) and one 9 carbon atoms (**Q7a**). Moreover, these three compounds have the same functional groups and are also the only compounds with DB1 as remaining double bond.

The first-generation products contain between 13 and 15 carbon atoms. Because of the very similar structure of many postulated compounds the clear assignment of the peaks was not always possible. The C15-dicarboxylic acid **Q11**, three C14-dicarboxylic acids (**Q10a-c**) and two C13-dicarboxylic acids **Q9a+b** could tentatively be identified.

The genealogy of products and their precursors is summarized in Figure 12.

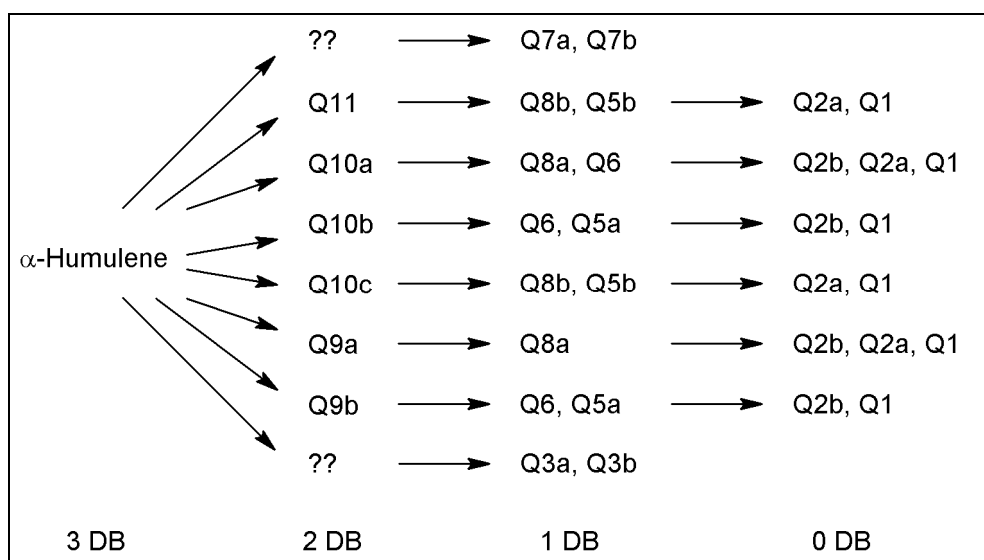


Figure 12. Pathways of assigned products in the ozonolysis of α -humulene. The products are listed in columns according to their formation route during each ozonolysis step, giving rise to products containing 2, 1 or no double bonds.

In total 37 compounds in the aerosol phase and five compounds in the gas phase could be tentatively identified. The relative yields of these products could be influenced by the different scavengers. Cyclohexane as OH-scavenger had rarely a positive effect on the yield, but it lowered the yield of some products up to 40 %. The CI scavengers increased the yield of some products up to factor 3. But there seems to be no general influence of the different scavenger on the products yield.

Only 20 products have been listed in Table III, but a detailed description of all assigned products has been summarized in a recent article submitted for publication in Phys. Chem. Chem. Phys. (Beck *et al.*, 2010).

Kinetic experiments and OH-radical yield for β -caryophyllene and α -humulene

The experimentally determined rate constant for the ozone attack of the second (less reactive) exocyclic double bond in β -caryophyllene was determined by simulation of the ozone consumption using Facsimile as $k_2 = 1.1 \times 10^{-16} \text{ cm}^3 \text{ molecule}^{-1} \text{ s}^{-1}$. This value is two orders of magnitude lower than the rate constant for the ozone attack of the first reactive endocyclic double bond in β -caryophyllene, $k_1 = 1.16 \times 10^{-14} \text{ cm}^3 \text{ molecule}^{-1} \text{ s}^{-1}$. The rate constant for the first, second and third ozone attack in α -humulene is 1.17×10^{-14} , 3.6×10^{-16} and $3.0 \times 10^{-17} \text{ cm}^3 \text{ molecule}^{-1} \text{ s}^{-1}$, respectively (Herrmann, 2006).

The OH-radical yields from the ozonolysis of several mono- and sesquiterpenes were indirectly determined using an OH-radical scavenger (cyclohexane), whose reaction product with the OH-radical (cyclohexanone) was quantified by PTR-MS, and from its product yield the OH-radical yield could be calculated (Herrmann *et al.*, 2010). For

β -caryophyllene, the OH-radical yield from the second double bond was twice as large (21 %) as for the first more reactive double bond (10.4 %). For α -humulene, the first two double bonds gave the same OH-radical yield of 10 %, the OH yield from the third double bond was not determined (Herrmann, 2006).

II.1.2 Determination of aerosol yields from sesquiterpene-ozonolysis

Determination of aerosol yields was focused on the ozonolysis of β -caryophyllene. Aerosol particle size distributions were measured by a Scanning Mobility Particle Sizer (SMPS), which enables to determine the aerosol yields.

The ozonolysis experiments for the determination of SOA mass yields were performed in the absence of OH scavenger. The experiments were performed under 1.5 to 3 fold terpene excess over O_3 . The aerosol number reaches its maximum within the first 10 minutes, with a particle diameter of about 50 nm. At longer reaction times particles grow in size, reaching a diameter of 120 nm after 60 minutes reaction time. Their number gradually decreases due to coagulation of the aerosol particle, condensation of semi-volatile compounds on existing particles, and/or loss by deposition on the reactor wall.

From the formed aerosol mass and the reacted β -caryophyllene SOA mass yields have been calculated. Table V lists the aerosol yields of β -caryophyllene ozonolysis from different experiments. Some of the experiments were performed in the presence of formic acid, formaldehyde and water as Criegee-Intermediate scavenger. As can be noticed from Table V, the aerosol yield increases by addition of water vapor and with higher concentrations of formic acid. This increase in aerosol yield is unexpected, since previous studies of the ozonolysis with monoterpenes have indicated that HCOOH acts as an effective Criegee intermediate scavenger (Bonn *et al.*, 2002). It is suggested that formic acid adds to the Criegee Intermediates CI-1 and CI-2 (see Figure 4) to generate a formate product (MW = 298) with sum formula of $C_{16}H_{26}O_5$, which can then undergo a rearrangement to yield the oxocarboxylic acid β -caryophyllonic acid (**P4** in Table I) and thus increases the aerosol yield.

Three experiments with α -humulene in excess and two experiments with 4-fold ozone excess were performed. The SOA-yield in the experiments with α -humulene excess varied between 13 and 16 %. A high excess of ozone increased the yield to almost 40 %. From the identification of the products by HPLC-MS, the different SOA yields can be explained by the degree of ozonolysis of the different double bonds. The SOA of the experiments with excess α -humulene should predominantly contain first-generation products. It could be assumed that these products have a relatively high

molecular weight, mostly possessing two or more functional groups. All these products are expected to have a relatively low volatility and therefore have high SOA formation potential. On the contrary, the SOA of the experiments with ozone in excess contained mainly products of the second-and third-generation. The latter compounds have a relatively low molecular weight, but because of their functional groups, they also possess a relatively low volatility.

A temperature-controlled flow tube was set up to investigate the temperature dependence of the SOA yield for the ozonolysis of β -pinene. It was found that under dry conditions the SOA yield increased for low particle mass concentration ($10 \mu\text{g m}^{-3}$) from 0.08 at 303 K to about 0.20 at 263 K (von Hessberg *et al.*, 2009).

Table V. Aerosol yields from β -caryophyllene (BC) with and without Cl-scavenger.

Ozone ppb	BC ppb	Reacted BC $\mu\text{g m}^{-3}$	Aerosol $\mu\text{g m}^{-3}$	Aerosol yield %	Scavenger ppb
100	309	920	50	6	-
180	562	2340	190	8	-
200	301	1930	170	9	-
200	300	2290	280	12	-
200	320	1540	270	18	-
100	258	1540	370	24	-
200	305	1580	310	19	HCOOH / 250
200	298	1900	470	24	HCOOH / 500
200	304	2220	660	30	HCOOH / 500
200	320	1900	620	32	HCOOH / 1000
200	331	1520	620	41	HCOOH / 1000
200	315	2130	180	9	HCHO / 7800
100	239	1050	130	12	HCHO 6800
200	295	1620	440	27	H ₂ O 12800 ppm *

* This corresponds to 36 % relative humidity

II.1.3 Identification and quantification of hydroperoxides from sesquiterpene ozonolysis

The reaction of Cl with H₂O is a NO_x-independent source of hydroperoxides (H₂O₂ and ROOH) and was investigated at various relative humidities. Experiments have been performed in the glass reactor at 730 Torr and room temperature. Formation of H₂O₂ and organic hydroperoxides during sesquiterpene ozonolysis has been monitored by HPLC with fluorescence detector. Samples were taken from the gas phase by drawing the air samples through a thermostated helix-shaped coil containing a continuous flow of a scrubbing solution (Sauer *et al.*, 2001; Valverde-Canossa *et al.*, 2006). All experiments were carried out at relative humidities between 50 to 60 %. Initial reactants' mixing ratios were 400 ppb of sesquiterpene and 270 ppb, 860 ppb and 1200

ppb of ozone, respectively. Excess cyclohexane (300 ppm) was added as an OH scavenger in some experiments.

For β -caryophyllene H_2O_2 yields were found to be 2% with excess alkene and 4% with excess ozone. Moreover, 0.2% of hydroxymethyl hydroperoxide (HMHP) were formed with excess ozone, while its concentrations were below the quantification limit with excess alkene. Under similar initial conditions, α -humulene produced four times more H_2O_2 . The addition of excess cyclohexane as an OH scavenger did not have any detectable influence on H_2O_2 yields for both sesquiterpenes. Extracted filter samples of organic aerosol showed significant quantities of hydroperoxides, with a relative percentage of long-chain (C_6 to C_{12}) organic hydroperoxides to H_2O_2 of up to 12 % (see Figure 13).

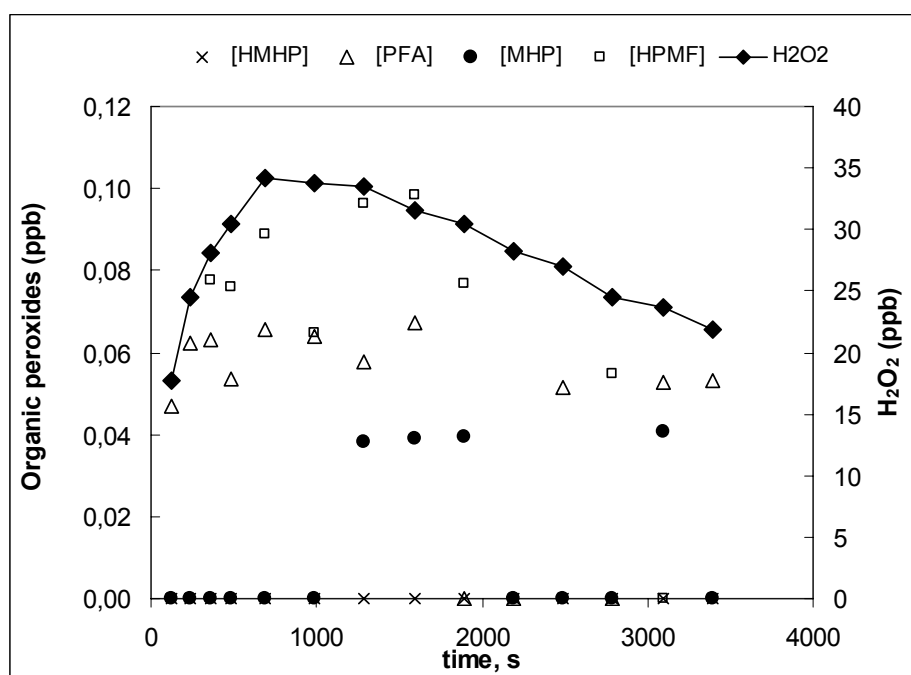


Figure 13: Time profile of hydrogen peroxide and organic peroxides mixing ratios in the gas phase from α -humulene ozonolysis. HMHP: α -hydroxy-methylhydroperoxide, PFA: performic acid, MHP: methylhydroperoxide, HPMF: hydroperoxymethylformate.

II.1.4 Formation of oligomers and polymers

In our recent studies we reported the discovery of oligomeric compounds by chemical analysis of secondary organic aerosol (SOA) formed during ozonolysis of enol ethers and structurally related small alkenes (Sadezky *et al.*, 2006, 2008). The formed SOA has been detected by a SMPS system and chemically characterized by a hybrid ESI/MS/MS-TOF technique in the mass range m/z 200–800. The chemical composition was confirmed by accurate mass measurements with an ESI Fourier Transform Ion cyclotron resonance (FTICR) mass spectrometer, which offers ultrahigh resolution and high sensitivity for the characterization of complex samples.

All detected oligomers have the basic structure of a linear oligoperoxide, $-\text{[CH(R)-O-O]}_n-$, with the repeated chain unit CH(R)OO having the same elementary composition as the main Criegee Intermediates (CI) in these ozonolysis reactions. The elemental compositions of parent ions, fragment ions and fragmented neutrals determined by accurate mass measurements with the FTICR technique allow us to assign a complete structure to the oligomer molecules, as exemplary shown in Figure 14.

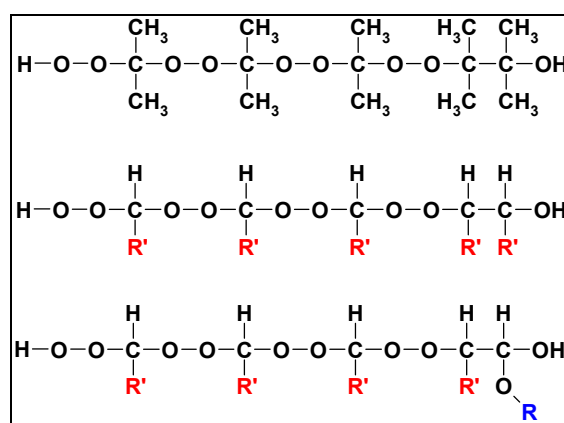


Figure 14. Oligoperoxidic structures suggested for the oligomers formed during gas-phase ozonolysis of enol ethers and symmetric alkenes: *top*: 2,3 dimethyl-2-butene; *middle*: *trans*-3-hexene with $\text{R}' = \text{C}_2\text{H}_5$ or *trans*-4-octene with $\text{R}' = \text{C}_3\text{H}_7$; *bottom*: enol ether e.g. ethyl butenyl ether with $\text{R} = \text{R}' = \text{C}_2\text{H}_5$.

We suggest that the formation of the oligoperoxidic chain units occurs through a new gas-phase reaction mechanism observed for the first time in this work, which involves the addition of stabilized CI to organic peroxy radicals (Sadezky *et al.*, 2008). This oligoperoxide formation involving CI-like chain units represents a new pathway for secondary organic aerosol and oligomer formation and shows its validity for a wide range of alkenes.

In the case of sesquiterpenes only the acyclic α -farnesene yielded oligomers in the range of m/z 200–800. For the ozonolysis of α -humulene also high molecular weight compounds up to mass 655 m/z were observed but it was impossible to deduce their individual oligomeric or polymeric structure. Here the mass spectrum of the products of the reaction of O_3 with excess α -humulene displays distinct peaks in the mass range 400 to 600 m/z . These peaks could possibly be attributed to dimer structures of mono- and dicarboxylic compounds, but no detailed analysis was performed. In the mechanism proposed by Sadezky *et al.* (2006, 2008), it was suggested that small stabilized Criegee Intermediates (C1 to C4) were added to peroxy radicals to form oligoperoxide structures. In the case of α -humulene the formed CIs were much larger (C15) and therefore stabilized to a greater extent, minimizing the probability to be involved in radical chain reactions, and that the formation of secondary ozonides (SOZ) seemed to be favoured, as observed in this study.

II.1.5 Determination of CCN activity of sesquiterpene ozonolysis products

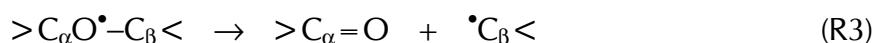
An important factor in cloud formation is the hygroscopicity of the aerosol particles, which is commonly determined by a Tandem-DMA method and from the hygroscopic growth factor conclusions about the cloud condensation nuclei (CCN) activity of aerosol particles are drawn. Interestingly, the CCN activity was recently measured (*Huff Hartz et al.*, 2005; *Asa-Awuku et al.*, 2008) and it was observed that the products of the sesquiterpene ozonolysis are less CCN-active than the products of monoterpene ozonolysis. The CCN activity for β -caryophyllene was found to be a strong function of temperature, suggesting that the hygroscopic fraction of the SOA is volatile. In view of these published results, it was decided not to repeat these measurements within the IBOOT project.

II.2 Development of predictive tools for mechanism construction

The predictive tools developed in this section are applicable to a wide range of compounds, with uses far beyond their application described in this report. Most of the SARs described here are derived from theoretical kinetic considerations using quantum chemical data, and provide not only a predictive tool but also a framework that allows for future extensions and improvements. The SARs are developed for reaction types that are not easily accessible by experimental means, and are expected to be of general use to the atmospheric chemistry community.

II.2.1 Alkoxy radical decomposition

The decomposition rate coefficient $k(T)$ for the alkoxy radicals formed as intermediates in the atmospheric degradation of most hydrocarbons can be well described as $k(T) = A \times \exp(-E_b/kT)$, with $A \approx 1.8 \times 10^{13} \text{ s}^{-1}$ for nearly all alkoxy radicals, and where the barrier height E_b to decomposition depends strongly on the α - and β -substituents on either side of the breaking $\bullet\text{OC}_\alpha\text{-C}_\beta$ bond



A previously developed SAR along these lines (*Peeters et al.*, 2004), which considered only alkyl-, hydroxy- and oxo-substituents, has now been extended to a large variety of substituents relevant in atmospheric chemistry. The quantum chemical methodologies applied to this reaction class includes the DFT functionals B3LYP, MPW1K, MPWKICIS1K, and BB1K, and the MP2 and CBS-QB3 *ab initio* methodologies combined with DIDZ, 6-31G(d,p), 6-311 + + G(2df,2pd), and aug-cc-VTZ basis sets, in combinations limited by our computational resources and selected based on the relative merit of the methodologies.

Based on results for over 80 transition states with different combinations of 10 substituents, the impact of α - and β -substituents s on the barrier height for alkoxy radical decomposition can be summarized as follows:

$$E_b / \text{kcal mol}^{-1} = 17.9 + \sum F_s \times n_s \quad (\text{Eq. 1})$$

where n_s is the number of substituents of type s on carbon α or β , F_s is the impact of a substituent of type s on the barrier height, and summed over all substituents on carbons α and β . The substituent activities F_s , in kcal mol^{-1} , are listed in Table VI.

Table VI: Alkoxy decomposition SAR activities.

Substituent	F_s	Substituent	F_s
α -alkyl	-2.3 ^a	β -alkyl	-3.4
α =O	-12.7	β =O	-8.5
α -OH	-8.9	β -OH	-7.5
α -OR (R = alkyl)	-9.2	β -OR (R = alkyl)	-9.1
α -OOH	-8.9	β -OOH ^c	-9.3
α -OOR (R = alkyl)	-6.4	β -OOR (R = alkyl) ^c	-7.2
α -NO	N/A ^b	β -NO	-16.0
α -NO ₂	-2.2	β -NO ₂	+0.4
α -ONO	-4.2	β -ONO	-6.0
α -ONO ₂	-3.8	β -ONO ₂ ^d	-2.8
α =C	+21.5	β =C	+5.0
α -C=C	-4.9	β -C=C	-9.6

^a If only one substituent is present on the α -carbon of the form $-\text{CHO}$, $-\text{CH}_2\text{OR}$, $-\text{CH}_2\text{OOH}$, or $-\text{CH}_2\text{OOR}$ (R = alkyl), use $F_s = -0.7$. ^b Compounds of the form $>\text{C}(\text{O}^\bullet)-\text{NO}$ spontaneously decompose to $>\text{C}=\text{O} + \bullet\text{NO}$ ^c Product radicals of the form $>\text{C}^\bullet\text{OOH}$ and $>\text{C}^\bullet\text{OOR}$ spontaneously decompose to $>\text{C}=\text{O} + \bullet\text{OH}$ or $\bullet\text{OR}$. ^d Product radicals of the form $>\text{C}^\bullet\text{ONO}_2$ spontaneously decompose to $>\text{C}=\text{O} + \bullet\text{NO}_2$.

In addition, the effect of ring strain has been examined for small rings. Three-membered rings with an oxy radical functionality are not stable and spontaneously break the ring. For systems where one of C_α and/or C_β is in a different ring system, the activities are listed in Table VII. These activities include the effect of the alkyl chain constituting the ring proper.

Table VII: Alkoxy decomposition SAR ring activities.

C_α in 3-membered ring : N/A ^a	C_β in 3-membered ring : +2.4
C_α in 4-membered ring : -2.0	C_β in 4-membered ring : -4.2
C_α in 5-membered ring : -2.0	C_β in 5-membered ring : -7.0
C_α in 6-membered ring : -2.0	C_β in 6-membered ring : -7.0

^a The 3-membered ring in substituted cyclopropoxy breaks without barrier.

Systems where C_α and C_β are part of the same ring, i.e. ring breaking reactions, are listed in Table VIII. These activities include the effect of the alkyl chain constituting the ring proper:

Table VIII: Alkoxy decomposition SAR activities for ring breaking

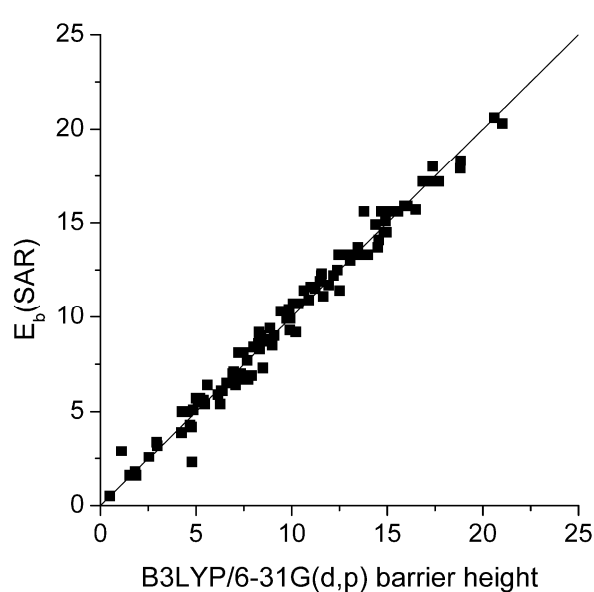
Breaking of 3-membered ring : -27.6

Breaking of 4-membered ring : -17.1

Breaking of 5-membered ring : -8.7

Breaking of 6-membered ring : -6.3

Compared to earlier work by our research group (Peeters *et al.* 2004) which examined the effect of alkyl-, hydroxy (-OH), and oxo (=O) substituents on the barrier height, the range of substituents was significantly extended to include more oxygen- and oxygen-nitrogen-bearing functionalities, including these in ethers, (hydro)peroxides, and -N_xO_y substituted compounds. This will enable us to predict the reactivity for a much wider range of (oxygenated) intermediates formed in the degradation of the larger biogenic hydrocarbons including terpenes and sesquiterpenes. Also, the effect of vinyl and allyl-substituents was investigated to support work on the degradation mechanism of poly-unsaturated hydrocarbons (including ring structures) such as isoprene and the terpenoids. Most substituents stabilize the product radical and carbonyl function and reduce the barrier height relative to the non-substituted template molecule ethoxy (CH₃CH₂O^{*}). The only exceptions occur where the α - or β -carbons are involved in a double bond (in addition to the breaking bond) or where C _{β} is part of a 3-membered ring. This observation simplifies the degradation mechanisms for some poly-unsaturated hydrocarbons. Compounds where the product radicals form a conjugated π -system with the newly formed C=O double bond, have a different A-factor by a factor of ~2. This work was published recently (Vereecken and Peeters., 2009).

**Figure 15:** SAR predictions against the underlying quantum chemical data.

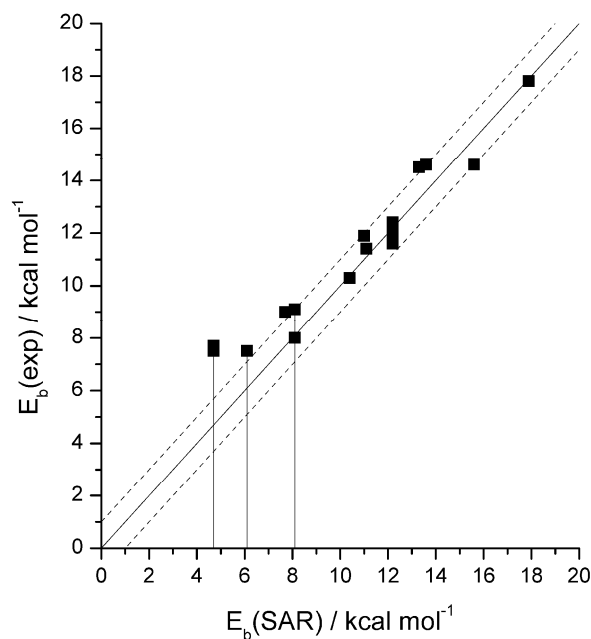


Figure 16: SAR predictions against the available experimental data.

II.2.2 Isomerization of alkoxy and alkylperoxy radicals by H-migration

Direct experimental data on H-migration in alkoxy radicals is very scarce, and is essentially limited to rate coefficients for 4 compounds, as reviewed by *Atkinson* (2007); for alkylperoxy radicals no direct data is available. The relative change in reactivity, i.e. barrier height and pre-exponential factor in the temperature-dependent rate coefficient equation, for different compounds can be estimated using an extensive set of conformer-specific B3LYP/6-31G(d,p) and CBS-QB3 calculations, examining the impact of changes in barrier height, TS rigidity, contributing conformers, and tunneling. These changes, relative to the experimental data for 1,5-H-shifts are examined in ongoing work for a wide set of isomerization reactions, 1,4-H-migration through 1,8-H-migration, with oxo- and hydroxy substitution at various positions relative to the migration hydrogen and radical oxygen.

The rate coefficient for isomerization of alkoxy radicals by 1,5-H-migration has been measured a number of times, and data is available for 1-butoxy, 1-pentoxy, 2-pentoxy, and 5-Me-hexoxy, i.e. for migration of primary, secondary and tertiary hydrogens (*Atkinson*, 2007). Using these data as reference values, it is possible to extrapolate these data to other H-shift reactions, using quantum chemical data to derive the transformation process. For migrations over a longer or shorter distance than a 1,5-H-shift, the rate coefficient will be affected by a number of reaction properties: the change in ring strain in the TS, change in TS rigidity, change in the number of contributing conformers in reactant and TS, and change in tunneling efficiency. Furthermore, if the migrating hydrogen is not any of the three aforementioned types (prim, sec, tert), the barrier height and reaction entropy will

further be influenced by substitutions around the migration H, and possibly substitution affecting the TS ring structure. Our focus for non-alkyl substitution went to carbonyl- (ketones, aldehydes) and hydroxy substitution (alcohols) as frequently present in the atmospheric oxidization of biogenic VOCs. A large set of CBS-QB3 data has been collected for a large set of compounds ranging from C₂ to C₉ compounds, and compared against B3LYP/6-31G(d,p) data. This data set has allowed for the derivation of correction factors for each of the parameters affecting the rate coefficient (*Vereecken and Peeters, 2010*). Rate coefficients at 298 K predicted in this way are listed in Table IX.

Table IX Predicted rate coefficients for alkoxy radical isomerisation (s⁻¹) at 298K as a function of migration span (1,4- to 1,8-Hshifts), degree of migration H (primary to tertiary), and nature of substitution. The correction factors used here are estimated directly from the quantum chemical data.

Substitution	Span	primary H	secondary H	tertiary H
alkyl only	1,4	2.1×10 ⁻²	0.23	0.82
	1,5	3.2×10 ⁵	3.3×10 ⁶	1.1×10 ⁷
	1,6	6.0×10 ⁴	5.7×10 ⁵	2.0×10 ⁶
	1,7	6.7×10 ²	6.7×10 ³	2.4×10 ⁴
	1,8	21	2.3×10 ²	8.5×10 ²
acyloxy	1,5	9.3×10 ³	3.1×10 ⁴	1.1×10 ⁵
	1,6	7.9×10 ³	5.1×10 ³	1.9×10 ⁴
aldehyde H	1,5	–	–	1.3×10 ⁷
	1,6	–	–	5.9×10 ⁵
	1,7	–	–	3.0×10 ⁴
endo-β-oxo	1,5	2.0×10 ²	1.5×10 ⁴	5.3×10 ⁴
	1,6	1.5×10 ³	3.0×10 ⁴	1.1×10 ⁵
generic endo-oxo	1,5	2.4×10 ⁵	2.5×10 ⁶	8.4×10 ⁶
	1,6	4.4×10 ⁴	4.7×10 ⁵	1.6×10 ⁶
exo-β-oxo	all	same as alkyl-only alkoxy radicals		
generic exo-oxo	all	same as alkyl-only alkoxy radicals		
>C(OH)O•	1,5	9.2×10 ⁵	9.2×10 ⁶	3.0×10 ⁷
α-OH	1,5	–	2.4×10 ⁷	7.5×10 ⁷
	1,6	–	1.8×10 ⁷	5.9×10 ⁷
endo-β-OH	1,5	7.3×10 ⁴	7.8×10 ⁵	2.7×10 ⁶
	1,6	7.0×10 ⁴	6.7×10 ⁵	2.3×10 ⁶
exo-β-OH	1,5	–	5.1×10 ⁶	1.7×10 ⁷
	1,6	–	1.3×10 ⁶	4.5×10 ⁶
generic endo-OH	1,5	same as alkyl-only alkoxy radicals		

In future work, it is intended to use a similar approach to develop a comprehensive SAR for H-migrations in alkylperoxy radicals. This work was prompted by our theoretical finding that H-migrations in the hydroxy-alkenylperoxy radicals from isoprene may be responsible for OH regeneration observed in pristine environments (see II.5.3, below). For

H-shifts in alkylperoxys, in addition to the effects mentioned above for alkoxy, additional factors need to be considered, accounting for the strong difference in reaction enthalpy (which affects both barrier height and tunneling), as well as the presence of an additional –O– group in the TS ring. Preliminary results suggest that isomerisation of some alkylperoxy radical types by H-shifts could be competitive against the traditional bimolecular reactions with HO₂ and NO at lower NO_x levels.

II.2.3 H-abstraction from substituted hydrocarbons by OH-radicals

The site-specific rate of H-abstraction by an OH-radical from substituted hydrocarbons correlates well with the bond strength of the C–H bond under investigation. We proposed to make a predictive SAR based on this correlation, using an extensive set of bond strength data obtained from a large set of quantum chemical calculations at the B3LYP-DFT and MPW1B95 levels of theory, using the 6-31G(d,p) and cc-pVTZ basis sets. The study covers all conformers of over 20 substituted alkanes, and all alkyl radicals potentially formed from these alkanes by H-abstraction. A minimal subset of these data (learning set) was then combined with experimental overall rate coefficients to derive Structure-Activity Relationships, based on several SAR models including linear, quadratic, exponential, and multifunctional models. These models predict the site-specific rate coefficient of H-abstraction by OH-radicals, and are verified against the complete set of data (test set).

The H-abstraction SAR is the first project in our research group based predominantly on the "Science project" software framework to manage the large amounts of data generated in the quantum chemical calculations, and their subsequent verification and incorporation in the SAR. This framework has been partly developed in the frame of IBOOT, and has reached a sufficient level of maturity to be used in a well-controlled production environment. The set of quantum chemical calculations for the SAR are available on our website http://arrhenius.chem.kuleuven.be/~luc/sar_habstr, currently listing over 20 alkanes and about 50 distinct H-abstraction products, with hundreds of conformers, using B3LYP/6-31G(d,p), B3LYP/cc-pVTZ, MPW1B95/6-31+G(d,p) and MPW1B95/cc-pVTZ levels of theory. These data are fitted to several SAR models, including linear, quadratic, and exponential models, as well as combination models. The statistical analysis of these fits is also published on the website. The MCM Review panel has provided us with an updated extensive list of available experimental data on VOC+OH-reaction for use in this task.

A study on the stability of α -nitroxy substituted alkyl radicals ($>C^{\bullet}ONO_2$) was published (Vereecken, 2008) as a spin-off of our research on H-abstraction in nitrates, formed abundantly in the tropospheric oxidation of hydrocarbons in polluted air.

II.2.4 Site-specific addition of OH radicals on substituted (poly)alkenes

An extensive set of experimental kinetic data is available for the addition of OH radicals on substituted alkenes, polyalkenes, and conjugated alkenes. Statistically examining the latest kinetic data recommendations allows for the derivation of a site-specific addition SAR, based on hypotheses compatible with the mechanistic knowledge as obtained from high-level theoretical work, and provided higher-order corrections are made for e.g. H-abstraction contributions and ring strain. The SAR developed is based on the verified hypothesis that the site-specific rate coefficient can be accurately estimated based on the stability type (primary, secondary, tertiary) of the radical site of the product radical, or based on the type of the multiple delocalization sites in conjugated alkenes (*Peeters et al.*, 1994, 1996)

In recently published work, (*Peeters et al.*, 2007) a SAR for the site-specific OH-addition on (poly)unsaturated hydrocarbons (*Peeters et al.*, 1994 and 1996) was further validated by an extensive statistical analysis of the latest kinetic data recommendation available in the literature. Statistical analyses of preliminary higher-order SAR expressions, e.g. accounting for H-abstraction contributions, were used to identify the source of the residual errors, including dependencies on ring strain, competing reaction channels, and the presence of conjugated π -systems or other functionalities. In addition, the hypotheses underlying the SAR were also compared against the mechanistic knowledge from high-level theoretical work in the literature, which is currently viewed as a double-TS approach. Finally, direct experimental measurements of the site-specificity of the OH-addition were extensively described.

Summarizing, the site-specific rate of addition can be predicted based on the stability type of the radical formed after addition (see Table below); the total rate of addition $k_{\text{tot}} = \sum k_i$ is equal to the sum of addition rates over all addition sites. Isolated double bonds lead to primary, secondary or tertiary product radicals, whereas conjugated double bonds potentially lead to allyl-resonance stabilized product radicals where the rate coefficient $k_{\text{first/second}}$ depends primarily on the first radical site next to the addition site, with an additional effect of the substitution around the second resonance radical site.

Table X: SAR parameters ($10^{-11} \text{ cm}^3 \text{ s}^{-1}$, 298K) for addition of OH on a (poly)alkene

k_{prim}	= 0.43	k_{sec}	= 3.0	k_{tert}	= 5.5
		$k_{\text{sec/prim}}$	= 3.0	$k_{\text{tert/prim}}$	= 5.7
		$k_{\text{sec/sec}}$	= 3.7	$k_{\text{tert/sec}}$	= 8.3
		$k_{\text{sec/tert}}$	= 5.0	$k_{\text{tert/tert}}$	= 9.9

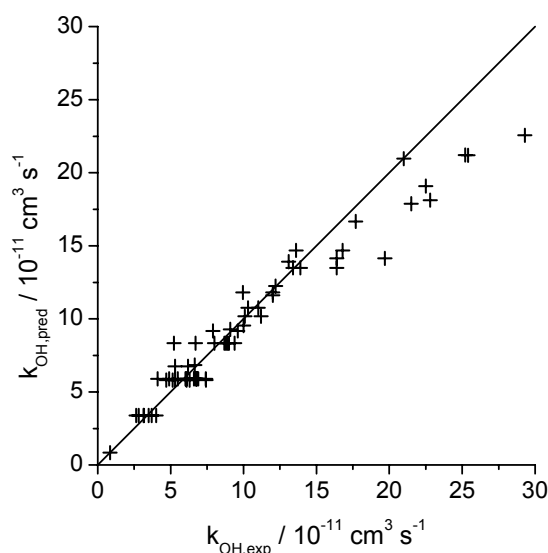


Figure 17: Comparison between SAR predictions and experimental total rate coefficients.

II.3 Development of oxidation mechanisms

The degradation of large biogenic hydrocarbons in the atmosphere is a key element in understanding the air quality, including the formation of SOA, smog and other photochemical pollutants. While the main degradation pathways are known, knowledge on the detailed degradation mechanisms or the product yields is tentative at best for most of the compounds emitted in the troposphere. In this section, we explore in great detail the oxidation mechanisms of a few typical BVOC, each representative of a specific class of compounds. α -pinene and β -pinene are prime contributors to the terpenes, with endo- and exo-cyclic double bonds, respectively. β -Caryophyllene is a representative of the highly reactive sesquiterpenes, a class of hydrocarbons with large emission strength but whose chemistry is largely unknown. The degradation mechanisms below show distinct chemistry, hitherto not examined in BVOC degradation but shown to be important, and as such the work in this section will serve as template studies for the development of degradation mechanisms for a wide range of compounds.

II.3.1 OH-initiated oxidation of β -pinene

The OH-initiated degradation mechanism for β -pinene was investigated using a combination of SAR-predictions, quantum chemical calculations, multi-conformer TST, and chemical activation estimates. A wide range of reaction conditions is examined, from NO_x-rich polluted environments to pristine environments, as well as the high concentrations for NO/HO₂/RO₂ typically found in experiments. The results are incorporated in a generic box model, accounting for variations in the concentrations of

NO_x, HO₂ and different classes of RO₂ radicals, with the aim that all relevant reaction pathways are investigated without devoting too much effort to pathways of lesser importance.

The initial reaction of OH radicals with β-pinene can occur on nine different sites, of which addition onto the exocyclic double bonded carbon is by far the dominant channel. The chemistry following this addition is strongly influenced by the non-traditional chemistry, e.g. (per)oxy radical ring closure (Vereecken and Peeters, 2004; Vereecken et al., 2007), found earlier to also influence the α-pinene degradation. This results in a complex, highly branched mechanism with a large number of competing H-shift and decomposition pathways. We also investigated the product distribution of the most important H-abstraction channel, leading initially to an allyl-resonance stabilized alkyl radical. These two entrance channels investigated account for over 90% of the product formation.

The product distribution predictions of the current generic model indicate good results for e.g. acetone and nopinone yields. Unfortunately, no detailed experimental data is available on the plethora of high-mass poly-substituted oxygenates predicted as the main products, where dozens of different compounds are expected in yields varying strongly on the reaction conditions. Exploratory experiments at NCAR by J. Orlando (personal communication) confirm that the OH-initiated oxidation of β-pinene yields an extraordinary wide range of products, most with low to medium yield. The mechanism for the OH-initiated oxidation of β-pinene is being finalized. Furthermore, one of our co-workers (Luc Vereecken) implemented this mechanism in the Master Chemical Mechanism (MCM) during a six-month stay at the University of Leeds, UK (October 2009-March 2010).

II.3.2 Specific pathways in the ozonolysis of α-pinene

The initial steps of this major process have been investigated theoretically in detail, using the B3LYP/6-311++G(3df,3pd) // B3LYP/6-311G(d,p) level of theory, complemented by TST and RRKM-Master Equation (ME) statistical-kinetics approaches. The computed barriers for the initial O₃-addition to form the trans- and cis-ozonides, of 1 and 2 kcal/mol, are in line with the experimental Arrhenius activation energy of 1-1.5 kcal/mol; also, the multi-conformer TST-calculated total rate coefficient, $k(T) = 5.6 \times 10^{-24} \times T^{2.9}$ for T = 200-500 K, is in agreement with the experimental data (Khamaganov and Hites, 2001; Atkinson et al., 1982). An important new finding is that the chemically activated trans- and cis-ozonides – which interconvert rapidly over an energy barrier of only 7 kcal/mol – result in four distinct activated Criegee intermediates (CI) (i.e. syn-CI-1, anti-CI-1, syn-CI-2 and anti-CI-2). Due to the high barriers of ca. 37 kcal/mol for the

syn/anti conversions, the interconversion of these chemically activated CI's is orders of magnitude slower than the fast 1,4-H shifts or ring-closures which initiate the hydroperoxide- and ester-channel pathways. For two of these activated CI, the hydroperoxide channel was found to be the dominant exit route by far, resulting in a predicted OH radical production of over 60%, consistent with experimental data.

The work on SOA formation in α -pinene oxidation (see Section II.4) incorporates a mechanism for α -pinene ozonolysis which still lacks (theoretically) confirmed routes for the formation of pinic acid as well as peroxy-pinic acid and hydroxy-pinonic acid. Note that we have shown that the proposed gas-phase formation routes for pinic acid are not viable, as crucial steps are completely outrun by competing channels (Peeters *et al.*, 2001; Capouet *et al.*, 2008; Vereecken and Peeters, 2009). Novel pathways that held promise for formation of these acids have been extensively explored theoretically, such as non-traditional peroxy radical reactions, akin to those already shown to be important in the OH-initiated oxidation of α -pinene, as well as some steps competing with the traditional hydroperoxide and ester channels of the Criegee Intermediates.

To that end, several of the isomerization/dissociation routes of the above-mentioned activated CI and of the dioxirane and bis-oxy radical intermediates have been investigated in detail. Contrary to the β -caryophyllene case, unimolecular formation of secondary ozonide from the Criegee Intermediates (featuring a -CHO functionality) is shown to be negligibly slow for α -pinene. Several novel pathways of intermediates involving H-shifts have been characterized; some may be of importance for the production of low-volatility SOA-precursors in near-pristine atmospheric conditions. However, despite close examination of many potential routes, an efficient pathway for pinic acid formation — in conditions of realistic, low peroxy radical concentrations — could not be identified so far; yet, some possible routes are still under investigation. On the other hand, a novel unimolecular reaction of an O₂-adduct of the oxo-alkyl co-product radical (with OH) from the hydroperoxide channel of one CI is predicted to be sufficiently fast to outrun the usual bimolecular reactions and to result efficiently in a number of highly oxygenated final products, including peroxy-pinic acid.

II.3.3 O₃-initiated oxidation of β -pinene

The ozone-initiated degradation of β -pinene were investigated using quantum chemical calculations at the B3LYP-DFT, MPW1B95, CBS-QB3, and CASPT2 levels of theory, combined with RRKM-master equation analysis studying the competition between the different product channels accessible to chemically activated intermediates, and collisional energy loss in those intermediates.

The initial O₃ attack on the endocyclic double bond proceeds predominantly on the anti side relative to the >C(CH₃)₂ bridge, and the TST-calculated rate coefficient shows a slight positive temperature dependence: $k(T) = 1.27 \times 10^{-22} T^{2.64} \exp(-714K/T) \text{ cm}^3 \text{ molecule}^{-1} \text{ s}^{-1}$. Note that here also, we newly identified two distinct conformers of the major initial CI, which cannot be interconverted, and give rise to different chemistries (see Figure 18).

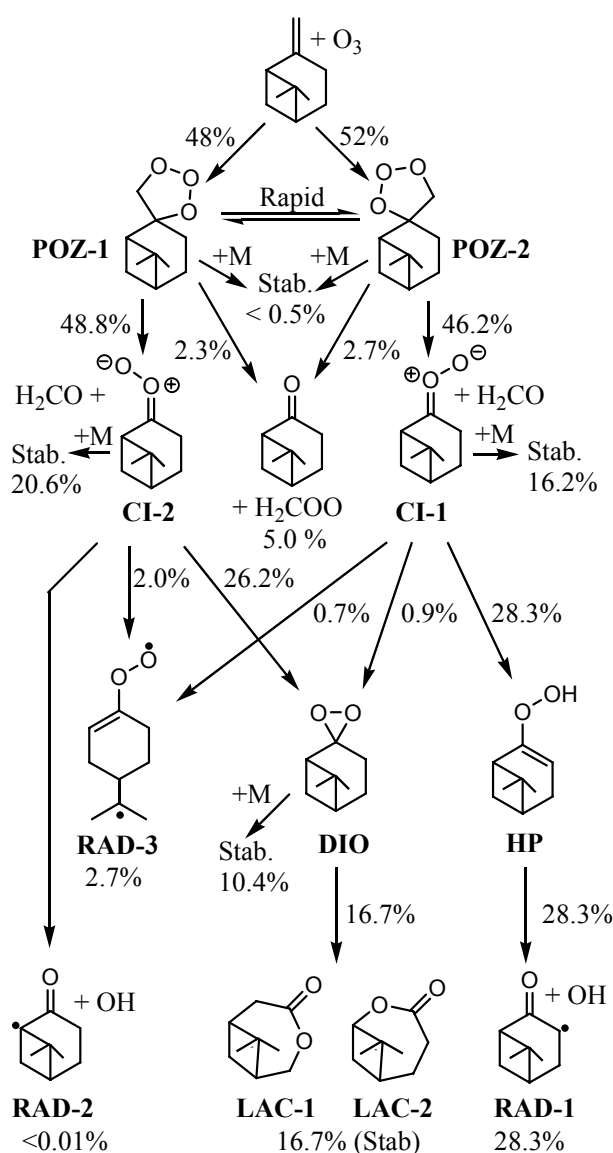


Figure 18: Schematic β-pinene ozonolysis mechanism and first generation oxidation product distribution. Branching ratios and product yields are given as absolute percentages.

Table XI: Predicted first-generation oxidation product branching ratios (%) of the β -pinene ozonolysis at 1 atm and 298K and comparison to selected literature data.

Product	This work	Zhang and Zhang, 2005	Winterhalter et al., 2000	Ma and Marston, 2008
Stabilized POZ	≤ 0.5 %			
Nopinone	5 % ^a	8 %	16 ± 4 %	16 ± 3 %
Stabilized CI	37 %	22 %	35 ± 5 %	> 21 %
CO ₂ (stab. DIO)	10 %		16 ± 5 %	} < 34 %
Lactones	17 % ^b	9 %		
OH + RAD-1/2	28 % (44 % ^c)	61 %	33 ± 5 %	30 %
RAD-3	2.7 %			

^a 10% additional nopinone likely from the stabilized CI-2 (see text)

^b Assuming 100 % CO₂ formation from stabilized dioxiranes, and 100 % lactone formation from chemically activated dioxiranes.

^c Assuming all stabilized CI-1 (16 %) decomposes thermally into OH + RAD-1.

^d Including aerosol phase.

The predicted first generation product distribution for atmospheric conditions is consistent with the available experimental data. Our results predict 5% of nopinone formation, 37% of stabilized Criegee intermediates (SCI), 17% lactones, 10% CO₂ formed after an intersystem crossing, 28% OH radicals with 2-oxo-alkyl radical coproducts, and 3% of a newly proposed biradical formed from prompt ring opening in the CI. In atmospheric conditions, additional OH production is expected from the stabilized CI-1 via the thermal unimolecular "hydroperoxide channel", whereas the other stabilized CI-2 can react with H₂O and its dimer to produce additional nopinone, bringing the theoretical predictions in line with experimental product determinations in air at 1 atm. Expected subsequent chemistries of the large coproduct radicals from reactions of the two CI have also been proposed. A paper detailing this research was recently published (Nguyen et al., 2009a).

II.3.4 O₃-initiated oxidation of β -caryophyllene

The O₃-initiated oxidation of β -caryophyllene was theoretically characterized for the first time using DFT quantum chemical calculations combined with statistical kinetic RRKM/Master Equation analysis and variational transition state theory. O₃-addition was found to occur primarily, $>95\%$, on the endocyclic double bond without a barrier, leading to a total rate coefficient of $8.3 \times 10^{-24} T^{3.05} \exp(1028K/T) \text{ cm}^3 \text{ molecule}^{-1} \text{ s}^{-1}$, with

a slight negative T-dependence. Thermal and chemically activated unimolecular reactions of the initially formed activated primary ozonides (POZ) and of the subsequent activated Criegee Intermediates (CI), including the so-called ester and hydroperoxide channels, as well as internal formation of the secondary ozonide, were characterized and quantified; a newly discovered reaction pathway through intersystem crossing from a dioxirane to a triplet bis(oxy) biradical intermediate is also incorporated in the mechanism. The first-generation product distribution at 298 K is predicted as 74% stabilized Criegee Intermediates (SCI), 8% OH• radicals together with vinoxy-type 2-oxo-alkyl radical co-products, 8% acids, 0.3% esters, and 9% CO₂ with two alkyl radical co-products. The thermalized CI can convert to the secondary ozonide in many reaction conditions, in particular the atmosphere; secondary ozonides are thus expected as dominant products of the β-caryophyllene ozonolysis.

These results are consistent with the experimental data obtained at MPI-Mainz and presented in Section II.1.1.2 of this report. The high molecular weight oxygenated products, including β-caryophyllonic acid and secondary ozonides, are expected to contribute to secondary organic aerosol formation. A manuscript detailing this research, and discussing also the temperature dependence and uncertainties of the product distribution, was recently published (*Nguyen et al., 2009b*) together with its experimental companion article (*Winterhalter et al., 2009*).

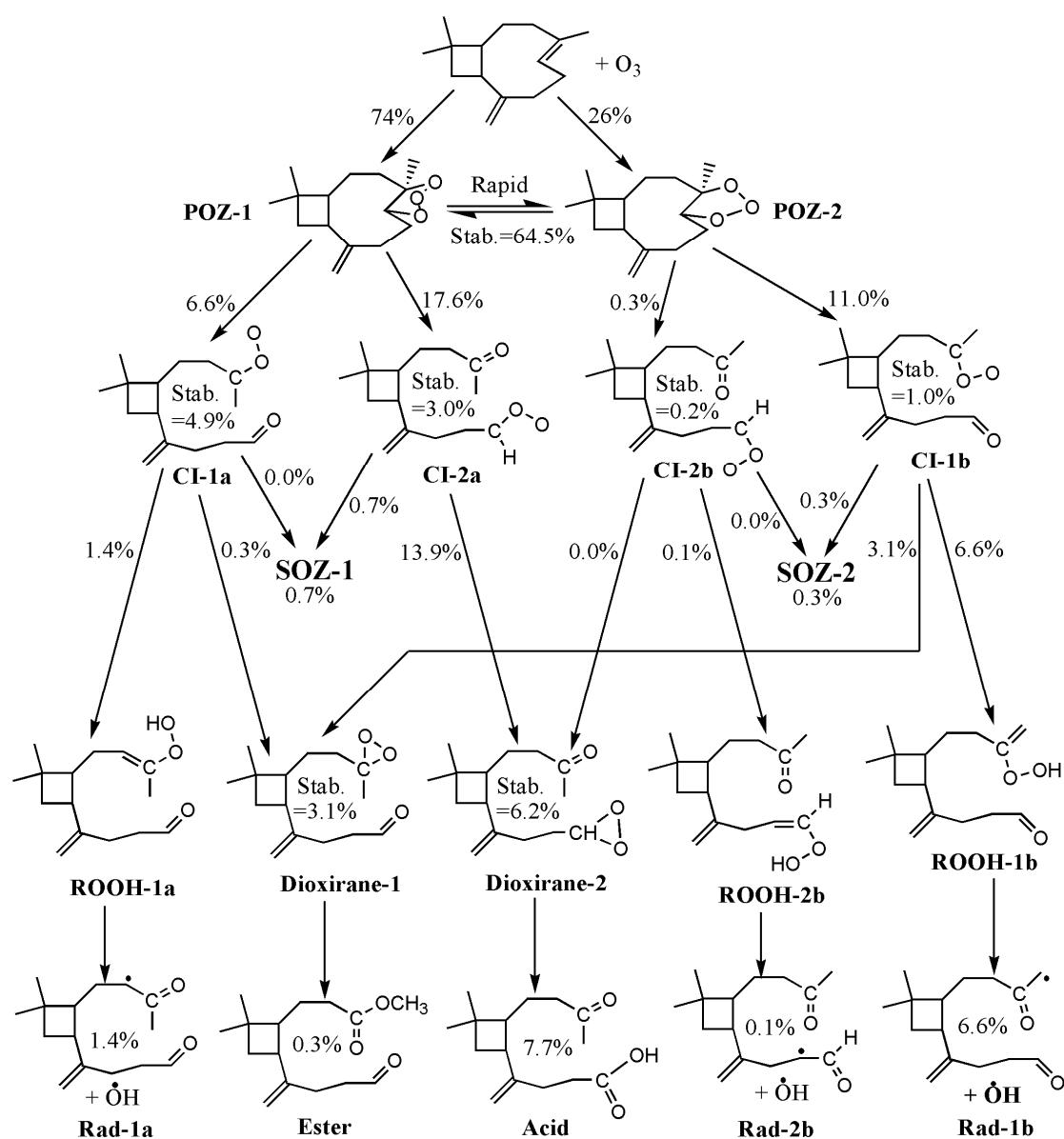


Figure 19: Schematic β -caryophyllene ozonolysis mechanism and first-generation oxidation product distribution. 'Stab' indicates the yield of collisionally stabilized intermediates. All branching ratios and product yields are absolute percentages.

II.4 Model simulations of terpene oxidation experiments

II.4.1 Gas phase mechanism

A near-explicit chemical box model has been developed for the oxidation of α -pinene by OH-radicals, ozone and NO_3 -radicals, as described in Capouet *et al.* (2004, 2008). It is based on advanced quantum calculations for the first reaction steps, on Structure Activity Relationships (SARs), and on available experimental results. As explained in Capouet *et al.* (2008), credible pathways are lacking for the production of low-volatility acids from the ozonolysis mechanism. Since these acids are known from experiments to

be produced in significant amounts (Yu *et al.*, 1999), we included an additional pathway to the ozonolysis mechanism, which leads to pinic acid (5% yield), pinalic acid and hydroxypinonic acid. Note however, that these yields might be dependent on photochemical conditions.

A fully explicit terpene oxidation mechanism is out of reach with the current capabilities since the number of reactions which would be required for the explicit oxidation mechanism of a C10 alkene would be prohibitively large (Aumont *et al.*, 2005). In our mechanism, high-yield compounds are treated explicitly, whereas the degradation of minor products (with yields < 5%) is assumed to generate generic and semi-generic radicals (Capouet *et al.*, 2008). The so-called *semi-generic compounds* are lumped species for which the carbon number and all the present chemical functionalities are known. The (fully) *generic compounds* are species classes for which the carbon number and only one functional group are specified. Since the explicit species represented by these generic species might contain other functional groups, volatility classes have been introduced to account for the effect of these functionalities on the vapor pressures. Eleven volatility classes are currently used. The generic chemistry is based on recent SARs for the OH-reaction rates. Photolysis rates are estimated by treating separately the different functionalities of the molecule, except for keto-nitrates and keto-aldehydes for which experimental data are available. We refer to Capouet *et al.* (2008) for more details.

Compared to Capouet *et al.*'s version of the model, the chemistry of generic alkoxy-radicals has been extended. They undergo (i) reaction with O₂ leading to a carbonyl and HO₂, (ii) decomposition into radicals leading to more volatile species, (3) isomerization leading to less volatile compounds. Since their precise structure is unknown, the channel ratios are obtained by averaging the channel ratios for explicit alkoxy radical in our mechanism. Thanks to these additions, the carbon balance is now preserved in the reactions of generic species.

The α -pinene degradation mechanism has been published in a user-friendly web page (<http://www.aeronomie.be/tropo/boream/>). The coupled model, BOREAM (Biogenic compounds Oxidation and RElated Aerosol formation Model), includes more than 10000 reactions and 2500 species, including the gas/particle partitioning reactions.

II.4.2 Oligomerization reactions

Recent work indicates that the oligomerization of α -pinene products can result in the formation of large, very condensable molecules. We investigated the possible impact of two such processes.

The reversible formation of peroxyhemiacetal from the reaction of aldehydes with hydroperoxides ($\text{ROOH} + \text{R}'\text{CHO} \rightarrow \text{ROOC}(\text{OH})\text{R}'\text{H}$) has been considered by Tobias

and Ziemann (2000) to explain formation of peroxides in the aerosol and was investigated by Antonovskii and Terent'ev (1967). We use forward and backward rate constants based on these experiments, although the nature of the solvent and the precise structure of the reactants could influence these rates significantly.

$$k_{fwd} = 42500 \cdot \exp(-4000/T) [M^{-1}s^{-1}] \quad (\text{Eq. 2})$$

$$k_{back} = 2600 \cdot \exp(-5000/T) [s^{-1}] \quad (\text{Eq. 3})$$

Based on reaction rate measurements by Tobias and Ziemann (2001), we included the gas-phase reactions of the Stabilized Criegee Intermediates (SCIs) with several acids (pinic, hydroxypinonic, pinalic, pinonic) and with pinonaldehyde. The reaction with 2-butanol is also significant in experiments where this alcohol is used as OH-scavenger. The products of such reactions have been identified by Heaton *et al.* (2007) during monoterpene ozonolysis. Note however, that Nguyen *et al.* (2009a) have shown that the β -pinene SCIs can also undergo unimolecular decomposition, thus competing with the bimolecular reactions.

II.4.3 Gas/particle partitioning model

II.4.3.1 General formulation

The partitioning model follows a kinetic approach, which at the equilibrium limit transforms to the formulation of Pankow (1994):

$$\frac{C_{p,i}}{C_{g,i}} = K_{p,i} M_0 \quad (\text{Eq. 4})$$

$$K_{p,i} = \frac{RT}{MW_{om} \gamma_i p_i^0} \quad (\text{Eq. 5})$$

with $C_{p,i}$, $C_{g,i}$, the equilibrium amount of species i per volume of air in aerosol phase and gas phase respectively, $K_{p,i}$ the partitioning coefficient, M_0 the aerosol mass per volume of air, MW_{om} the mean molecular mass in the aerosol, T the temperature, p_i^0 the vapor pressure and γ_i the activity coefficient.

II.4.3.2 Activity coefficients

Since the aerosol is a complex mixture, the interactions between the molecules are not the same as in a pure liquid, and the activity coefficient differs from unity. As opposed to the vapor pressure, it depends on the concentration of all other species. We adopted the popular UNIFAC method (UNiversal Functional group Activity Coefficient, Fredenslund *et al.*, 1975) which approximates the liquid phase as a mixture of

functional groups. The activity coefficient is decomposed into a combinatorial part γ_i^C and a residual part γ_i^R :

$$\ln \gamma_i = \ln \gamma_i^C + \ln \gamma_i^R \quad (\text{Eq. 6})$$

As most condensable oxidation products in BOREAM have roughly the same size, the impact of the combinatorial part, taking into account the size differences, is relatively unimportant, except for the small H₂O molecule. The residual part takes the difference of interaction between molecules into account and is the most important part of the activity coefficient. It is determined by group-group interaction parameters. Interaction parameters for several functional groups of atmospheric relevance, such as nitrates or hydroperoxides, are either not known or not public. Therefore, we utilized the on-line SPARC calculator (<http://ibmlc2.chem.uga.edu/sparc/>, Hilal et al., 2004) to generate activity coefficients to which we fitted the unknown interaction parameters. In SPARC, interactions between molecules are expressed in terms of molecular descriptors (molar volume, polarizability, dipole moment), which in turn are calculated from molecular structure.

Having obtained these parameters, UNIFAC has been successfully implemented in our model. At the moment, five different parameterizations are included (Hansen et al., 1991; Magnussen et al., 1981, Ming and Russell, 2002, Peng et al., 2001; Raatikainen and Laaksonen, 2005). As the parameterization of Raatikainen and Laaksonen (2005) (UNIFAC-Raatikainen) is fitted to polyfunctional compounds, we normally use this method for our simulations.

In a recent publication (Compernelle et al., 2009), we investigated the impact of the activity coefficients on SOA yields in simulated smog chamber. The main conclusions are

- For dry, high-VOC experiments, the activity coefficient has a negligible impact.
- For dry, low-VOC ozonolysis experiments, UNIFAC-Raatikainen predicts a higher yield compared to the ideal case (see Figure 20).
- The activity coefficient has an important impact on water uptake. It generally lowers the water uptake, and as a consequence lowers the SOA yield (see Figure 20).

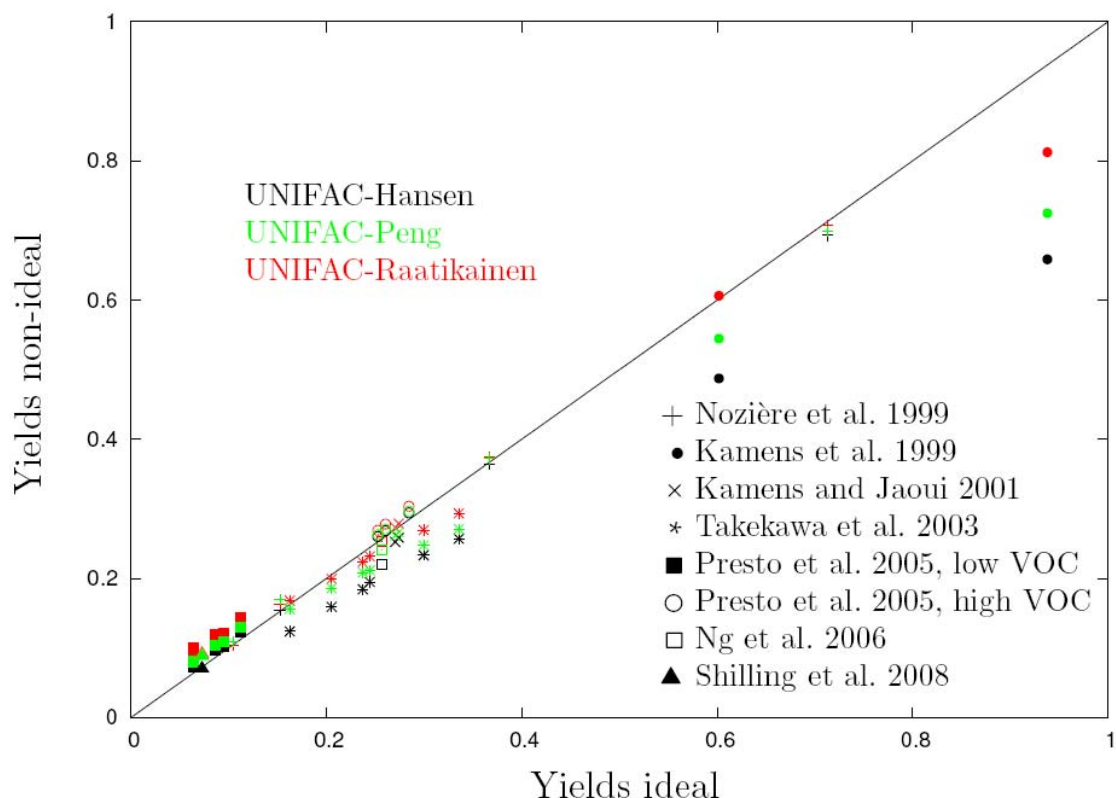


Figure 20. Simulated SOA yields in several smog chamber experiments, with inclusion of non-ideality, vs. yields where ideality is assumed.

II.4.3.3 Vapor pressures

The vapor pressure is the most important single-molecule property determining partitioning to the aerosol phase. This quantity varies over many orders of magnitude and hence SOA yield depends much on the vapor pressure values. As no experimental vapor pressure is available for the large majority of condensable species in our BOREAM model, an estimation method is required.

Up to now, vapor pressures of explicit molecules in BOREAM were calculated by the group contribution method of *Capouet and Müller (2006) (CM)*

$$\log_{10}(p^0) = \log_{10}(p_{\text{hc}}^0) + \sum_k v_k \tau_k \quad (\text{Eq. 7})$$

with p^0 the estimated saturation vapor pressure, p_{hc}^0 the vapor pressure of the parent hydrocarbon, and τ_k contributions due to functional groups (carbonyl, hydroxyl,...). The parent hydrocarbon of a molecule is obtained by removing all non-carbon atoms and adjusting with the appropriate amount of H atoms. p_{hc}^0 is either known experimentally, or it can be estimated with relatively good accuracy by existing estimation methods. The τ_k group contributions are fitted to experimental data.

The CM method is simple to implement and use, but the parameters were fitted to a relatively small set of molecules. Also, the contributions of the functional groups are assumed to be independent of their environment (i.e. no second order groups) and the contributions are assumed to be additive to $\log_{10}(p)$. This last assumption breaks down especially for hydrogen-bonding groups.

Therefore, we assembled vapor pressure data from 788 compounds, of which 130 hydrocarbons, 438 monofunctional and 220 polyfunctional. Based on these data, we developed a new method, called EVAPORISATION, which stands for Estimation of VAPOR Pressure of Organics, Including effects Such As The Interaction of Neighbours. The method is applicable to ether, peroxide, nitrate, carbonyl, ester, peroxy acyl nitrate, alcohol, acid, hydroperoxide and peracid species. To describe the temperature-dependence, following empirical formula was employed:

$$\log_{10} \frac{p^0}{\text{Torr}} = A + \frac{B}{T^{1.5}} \quad (\text{Eq. 8})$$

For $\log_{10} p^0$, additivity of functional groups fails, especially for hydrogen bonding groups. This is incorporated in EVAPORISATION by making A nonadditive for carbonyl-like and hydrogen bonding functional groups, while B stays additive.

$$A = A_{\text{lin}} + A_{\text{CO}} + A_{\text{HB}} \quad (\text{Eq. 9})$$

$$A_{\text{lin}} = \sum_{k \in \text{lin}} c_k a_k, A_{\text{CO}} = \sum_{k \in \text{CO}} \frac{c_k a_k}{\sqrt{N_{\text{CO}}}}, A_{\text{HB}} = \sum_{k \in \text{HB}} \frac{c_k a_k}{\sqrt{N_{\text{HB}}}}$$

where CO stands for carbonyl-like groups (carbonyls, esters, peroxy acyl nitrates), HB for hydrogen bonding groups, and lin for the additive groups (carbon, ether, peroxide, nitrate). k runs over descriptors describing the carbon skeleton, functional groups and some second order effects –including local group-group interactions– that modify the functional group contributions: e.g. the conjugation of a carbonyl with a double bond, and the intramolecular bonding of an alcohol with a neighbouring functional group. The nonadditivity for A has a physical ground: A is closely related to the entropy of boiling, and the ordering of the liquid increases less than linear with the number of strongly polar groups. The result is that polyfunctional molecules with polar groups tend to have a lower vapor pressure than predicted by a simple group contribution method.

Recently new vapor pressure data on diacids and functionalized diacids at room temperature became available (e.g. *Booth et al.*, 2010, *Soonsin et al.*, 2010). Unfortunately, there is a considerable inconsistency between data of different research groups. An additional complication is that much of the data is for the solid rather than, as required, for the liquid. Fusion enthalpy and temperature are needed to convert the data to the correct form, but these are not always available. Therefore, we developed a simple method to estimate these quantities (*Compernelle et al.*, 2011).

Despite the uncertainties, one conclusion seems to be that functionalized diacids can have a much higher vapor pressure than expected from a group contribution argument or from the above formulation. Therefore, the following empirical correction is made to the group coefficients of functionalized diacids:

$$c'_k = \frac{c_k}{N_{\text{lin}} + N_{\text{CO}} + N_{\text{HB}}} 2.4 \quad (\text{Eq. 10})$$

The group parameters are obtained by multiple linear regression. In Table XII the performance of the method for the various molecule types is given. In obtaining the predicted residual sum of squares (PRESS) iteratively one molecule is left out of the training set, and its vapor pressure is estimated. The PRESS is a measure of the predictivity of the method.

Table XII: Performance of $\log_{10} \frac{p^0}{\text{Torr}}$ as predicted by EVAPORISATION. Given are the mean absolute error (MAE), the standard deviation (STD) and the predicted residual sum of squares (PRESS).

molecule type	# molecules	MAE	STD	PRESS
hydrocarbons	130	0.09	0.12	0.13
<i>monofunctional</i>				
nitrates	23	0.08	0.12	0.12
carbonyls	128	0.08	0.11	0.12
ethers	52	0.07	0.11	0.11
esters	53	0.05	0.07	0.07
peroxides	11	0.32	0.39	0.41
peroxy acyl nitrates	5	0.10	0.17	0.30
alcohols	120	0.08	0.12	0.12
acids	38	0.09	0.12	0.12
hydroperoxides	4	0.05	0.06	0.10
peracids	4	0.21	0.25	0.35
<i>bifunctional</i>				
dinitrates	10	0.29	0.33	0.36
dicarbonyls	18	0.08	0.10	0.14
diols	32	0.12	0.17	0.18
diacids	31	0.21	0.31	0.33
diethers	16	0.10	0.13	0.13
diesters	13	0.10	0.13	0.14
carbonyl esters	12	0.07	0.09	0.09
carbonyl acids	16	0.25	0.30	0.32
hydroxy ethers	11	0.09	0.11	0.11
hydroxy nitrates	4	0.35	0.42	0.43
hydroxy peroxides	1	0.35	-	-
hydroxy carbonyls	17	0.13	0.18	0.19
hydroxy acids	5	0.13	0.18	0.18
<i>More than 2 functionalities</i>				
at least 2 acids	11	0.59	0.74	0.84
other	5	0.40	0.47	0.81
all	788	0.10	0.15	0.16

The performance of the method for most mono- and bifunctional molecule types is good, and where it is less, this is probably due to the sparseness of experimental and/or the inconsistency between different reference sources. Probably new experimental data

can reduce these errors significantly, by updating the parameters but without having to modify the model framework.

The errors for molecules with more than 2 functionalities are still considerable. Apart from the inaccuracy of experimental data, it is likely that this is also due to the relative simplicity of our model, while the true group interactions will be complex. However, more consistent experimental data are a prerequisite for the development of more detailed models.

We also implemented in BOREAM several vapor pressure methods available in the literature: SIMPOL (*Pankow and Asher, 2008*), SPARC (version 4.2, *Hilal et al., 2003*, <http://ibmlc2.chem.uga.edu/sparc/>), and methods needing a boiling point as input: *Myrdal and Yalkowsky (1997)* (MY), *Nannoolal et al. (2008)* (Nan), and *Moller et al. (2008)* (Mol). As this boiling point is generally not experimentally available, it is calculated by the methods of *Joback and Reid (1987)* (JR), or *Nannoolal et al. (2004)* (Nan). Such a combination of methods we denote here as e.g. MY-JR, or Mol-Nan.

Except for SIMPOL and SPARC, all of the above mentioned methods had to be extended such that hydroperoxides, peracids and peroxy acyl nitrates (shortly called *per*-groups here) could be treated. A study of these methods was done (*Compernelle et al., 2010*) and we showed that some of them (*Joback and Reid, 1987, Moller et al., 2008*) gave anomalous results when applied to polyfunctional molecules.

A comparison was made of our newly developed method EVAPORISATION to these implemented methods. In Figure 21 we chose the popular methods SIMPOL and *Nannoolal et al., 2008*, the last one combined with the boiling point estimation method of *Nannoolal et al., 2004* (Nan-Nan), as well as our CM method.

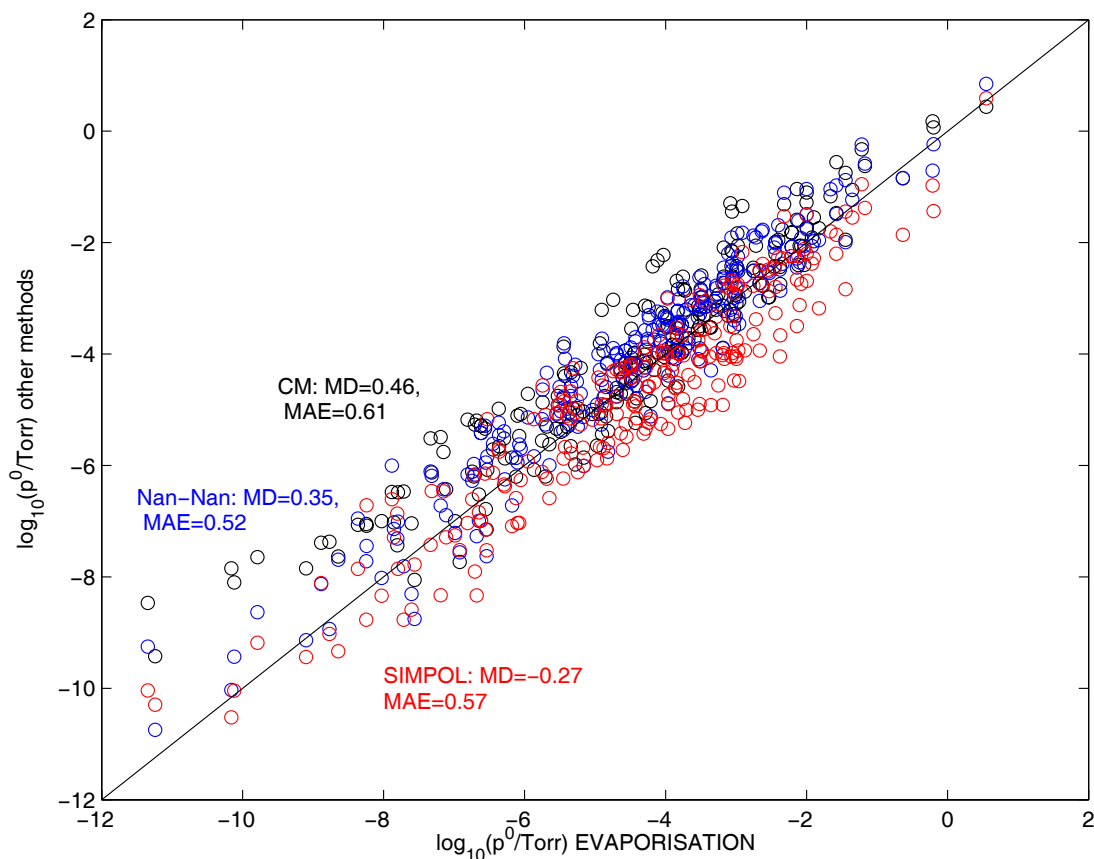


Figure 21. Vapor pressure estimation intercomparison of EVAPORISATION with some other methods.

It turns out that our method predicts on average lower vapor pressures than the CM method. Larger predicted SOA yields can thus be expected after implementation of this method.

II.4.4 Model evaluation against smog chamber experiments

The BOREAM model for has been evaluated against a large number of smog chamber experiments. Three BOREAM versions have been tested:

- BOREAM A which was used in *Capouet et al. (2008)*
- BOREAM B, with updates to the generic chemistry of alkoxy radicals (cf. Section II.4.1), water uptake, and non-ideality (Section II.4.3.2)
- BOREAM C, with a lower pinic acid yield (3% in agreement with *Ma et al. 2007*) and a higher vapor pressure for compounds bearing the peroxy-acyl nitrate group (PAN). This is justified by the large uncertainty of the vapor pressure estimate for such compounds, since the contribution of the PAN functionality to the vapor pressure is based on the experimental vapor pressure of only one compound in *Capouet and Müller (2006)*.

We divide the experiments into two categories: photo-oxidation, where the smog chamber is irradiated with visible or UV light, and dark ozonolysis.

II.4.4.1 Photo-oxidation experiments

The SOA yields of 28 photo-oxidation experiments were simulated. As seen in Figure 22, the modeled yields agree with the observations within a factor of 2 or better in most cases, although large overestimations are noted with version B for experiments by *Nozière et al.* (1999), *Presto et al.* (2005) and *Takekawa et al.* (2003). Large underestimations are also found with version A in the case of high-temperature experiments by *Hoffmann et al.* (1997). Version C provides the best overall agreement, although with significant overestimations, in particular for the low-VOC experiments by

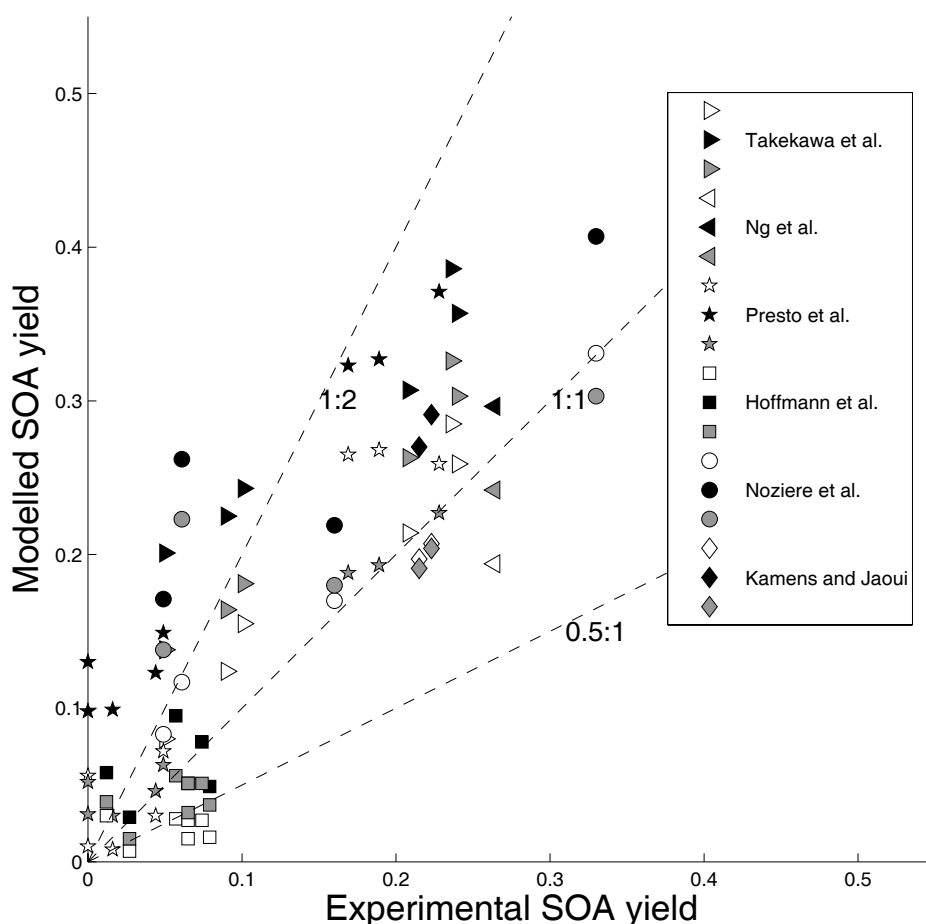


Figure 22 . Modeled versus experimental SOA yields for photo-oxidation experiments. Results are shown for three BOREAM versions: A (white), B (black), and C (grey).

II.4.4.2 Dark ozonolysis experiments

In *Ceulemans et al.* (2010), the yields simulated with BOREAM (version B) are compared with measured yields for more than 100 dark ozonolysis experiments. In most cases, an OH-radical scavenger was used during these experiments. In most cases, the measured SOA yields are reproduced within a factor 2 or less (Figure 23). However, larger discrepancies are also found. In particular, the modeled yields decrease strongly with temperature, in contrast with the weaker temperature dependence exhibited by the observed SOA yields. As a consequence, model overestimations of up to a factor 2 are found at lower temperatures, whereas underestimations by up to an order of magnitude are found at high temperature ($> 40^{\circ}\text{C}$). Similar conclusions regarding the temperature dependence of the yields can be drawn from comparisons with the experiments by *Pathak et al.* (2007) conducted between 0° and 40°C (Figure 24). A quantitative analysis of the biases is given in Table XIII for these experiments.

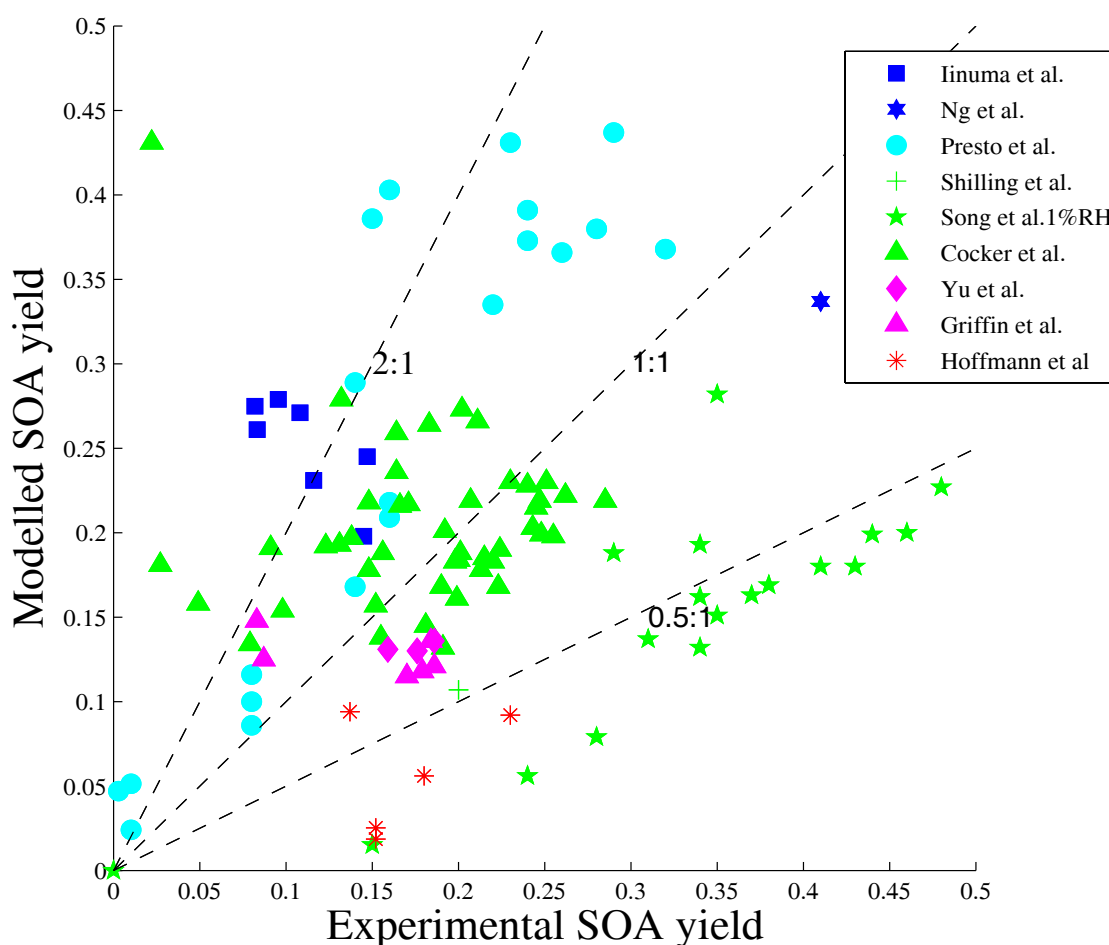


Figure 23. Modeled vs. experimental SOA yields for several dark ozonolysis experiments.

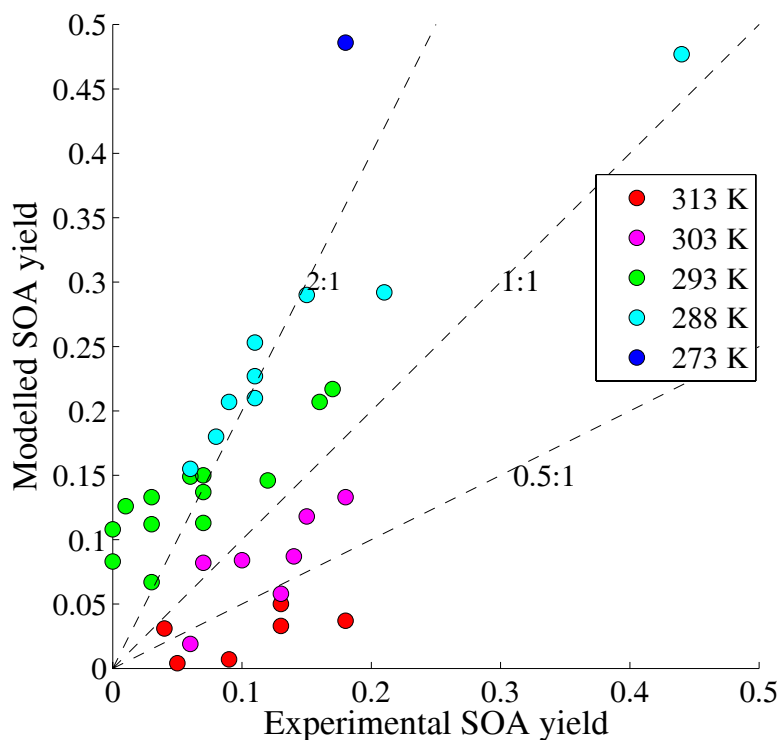


Figure 24. Modeled vs. experimental SOA yields for dark ozonolysis experiments from *Pathak et al.* (2007). BOREAM (version B) was used.

Sensitivity tests were performed to investigate the dependence of SOA yields on several parameters (Table XIII). The formation of oligomer products from the reactions of SCI with carboxylic acids is found to contribute significantly in the case of low yield experiments performed at very low RH. In such cases, the model agreement was improved when these reactions were taken into account. This result should be regarded with caution, since the model does not include the possible thermal hydroperoxide channel of SCI (*Kroll et al.*, 2001).

Table XIII. Geometrically averaged ratios of modeled to observed SOA yields for the *Pathak et al.* (2007) experiments at different temperatures, and for several model sensitivity tests. STD: standard model (BOREAM B); R1: without SCI oligomers; R2: vapor pressure from SIMPOL; R3 vapor pressures from *Myrdal and Yalkowsky* (1997) with *Nannoolal et al.* (2004) boiling point; R4: vapor pressures of *Nannoolal et al.* (2008) with *Nannoolal et al.* (2004) boiling point. R5: ideality assumed. R6: with addition of non-volatile product; R7: modified T-dependence of vapor pressures; R8: combination of R6 and R7.

	STD	R1	R2	R3	R4	R5	R6	R7	R8
273 K	2.1	1.58	2.5	0.82	2.0	2.2	2.17	1.03	1.14
288 K	1.91	1.71	2.9	0.83	1.80	2.3	2.1	1.43	1.61
293 K	1.71	1.60	2.9	0.74	1.66	1.62	2.0	1.48	1.8
303 K	0.65	0.47	1.56	0.19	0.63	0.48	0.97	0.80	1.11
313 K	0.22	0.05	0.67	0.02	0.25	0.15	0.64	0.44	0.90

The vapor pressure estimation is of great importance for SOA yields (tests R2-R4). For example, the use of SIMPOL (test R2) increased SOA yields by up to a factor of three at high temperature, whereas the *Myrdal and Yalkowsky* (1997) method (with *Nannoolal et al.* (2004) boiling point) (test R3) decreased SOA yields by up to an order of magnitude.

The model performance in terms of temperature dependence is improved when formation of additional highly condensable products is assumed (test R6) or when the temperature dependence of vapor pressures is decreased (test R7). It appears possible that species are missing in the model, with formation pathways which could be temperature dependent. Their formation could result from gas-phase, heterogeneous or particle-phase processes. Improvements of the α -pinene SOA model should be aimed at resolving these issues.

II.4.4.3 Comparison with other box model studies

Xia et al. (2008) simulated smog chamber experiments using the MCM mechanism for α -pinene coupled to an aerosol partitioning module (Figure 25). Although a good agreement was found in some cases, severe underestimations were found for many experiments (*Pathak et al.*, 2007; *Takekawa et al.*, 2003; *Presto et al.*, 2005; *Presto and Donahue*, 2006) which reached up to three orders of magnitude, i.e. much more than in the case of BOREAM. Reasons for the different model performance might include differences in the gas phase mechanism and in the estimation of partitioning coefficients.

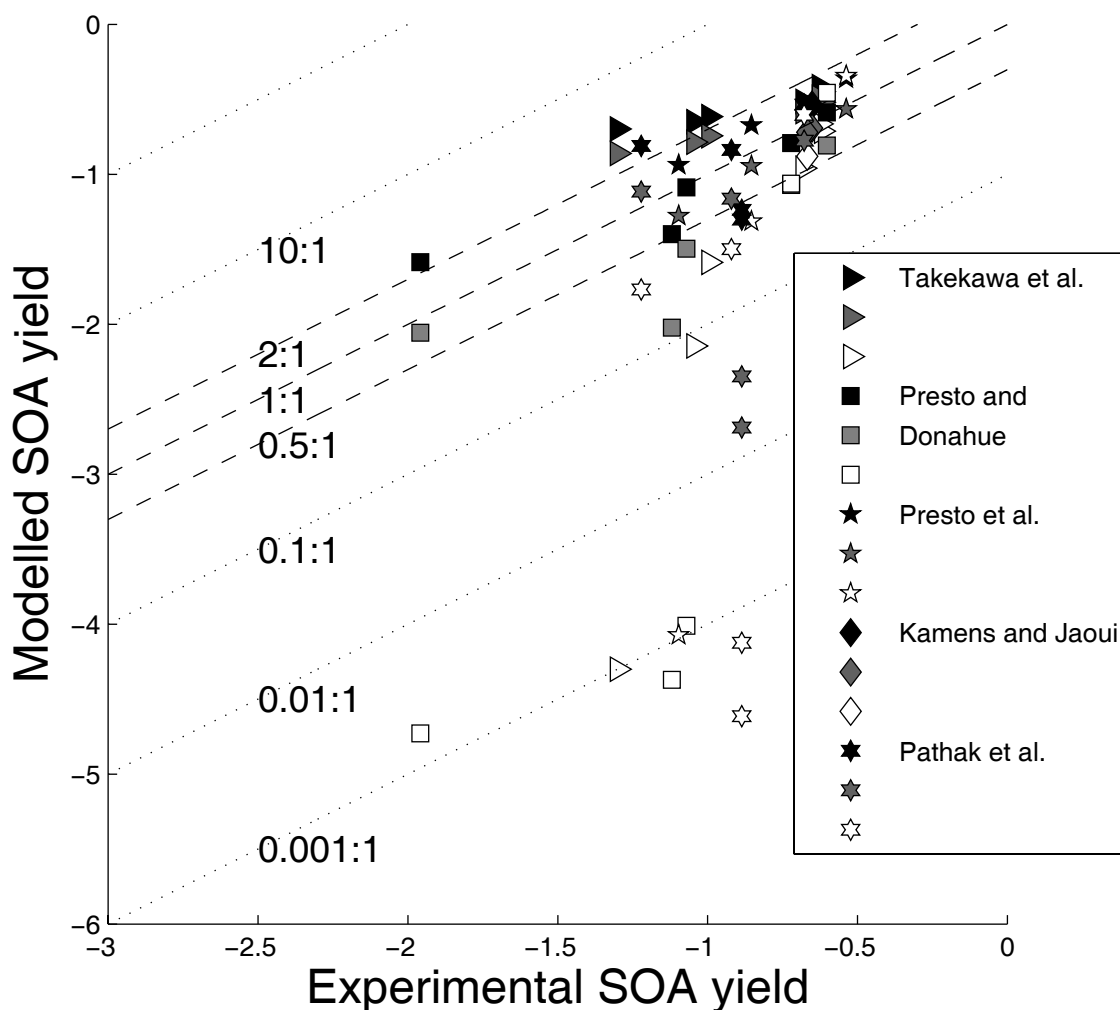


Figure 25. Modeled vs. experimental SOA yields for several smog chamber studies using a log₁₀ scale. Black symbols: BOREAM B; grey symbols: BOREAM C; open (white) symbols: Xia et al. (2008).

II. 5 Atmospheric oxidation of oxygenates.

Isoprene oxidation and its impact on the oxidizing capacity of the atmosphere

The potential energy surface of several reactions of oxygenates with OH and HO₂ radicals, as well as of newly identified crucial reactions of the hydroxy-peroxy radicals from isoprene oxidation, were investigated using many levels of theory, ranging from DFT to high-level CBS-QB3 and CBS-APNO calculations. The results are incorporated in RRKM-Master equation analysis, as well as multi-conformer Transition State Theory and other theoretical kinetic methodologies, in order to obtain temperature-rate coefficients and/or product distributions. For the oxidation of isoprene, with its huge emissions of 500 Tg/yr, the goal was to identify the pathways that result in OH radical regeneration, with considerable impact to the global oxidizing capacity of the troposphere.

II.5.1 Pressure and temperature dependence of reactions of oxygenates with OH

The reactions of oxygenates with OH are characterized by the formation of H-bonded pre-reactive complexes (PRC), affecting the energy of the abstraction transition states (TS); in certain cases this even lowers the abstraction TS to below the energy of the free reactants.

Because of the PRC-"well" between reactants and TS, one can expect here in principle two limiting pressure regimes for the rate coefficient: (i) a low-P regime where there are no stabilized PRC, but only nascent, activated ones, and (ii) a high-P regime where there is a thermal population of stabilized PRC, from the bottom of the well up. Following an analytical, statistical-rate-theory-based approach, supplemented by multi-conformer TST calculations and RRKM-ME analyses (*Peeters and Vereecken, 2006*; a full paper is still in preparation) we showed that two (extreme) cases must be considered, depending on the energy of the abstraction transition states relative to the initial reactants.

- For TS well above the free reactants, a positive T-dependence is expected, without significant P-dependence, i.e. the rate coefficients in the high- and low-P regimes are quasi-equal, and straightforward TST theory is applicable, without any effect of the PRC or its properties. At low temperatures some curvature of the Arrhenius plot can occur due to tunneling through the barrier, this being slightly more important in the high-P regime. A typical example is the reaction of acetone with OH, for which the PRC lies around 4 kcal/mol below but the TS some 3.5 kcal/mol above the reactants. Using our analytical approach, and confirmed by RRKM-ME calculations, we found that from 0 to 1 atm, this process (although formally still in the low-P regime) has a rate near-equal to the TST value (high-P limit), thus confirming an earlier computational study (*Caralp et al., 2006*), who found no pressure dependence up to 1 atm.

- For TS well below the free reactants, the rate is predicted to differ markedly in the low-P and high-P regimes, in particular at lower temperatures. The reason is that collisional stabilization of the PRC alters the competition between redissociation of the PRC and its product-forming reaction in favor of the latter. Further, a negative T-dependence is predicted, due to the energy dependence of the mentioned competition, the negative T-dependence of the initial, barrierless H-bond formation, and to a lesser extent tunneling. A prime example is the reaction of methylhydroperoxide with OH, with the PRC lying 4 kcal/mol and the exit TS's 2 kcal/mol below the reactants, the reaction being at 1 atm in the low-P regime (a paper is in preparation). Other examples include reactions of aldehydes and hydroxyacetone with OH.

- Recently, we showed that an intermediate regime can exist, provided that the barrier height is within a narrow region close to the energy of the free reactants, leading

to a near-T-independence over fairly large T ranges. Experimental work by Crowley et al., in a joint study with us, found glycolaldehyde to exhibit this extraordinary behavior between at least 240K and 360K at pressures near the low-P limit (Karunanandan et al., 2007).

The above first-principle results are compatible with all the available experimental literature data on the OH-initiated oxidation of partially oxygenated hydrocarbons, and represent the culmination of our theoretical work performed in previous years in the UTOPIHAN project and our collaboration with MPI-Mainz (Dr. J. Crowley).

Another major example of an intermediate case is the atmospheric reaction of OH with acetic acid, $\text{CH}_3\text{C}(\text{O})\text{OH}$. In a continued experimental investigation we have complemented the rate coefficient measurements over the 300 - 800 K range (Khamaganov et al., 2006) by branching fraction measurements for the carboxyl-H-abstraction (300 to 500 K range), and by new PLP-LIF determinations of the rate coefficients of both the $\text{OH} + \text{CH}_3\text{C}(\text{O})\text{OH}$ and $\text{CD}_3\text{C}(\text{O})\text{OD}$ reactions over the 295 - 800 K range. The data confirm the gradual transition from a low-T, acidic-H-abstraction mechanism through an H-bonded PRC, showing a negative T-dependence, to (direct) methyl-H abstraction at high T – featuring a pronounced positive T-dependence. Theoretical, QC-based, analytical and RRKM-ME treatments are consistent with these views, showing that the barrier for the major, acid-H abstraction channel is barely submerged (TS only ≈ 0.8 kcal/mol above the reactants) and quite narrow, such that at low T tunneling becomes important and pressure-dependence significant (the reaction at 1 atm being closer to its low-P limit), whereas at $T > 500$ K, the rates in the low-P and high-P regimes are nearly identical. A paper on this subject is still in preparation.

II.5.2 Reactions of carbonyl-bearing compounds with HO_2 -radicals

As a follow-up of our earlier work on the HO_2 -initiated oxidation of formaldehyde and acetone at the low temperatures of the tropopause (Hermans et al., 2004 and 2005), theoretical studies have been conducted on reactions of the HO_2 radical with major dicarbonyl oxidation products of isoprene and terpenes. The rationale is that at these low temperatures the initial α -hydroxy-alkylperoxy adduct is stable enough to undergo subsequent, effective chemical degradation reactions with NO and HO_2 . Present theoretical investigations on glyoxal and methylglyoxal have shown that such HO_2 -initiated oxidation mechanisms can indeed constitute effective sinks for both these dicarbonyls at tropopause temperatures, as well as in high- $[\text{HO}_2]$ laboratory conditions. One key quantity is the energy of the α -hydroxy-alkylperoxy adduct relative to the carbonyl + HO_2 reactants; the *ab initio* computed value for methylglyoxal is consistent with earlier laboratory observations at room temperature (Staffelbach et al., 1995; Tyndall et al., 1995). For glyoxal, we identified also a unimolecular pathway of the

OCH-CH(OH)OO adduct to OH + CO + HC(O)OH; this route could play some role in laboratory experiments on glyoxal involving HO₂. A paper is to be submitted.

In this context, we have also theoretically investigated the subsequent reactions of α -hydroxy-alkylperoxy adducts with HO₂, aiming to rationalize the new findings (Jenkin *et al.*, 2007) that the HOCH₂OO + HO₂ reaction also generates both the OH and HOCH₂O radicals, besides the corresponding hydroperoxide plus O₂ and the acid HC(O)OH + H₂O + O₂. Note that the recent finding of other, non-terminating RO₂ + HO₂ routes besides the "traditional", terminating ROOH-forming channel, has provoked great interest in the atmospheric chemistry community. We have characterized the various reaction channels involved, occurring on the triplet and singlet PES surfaces, both proceeding through H-bonded pre-reactive complexes (PRC). Our theoretical study rationalizes the three observed reaction channels and their branching ratios, but shows the radical channel to yield HC(O)OH + OH + HO₂ instead of HOCH₂O + OH + O₂ as assumed by Jenkin *et al.* (2007). Rate coefficients at 210 K on both the singlet and triplet PES are expected to be capture limited (i.e. formation of the PRC controlling the rate; *k* of order 10⁻¹⁰ cm³ s⁻¹), which should enhance the efficiency of the carbonyl removal initiated by HO₂ near the tropopause at high HO₂ levels. A paper on HOCH₂OO + HO₂ was recently published (Nguyen *et al.*, 2010a).

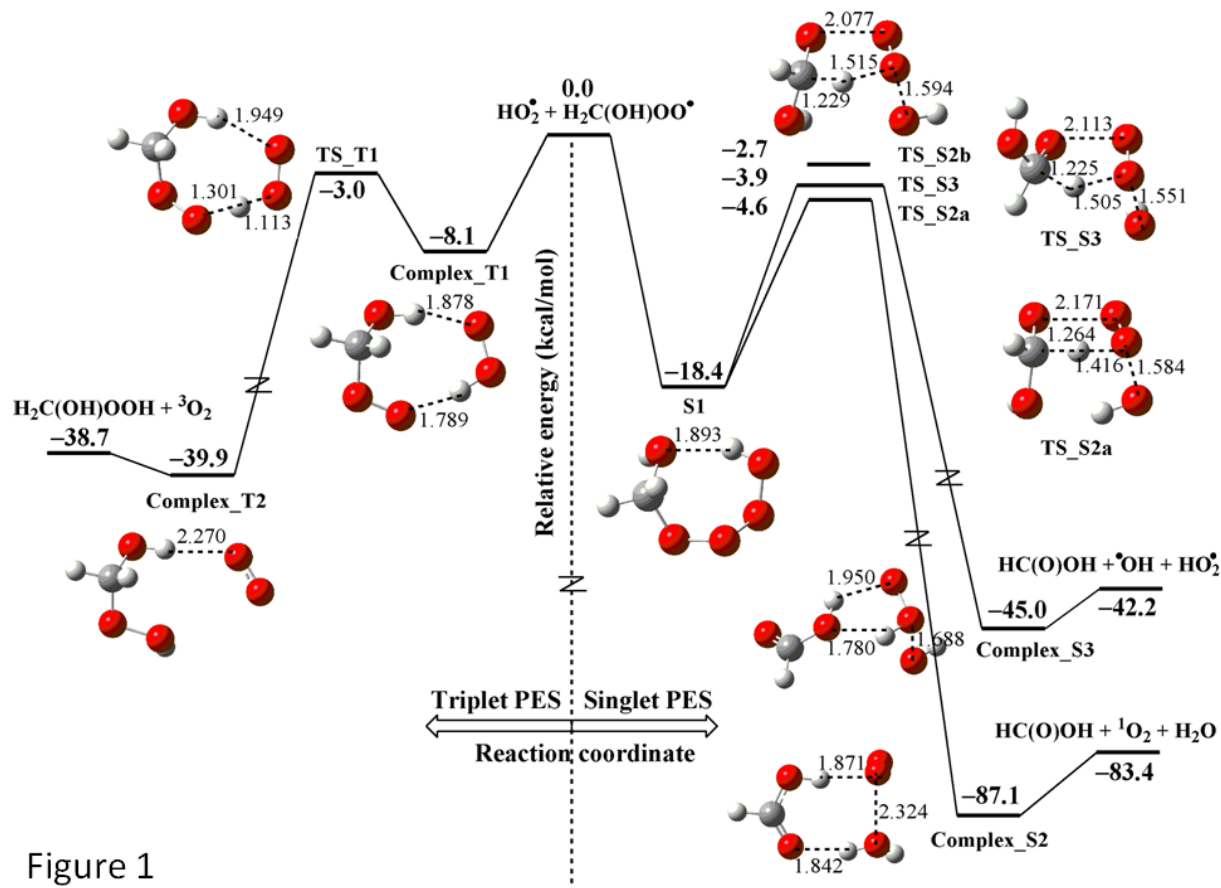


Figure 1

Figure 26. Schematic profile of the lowest-lying triplet and singlet PES for the HO₂ + HOCH₂OO^{*} reaction characterized using various high levels of theory (mainly CBS-APNO). Relative energies, including ZPE, in kcal/mol and bond distances in Angstrom.

II.5.3 HO_x radical regeneration in the oxidation of isoprene

Isoprene, with its huge global emissions of 500 Tg/yr — much of it by tropical forests, has a vast impact on the oxidizing capacity of our atmosphere. Whereas according to currently accepted oxidation mechanisms isoprene should strongly reduce hydroxyl radical levels, several recent campaigns in and around near-pristine forest areas such as the Amazon Basin, have measured unexpectedly high OH concentrations, up to ten times larger than predicted by the models (see among others *Lelieveld et al.*, 2008). Severe underestimations of OH and HO₂ radical concentrations have been also reported over isoprene-rich areas at mid-latitudes, e.g. in the United States and China. In an attempt to explain this, Lelieveld et al. (2008) proposed the artificial production of 2 OH radicals in the reactions of HO₂ with the initial peroxy radicals from isoprene: RO₂ + HO₂ → ROOH + 2OH. However, since then, it was shown that regeneration of OH in the reactions of (similar) hydroxy-peroxy radicals with HO₂ radicals is negligible (*Dillon and Crowley*, 2008, *Dillon et al.*, 2010).

Due to the far-reaching global implications of these unexplained findings, a great part of the IBOOT-effort of KULeuven during 2008-2010 has been re-directed towards unraveling the precise chemical mechanisms by which OH is apparently being (re-)generated in isoprene oxidation.

Bringing to bear theoretical methodologies, including extensive *ab initio* PES computations at the high CBS-APNO level of theory as well as multi-conformer TST, we have been able to put forward and confirm quantitatively four novel types of reactions in isoprene oxidation of key importance at low to moderate NO_x levels (*Peeters et al.*, 2009). The figure below shows the resulting novel "Leuven Isoprene Mechanism" (LIM), with the new reaction steps introduced by us indicated (by arrows) in color.

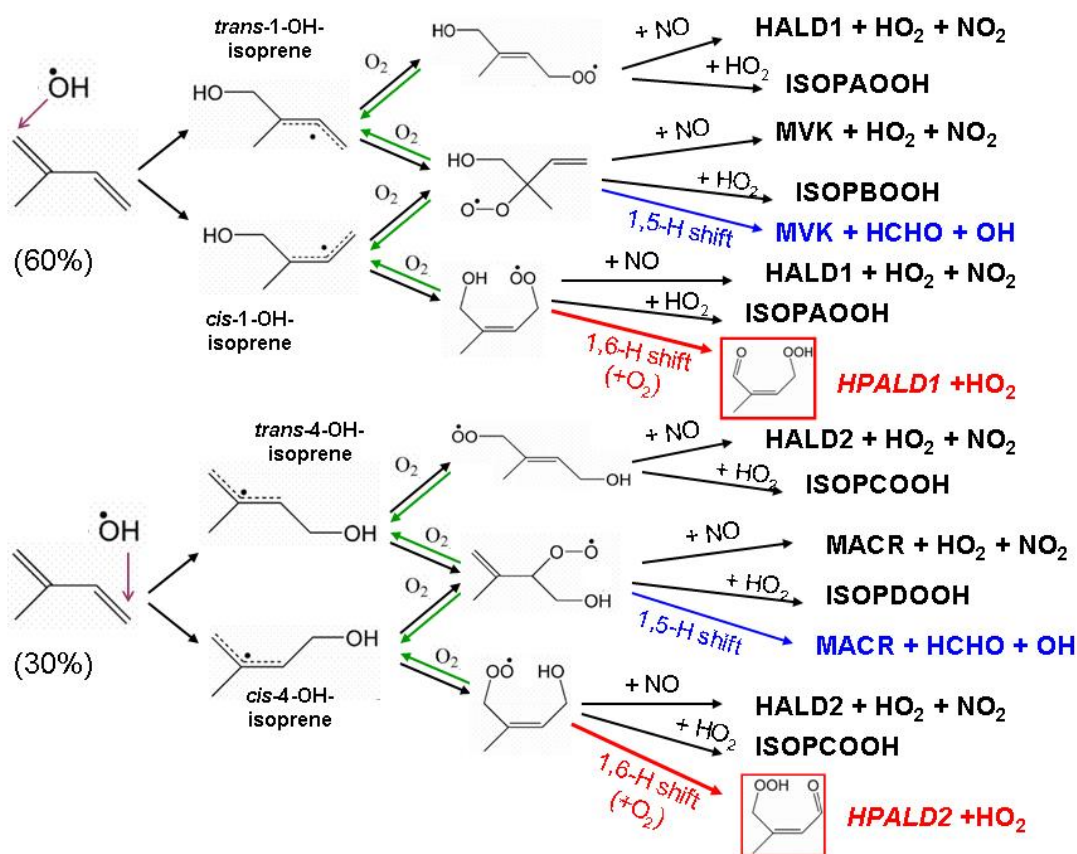
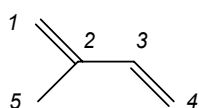


Figure 27. The "Leuven Isoprene Mechanism" (LIM) for isoprene oxidation at low- and moderate NO_x levels. The new reactions are denoted (by arrows) in color. Green: fast re-dissociation of the peroxy radicals to the initial allyl-stabilized OH-adducts. Red: fast isomerisation of the Z-delta-hydroxy-peroxys by 1,6-H shifts to yield photolabile 4-hydroperoxy-methyl-but-2-enals (HPALDs). Blue: slower 1,5-H shifts in the beta-hydroxy-peroxys to yield directly methylvinylketone/methacrolein+ HCHO + OH.

These new reaction steps, detailed below, are all assisted by allyl-resonance stabilisation of the intermediates or product radicals involved, and are therefore specific to a VOC with a C=C-C=C structure. Note also that we have duly considered all relevant isomers and conformers of the initial hydroxy-adducts and of the resulting peroxy radicals.

(i) The major hydroxy-peroxy radicals with O₂ only weakly bonded were found to eliminate O₂ so rapidly that the various isomers/conformers can easily interconvert in low-NO_x conditions to a near-equilibrium population, which allows for the bulk of the total peroxy radical pool to be channeled through the most reactive radical.

(ii) For both the major initial 1-OH-isoprene- and 4-OH-isoprene radicals (see C-atom labeling scheme:),



the most reactive O₂-adduct conformers are shown to be the Z-1-OH-4-peroxy and Z-4-OH-1-peroxy radicals from isoprene (i.e. the Z-delta-OH-peroxys), which undergo a fast

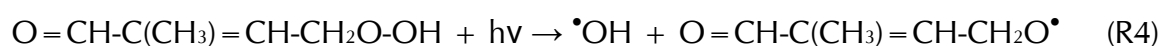
1,6-H shift (details given by *Nguyen et al.*, 2010b) and via subsequent reaction with O₂ generate highly photolabile 4-hydroperoxy-methyl-but-2-enals (HPALDs) plus HO₂ radicals. The HO₂ + HPALD yield per isoprene oxidized is estimated close to 0.7 in pristine tropical forest conditions (303 K, 40 ppt HO₂ and 20 ppt NO), while IMAGESv2-based global modelling (*Peeters and Müller*, 2010; see below) predicted a globally averaged yield as high as 0.6, both values being fairly robust against variations of the controlling rate parameters within their uncertainty range. This gain of 0.5 to 0.7 HO₂ per initial isoprene-peroxy is diametrically opposed to the 0.6 to 0.8 HO₂ lost in traditional isoprene chemistry by HO₂ reaction with the peroxys to yield hydroperoxides.

(iii) We have characterized a moderately fast 1,5-H-shift reaction of both the major β-OH-peroxy adducts, which directly regenerates OH for an overall fraction estimated at 0.01 - 0.10 in the pristine conditions mentioned above.

(iv) We presented sound argumentation that major OH-regeneration occurs directly via photolysis of the labile unsaturated hydroperoxy-aldehyde coproducts of HO₂ (O=CH-C(CH₃)=CH-CH₂O-OH and O=CH-CH=C(CH₃)-CH₂O-OH), with a potential for additional OH regeneration by the subsequent photochemistry.

Worth to mention is that the new reactions we introduced were previously unsuspected due to the very high NO levels which characterized most laboratory investigations of isoprene oxidation by OH; under such conditions, the NO-reaction of the isoprene peroxy radicals is indeed largely dominant.

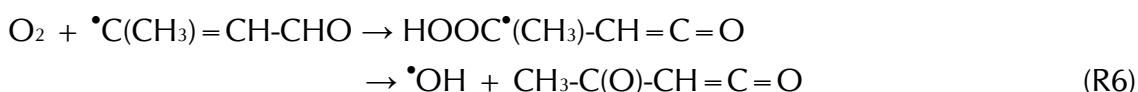
In a second paper (*Peeters and Müller*, 2010), we could present experimental evidence construed from the recent literature in support of various key features of our new isoprene mechanism (LIM). Among others, the HPALDs we predicted from the 1,6-H shifts of the Z-delta-OH-peroxys have been observed in the laboratory by Paulot et al. (2009b) in concentrations consistent with their estimated yields and very fast photolysis as we had contended. From the published experimental observations we also concluded to the occurrence (unnoticed by Paulot et al.) of an additional hydroxy-peroxy radical removal route beside the accepted pathways; we consider this to be the unimolecular 1,6-H shift we identified and quantified theoretically. Further, by confrontation of our mechanism with product (yield) measurements in several photoreactor and field studies, we could more precisely quantify the rates of the 1,6-H and 1,5-H shifts of the isoprene-peroxys and/or reduce their uncertainty margins; for the 1,6-Hshifts, the best value for the two cases appears to be somewhat lower than the geometric average of our original first-principles predictions. Regarding the HPALDs photolysis, we expect this to be fast due to the combination of an efficient near-UV absorbing conjugated O=C-C=C α,β-enone chromophore (max σ around 335 nm) and a hydroperoxide chromophore with its weak O-OH bond, resulting in efficient OH regeneration:



We argued that the process most likely proceeds through an avoided crossing along the O–OH coordinate of the initial excited singlet (n_1, π^*) surface and the repulsive (n_2, σ^*) singlet surface of the O–OH functionality, and could so quantify the rate-controlling energy barrier and hence estimate the photolysis frequency for a near overhead sun at $4 \times 10^{-4} \text{ s}^{-1}$. The resulting oxy radical is expected to undergo a fast 1,5-formyl-H shift followed by O_2 addition, and after another 1,6-H shift and subsequent reaction with O_2 to yield HO_2 plus an even more photolabile unsaturated peroxy-acid-aldehyde, $\text{HOOC(O)-C(CH}_3\text{)=CH-CHO}$ (PACALD). With its bi-conjugated O=C-C=C-C=O chromophore and very weak HO–O bond, the PACALD is expected to photolyze at an even faster rate of 10^{-3} s^{-1} , (far outrunning reaction with OH), yielding OH and likely eliminating promptly CO_2 :



Fast O_2 addition and an 1,5-H shift can directly result in another OH:



The secondary photochemistry subsequent to HPALD photolysis can therefore result in an additional 1 to 2 OH radicals. Also reported in the same paper, a global modeling study using the IMAGESv2 CTM demonstrated that the new LIM chemistry has indeed the potential to greatly impact isoprene oxidation chemistry, in particular over rainforests, and profoundly influence the self-cleansing capacity of the atmosphere in the boundary layer in such areas. It was shown that LIM may rationalize the unexpectedly high hydroxyl radical concentrations measured, not only over the Amazon forest, but also over other isoprene-rich areas. The new chemistry should play a significant role at moderate pollution levels too, even at our latitudes, and modify there the ozone forming potential of isoprene. A recent extensive box- and global modeling study by Archibald et al. (2010) fully supported the potentially major impact of our new isoprene mechanism

Our most recent modeling study on this issue (*Stavrakou et al.*, 2010) evaluated and quantified the impacts of different mechanism updates on the boundary layer concentrations of OH and HO_2 radicals using the IMAGESv2 global chemistry transport model. The model results for HOx, isoprene, NO, and ozone are evaluated against air-based observations from the recent GABRIEL campaign over the Amazon basin and from the INTEX-A campaign over the Eastern US. The Mainz Isoprene Mechanism version 2 (MIM2, *Taraborelli et al.*, 2009) used as reference mechanism in our simulations, has been modified to test (i) the artificial OH recycling proposed by Lelieveld et al. (2008), (ii) the epoxide formation mechanism proposed by Paulot et al. (2009b), and finally (iii) the HOx regeneration of our Leuven Isoprene Mechanism (*Peeters et al.*, 2009; *Peeters and Müller*, 2010), with preliminary mechanisms for the OH-reaction of the HPALDs and for the chemistry of the HPALD-

and PACALD (photo-)products (LIM0). The simulations show that the LIM0 scheme holds by far the largest potential impact on HO_x concentrations over densely vegetated areas in the Tropics as well as at mid-latitudes. Strong increases, by up to a factor of 4 in the modeled OH concentrations, and by a factor of 2.5–3 in the HO₂ abundances are estimated through the LIM0 mechanism compared to the traditional MIM2 scheme. Comparatively much smaller OH increases are associated with the mechanism of Paulot et al. (2009b) and even further suppressed when combined with the LIM0 scheme. Hydroperoxy-aldehydes (HPALDs) are found to be major first-generation products in the oxidation of isoprene by OH, with a combined globally averaged yield of 50–60%. The LIM0 chemistry can reproduce the observed boundary-layer mixing ratios of OH and HO₂ to within 30%, performing far better than the other mechanisms. In spite of the remaining uncertainties in the theoretically-predicted rates of critical radical reactions leading to the formation of HPALDs, and even more in the subsequent degradation of these new compounds, the current findings make a strong case for the newly proposed chemical scheme. Still, direct experimental confirmation and quantification is urgently needed for the formation of HPALDs and for their fast OH-generating photolysis.

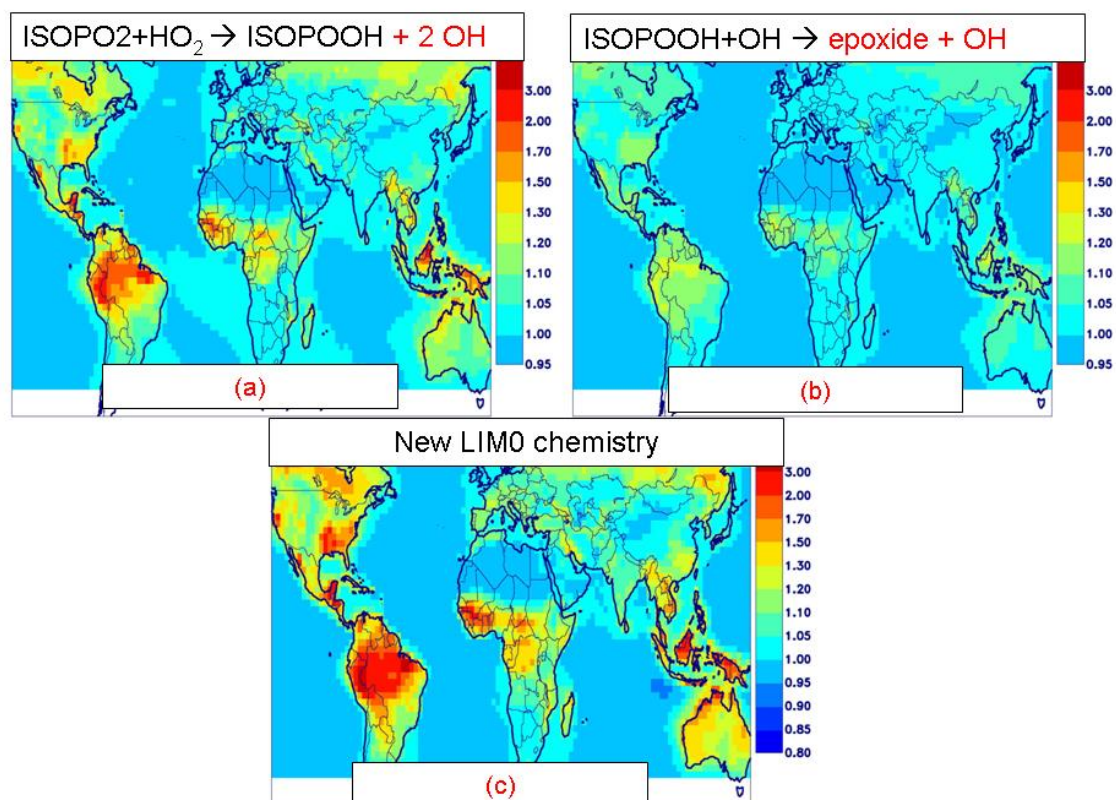


Figure 28. Calculated impact on OH concentrations (July 2005, below 1.5 km) of (a) the artificial production of 2 OH in the RO₂ + HO₂ reactions (Lelieveld et al., 2008); (b) the Paulot et al.2009b "epoxide" mechanism; (c) the LIM0 mechanism update with 3 OH formed per HPALD photolyzed.

In follow-up research, the KULeuven and BISA teams will be jointly involved in a mechanism-construction and modeling effort. Much of the work will be directed towards the further theory-based development of a detailed new isoprene oxidation mechanism upgrade, LIM1, with a prime focus on the subsequent efficiently OH-regenerating chemistry of the photolabile HPALDs and their products. The LIM1 oxidation mechanism will also include the competing OH-initiated oxidation of the HPALDs and PACALDs and their products, as well as the revised chemistry of the initial hydroperoxides that were recently shown to yield mainly epoxides (Paulot *et al.*, 2009), and the chemistry of methylvinylketone and methacrolein likewise formed from the initial hydroxy-peroxys. Extensive modeling using LIM1 will be made in order to verify to which extent we will be able to reproduce the fast OH-regeneration observed in and near pristine forests, while at the same time examining the HO₂ budget. Constrained modeling of the presently available (and hopefully new, future) isoprene oxidation photo-reactor experiments in near-pristine (low-NO_x) conditions will also be in order. Finally, modeling studies will be conducted for more generally occurring conditions in and near forested areas in temperate zones (such as in the US and China), in order to accurately assess the impact of the OH-regenerating isoprene oxidation chemistry on the oxidizing capacity of the troposphere and on the global budget of tropospheric ozone.

II.6 Global Modeling

II.6.1 Development of reduced mechanism for the oxidation of terpenes

Due to its large global emissions, isoprene is expected to have a much larger impact than any other biogenic VOC on the gas-phase composition of the troposphere, in particular on the budget of oxidants. Still, the mono- and sesquiterpenes are believed to be a large source of SOA, of the same order as the SOA production due to isoprene (Henze *et al.*, 2008). Therefore, our priority has been the development of a parameterization for the formation of SOA from α -pinene. The development of a reduced α -pinene mechanism which would mimic the effect of the explicit mechanism on the gas-phase composition would be unnecessarily complex, given the large uncertainties associated to the oxidation of isoprene. Indeed, as discussed in Section II.5.3, there is now overwhelming evidence from field campaigns (e.g. Lelieveld *et al.*, 2008) and from the theoretical studies performed within IBOOT (Peeters *et al.*, 2009) that the isoprene chemical mechanism currently used in models needs to be radically revisited. The elaboration of a revised mechanism and its reduction for use in global models will be addressed in future research.

II.6.2 Development of SOA parameterization for use in a global model

II.6.2.1 General formulation

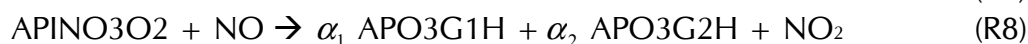
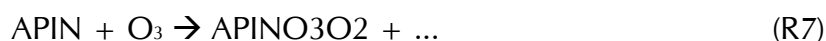
We consider three sources of organic aerosol (OA) in our global model IMAGESv2 (Stavrakou and Müller, 2006):

- Direct emission of Primary Organic Aerosol (POA) due to anthropogenic sources (Bond *et al.*, 2004) and biomass burning (van der Werf *et al.*, 2006; Andreae, pers. comm.). POA has hydrophilic and hydrophobic components. Conversion of hydrophobic to hydrophilic POA due to aging is represented by an e-folding time of 1 day (Martin *et al.*, 2003).
- Reversible SOA formation due to the partitioning of semi-volatile organic compounds. We adopt the approach of the two-product model (e.g. Henze *et al.*, 2008) for estimating this production of SOA from isoprene, terpenes and aromatics. In most cases, the precise pathways leading to SOA are unknown, and the two-product model parameters are obtained from laboratory data. For monoterpenes (represented by the model compound α -pinene), these parameters are fitted from BOREAM model simulations, as presented in the next subsection.
- Irreversible SOA formation due to the production of essentially non-volatile compounds (e.g. oligomers and polymers). Non-volatile SOA arises from a multitude of poorly elucidated pathways believed to occur at the surface or in the bulk phase of aerosols and cloud droplets. For example, very common short-chained aldehydes (glyoxal, methylglyoxal, methacrolein, glycolaldehyde, etc.) oligomerize rapidly in aqueous aerosols and/or in cloud droplets.

Isoprene and monoterpene emissions are obtained from the inventories of Müller *et al.* (2008) and Guenther *et al.* (1995), respectively. The gas-phase degradation of isoprene is based on the Mainz Isoprene Mechanism version 2 (Taraborelli *et al.*, 2009) and has been further modified to include a production of two OH radicals in the reaction of first generation peroxy radicals from isoprene with HO₂, as recommended by Lelieveld *et al.* (2008) as a crude way of including OH regeneration in the oxidation of isoprene. The model accounts for wet and dry deposition of gases and aerosols. The wet removal scheme is based on ECMWF cloud and precipitation fields. The semi-volatile gaseous SOA precursors are assumed to be as soluble in water as glyoxal, based on the high solubility of typical multi-functional SOA components.

II.6.2.2 Parameterization for reversible SOA formation

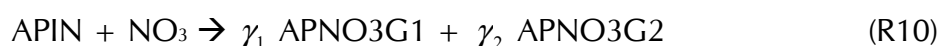
The product yields and partitioning parameters of the condensable compounds from aromatics (benzene, toluene and xylene), isoprene and sesquiterpenes are obtained from *Henze et al. (2008)*, *Henze and Seinfeld (2006)* and *Chang and Pankow (2008)*, respectively. For α -pinene, we account for the dependence of the SOA yields on the NO_x regime and on the nature of the oxidant (O₃, OH or NO₃). For example, the O₃-initiated oxidation is represented through the reactions:



The formation yields α_i are temperature-dependent:

$$\alpha_i(T) = \alpha_i^0 \cdot \exp(\alpha_i^1 \cdot (T - 298)). \quad (\text{Eq. 11})$$

Reactions analogous to reactions R7-R9 describe the OH-oxidation. Only the high-NO_x case is considered for the NO₃-initiated oxidation:



The partitioning coefficients $K_{p,i}$ [$\text{m}^3 \mu\text{g}^{-1}$] follow the expression

$$K_{p,i}(T) = K_{p,i}(T_r) \cdot \left(\frac{T}{T_r}\right) \cdot \exp\left(\frac{\Delta H_i}{R} \cdot \left(\frac{1}{T} - \frac{1}{T_r}\right)\right) \cdot \left(\frac{m}{m_r}\right) \quad (\text{Eq. 12})$$

where $K_{p,i}(T_r)$ is the partitioning coefficient at the reference temperature T_r and for an average molecular weight of the absorbing aerosol (m) equal to its reference value m_r . ΔH_i is the enthalpy of vaporization, and R the gas constant. The yields and partitioning parameters (Table XIV) were obtained by fitting the SOA yields calculated by the BOREAM model in a wide range of conditions, as described below.

Table XIV. Two-product model parameters for alpha-pinene SOA derived in this study. α_i^0 and α_i^1 define the product yields (Eq. 11). $K_{p,i}(298)$ and ΔH_i define the partitioning coefficients (see

Eq. 12). m_r is the reference average molecular weight of the aerosol.

reaction	product	α_i^0	α_i^1	$K_{p,i}(298)$ $\text{m}^3 \mu\text{g}^{-1}$	ΔH_i kJ mol^{-1}	m_r
α -pinene + OH, low NO _x limit	1	0.194	-0.022	6.98	87	215
	2	0.134	-0.013	0.117	22	215
α -pinene + OH, high NO _x limit	1	0.0149	-0.040	0.762	10	253
	2	0.0586	-0.025	0.0049	162	253
α -pinene + O ₃ , low NO _x limit	1	0.182	-0.132	4.16	87	211
	2	0.092	-0.025	0.0158	77	211

α-pinene + O₃,	1	0.0095	-0.057	0.837	162	236
high NO_x limit	2	0.123	-0.054	0.0033	111	236
α-pinene + NO₃	1	0.0097	-0.049	0.493	172	251
(high NO_x)	2	0.136	+0.015	0.00092	148	251

In each simulation, α -pinene is allowed to react with only one oxidant. The high-NO and low-NO conditions are obtained by setting the NO₂ concentration to either a quite large (10 ppbv) or a negligible value, so that the reactions of peroxy radicals with NO are either by far dominant or negligible. Temperature is varied between 273 and 303 K. The photolysis rates and the concentrations of oxidants (O₃, OH, HO₂) and α -pinene are prescribed, but they follow diel cycles typical of atmospheric conditions. The condensable compounds undergo deposition, with a lifetime set to 6 days, so that the system reaches a quasi-steady state after about 2 weeks of simulation. The SOA yield is estimated from the concentrations calculated during the last day of the simulation. BOREAM version C (see Section II.4.4) is used, since it provides a better agreement with the laboratory yields. The effect of water uptake is taken into account in the parameterization through the use of RH-dependent activity coefficients γ_{water} (for H₂O) and γ_{org} (for organics) estimated from BOREAM model calculations at relative humidities varied between 0.5 and 99.5% with a 1% step.

II.6.2.3 Parameterization for irreversible SOA formation from dicarbonyls

The formation of SOA from glyoxal and methylglyoxal is included in the model as an irreversible process (*Fu et al.*, 2008). It is assumed to be very fast in liquid clouds. On aqueous inorganic aerosols, a constant reactive uptake coefficient ($2.9 \cdot 10^{-3}$) is assumed (*Liggio et al.*, 2005). The sources of glyoxal and methylglyoxal include direct emissions as well as secondary formation in the oxidation of other NMVOCs, most importantly isoprene. The detailed budget of glyoxal has been presented in *Stavrakou et al.* (2009a). Inorganic aerosols are calculated with the EQSAM model (*Metzger et al.*, 2002). Their hysteresis behavior is accounted for by assuming that they are liquid when the relative humidity exceeded the deliquescence relative humidity in the last 24 hours.

II.6.3 Results: distribution and budget of organic aerosols (OA)

Three model simulations were performed:

- I1: α -pinene SOA parameters as in Table XIV, but neglecting absorption of organic compounds in aerosol water.

- I2: as I1, with a temperature dependence based on laboratory measurements (Offenberg *et al.*, 2006): $\alpha_i^1 = 0$ and $\Delta H_i = 42 \text{ kJ mol}^{-1}$ in Eqs.11-12;
- I3: as I1, allowing absorption of organics in aerosol water (i.e. M_0 in Eq. 4 includes organic aerosol and liquid water).

The calculated global annual distribution of OA concentration is displayed in Figure 29 for simulation I2. Over continents, OA concentrations typically range between 1 and 30 $\mu\text{g m}^{-3}$. The largest values are found in Tropical regions, over regions characterized by intense vegetation fires.

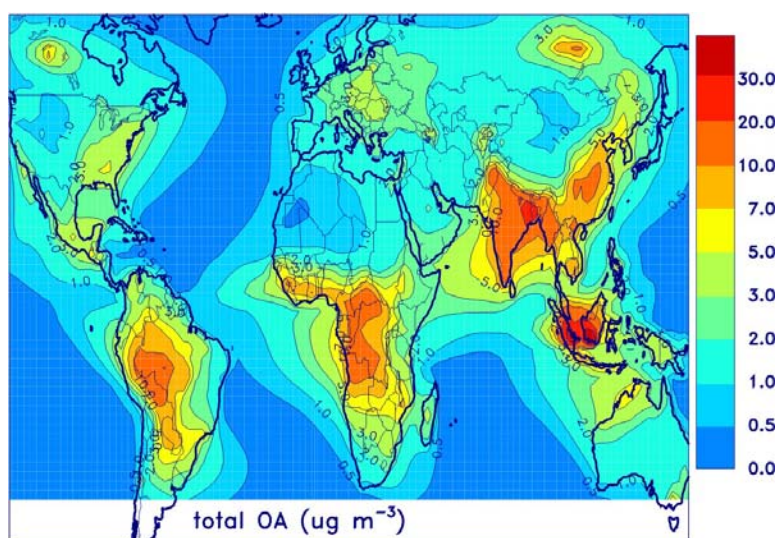


Figure 29. Annually averaged concentration of organic aerosol ($\mu\text{g m}^{-3}$) at surface level calculated by the IMAGES model in simulation I3.

The relative contributions of the major sources of OA (POA, SOA from dicarbonyls, from isoprene, from monoterpenes) to the total OA concentration are displayed in Figure 30. The global budget of SOA is summarized in Table XV. POA is found to be largely dominant over Equatorial and Southern Africa as well as over India and China. However, on the global scale, SOA is the dominant form of OA, with a global production of about 100 Tg/year, for a global POA source of 62 Tg/year. The SOA production due to the oligomerization of dicarbonyls in clouds and aqueous aerosols is calculated to represent as much as 37 Tg/year or about a third of the total SOA production. This estimate is of course very uncertain and calls for further studies of this important process. The oligomerization of other oxygenated VOCs requires also more attention.

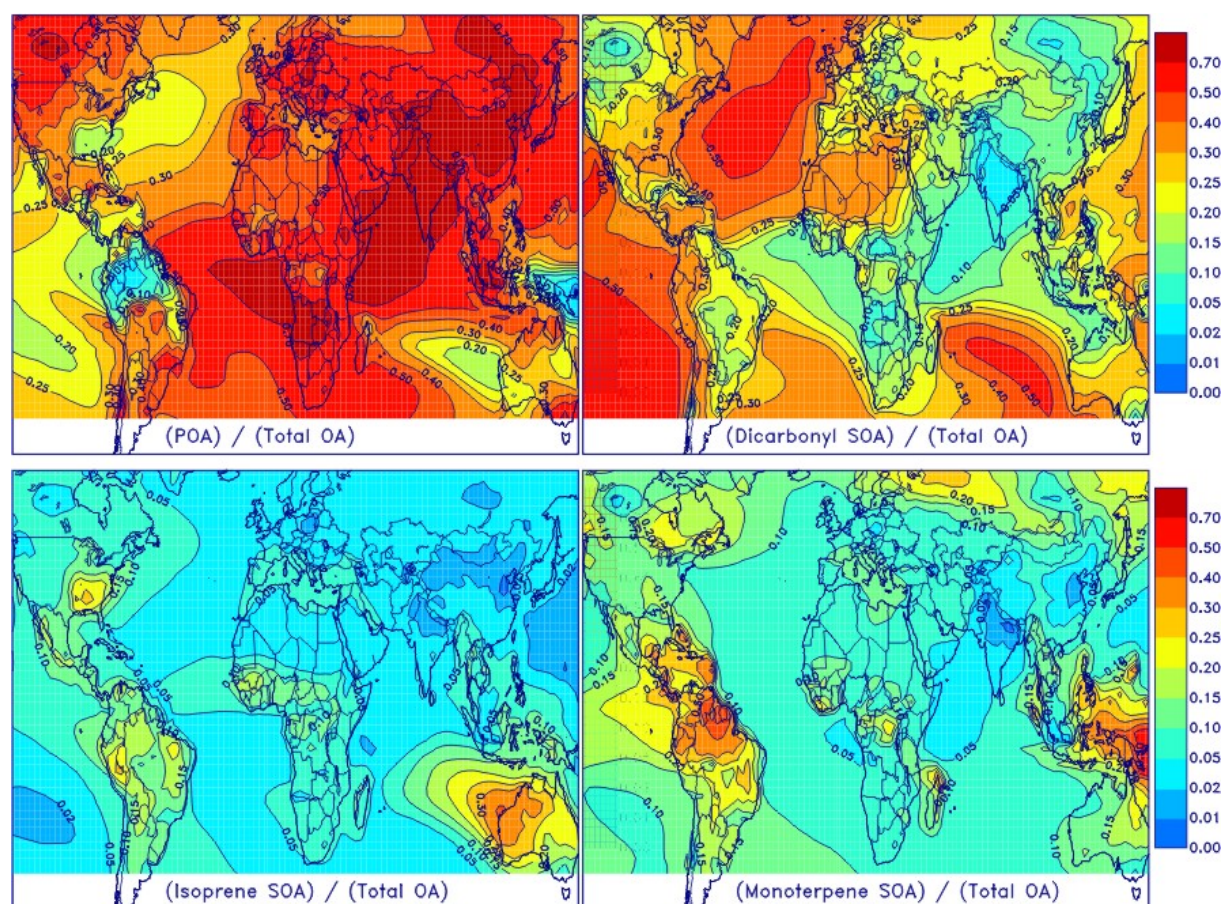


Figure 30. Relative contribution of the major sources of OA to the total OA concentration at surface level: POA (upper left), SOA from dicarbonyls (upper right), from isoprene (lower left), and from monoterpenes (lower right). Results shown for simulation I3, annual mean.

Table XV. Global SOA production (Tg/yr) and burden (Tg) in this work (runs I1, I2 and I3, see text for details) and in previous model studies.

	<i>I1</i>	<i>I2</i>	<i>I3</i>	<i>Henze et al.</i> (2008)	<i>Tsigaridis &</i> <i>Kanakidou</i> (2007)
Monoterpenes	27.5	21.4	30.2	8.7	12.1
Sesquiterpenes	6.5	6.5	8.8	2.1	0
Isoprene	19.5	19.1	26.8	14.4	4.6
Aromatics	3.9	3.8	4.1	3.5	1.8
Dicarbonyls	37.1	37.1	37.1	0	0
Total SOA production	94.5	87.9	107	30.3	18.6
SOA Burden (Tg)	1.68	1.50	1.92	0.81	0.82

The calculated SOA production due to the oxidation of aromatics and isoprene (not counting the contributions of dicarbonyls) are in good agreement with the previous estimates of *Henze et al.* (2008) and *Henze and Seinfeld* (2006) using the GEOS-Chem model. For monoterpenes, however, our estimated SOA production is 2-3 times higher

than in previous modeling studies. Note that due to the importance of wet deposition, this discrepancy would have been even higher if the gaseous SOA precursors had been assumed to be only weakly soluble, as in the study of *Tsigaridis and Kanakidou (2007)*. In the latter study, however, the SOA formation due to the OH-initiated oxidation of monoterpenes was neglected, whereas in our study, it represents 67% of the total SOA production from α -pinene. This very large contribution has two main reasons:

(1) The high SOA yields calculated by BOREAM in low-NO_x conditions when OH oxidizes α -pinene, of the order of ~ 0.4 at 298 K for typical M_0 concentrations ($3\text{--}20 \mu\text{g m}^{-3}$). These high yields are due to the formation of hydroxy dihydroperoxides, with vapor pressures of the same order as (or even lower than) pinic acid. Laboratory data are unfortunately lacking to confirm this model prediction.

(2) The high OH abundances calculated over remote areas characterized by large isoprene emissions, due to the trick proposed by *Lelieveld et al. (2008)* and used in our model to bring the modeled OH concentrations in line with field measurements such as those of the GABRIEL campaign. For these reasons, monoterpene SOA are calculated to represent 20-50% of OA over remote forests at tropical and boreal latitudes (see Figure 30).

II.6.4 Validation by comparison with observations

II.6.4.1 Glyoxal and formaldehyde

The model results for glyoxal and formaldehyde have been extensively compared with ground-based, aircraft and satellite data (*Stavrakou et al., 2009a, 2009b, 2009c*), and the inverse modeling technique has been used to suggest emission updates bringing the model distributions closer to the measurements. In particular, the use of satellite and ground-based glyoxal measurements indicates the existence of a large biogenic source of glyoxal precursor(s) with a chemical lifetime of the order of a few days (*Stavrakou et al., 2009a*). The emissions of isoprene over the Eastern US are estimated to be $\sim 30\%$ too high in the current inventories, in agreement with an analysis based on isoprene aircraft measurements (*Warneke et al., 2008*).

II.6.4.2 Organic aerosol

As seen in Figure 31, the simulated organic aerosol concentrations compare reasonably well with the ground-based measurements of the IMPROVE network in the United States. Significant underestimations are noted over the Northwestern US as well as at various sites in Europe, Asia and Africa, where either the POA source or the production of anthropogenic SOA might be largely underestimated by the model. Over regions

where the biogenic VOC emissions are large (Amazonia, the Eastern US), a fairly good agreement is obtained, contrasting with several previous studies. The large total SOA source inferred from our calculations is therefore supported by this comparison with ground-based data.

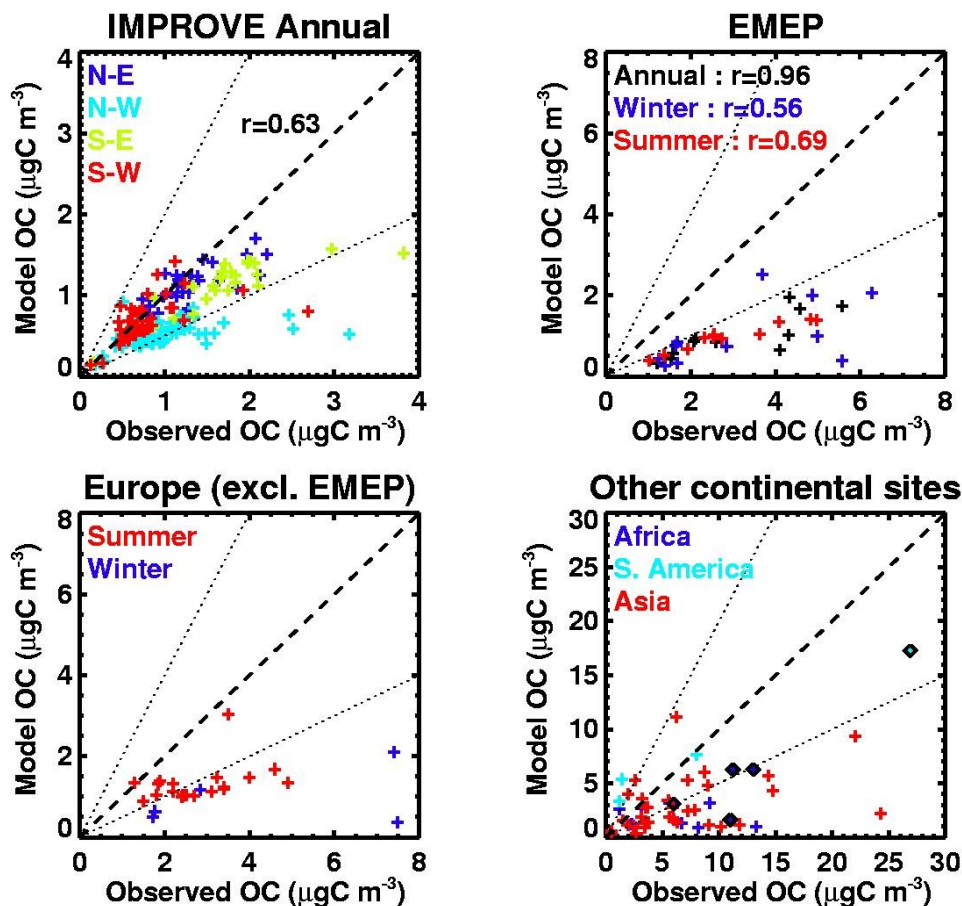


Figure 31. Modeled (simulation I3) vs. observed organic carbon concentrations (annual averages, $\mu\text{gC m}^{-3}$) at surface sites in the United States (top, left), in Europe (top, right and bottom, left) and in other continents (bottom, right).

III. POLICY SUPPORT

Environmental policy should be based on accurate information regarding the roles of natural and anthropogenic emissions on the abundance of pollutants. IBOOT has fulfilled its major objective, which was to narrow down the uncertainties associated with the role of biogenic volatile organic compounds (BVOCs). Although of natural origin, the BVOCs are central to our understanding of the role played by human activities (e.g. land use changes and anthropogenic emissions) in climate change and air quality issues. Most importantly,

- they influence the oxidizing capacity of the atmosphere and therefore the abundance of many key gases, especially the greenhouse gas methane, but also air quality compounds (e.g. carcinogenic benzene) and chemicals contributing to stratospheric ozone depletion (e.g. HCFCs)
- in polluted areas, they participate to summertime “ozone smog” episodes, i.e. to the build-up of noxious pollutants, primarily ozone, due the catalytic action of nitrogen oxides of anthropogenic origin
- they are a source of Secondary Organic Aerosol (SOA) which make up a substantial fraction of fine aerosols (i.e. particulate matter or PM).

Aerosols play a central role in climate through direct radiative effects and through their influence on clouds. Along with ground-level ozone, fine aerosols are also a major component of smog over polluted regions. They have acute adverse effects on human health, in particular on the respiratory and cardiovascular systems; over Europe, PM pollution has been estimated to cause ~200,000 premature deaths per year.

Regulation measures in the United States and Europe are tightening as a growing body of scientific evidence suggests that there is no safe level of exposure to ozone or PM. Although anthropogenic emissions of ozone precursors have generally decreased in Europe since the 1990s, exposure to ground-level ozone has failed to decline substantially, and the number of premature deaths due to ground level ozone worldwide is expected to quadruple by 2030. This global pollution trend has also negative consequences for crop yields and for ecosystems and their ability to take up atmospheric carbon dioxide.

Although crucial to these issues, the effects of BVOCs remain poorly quantified, however. IBOOT has contributed to answer the following key questions:

Do BVOCs deplete the oxidizing capacity of the atmosphere?

BVOCs were previously believed to deplete hydroxyl radical (OH) concentrations and to reduce the oxidizing capacity of the atmosphere. However, recent observations have indicated that the oxidation of isoprene, the single-most important BVOC, regenerates OH radicals in remote areas, and that the overall effect of isoprene emissions on the oxidizing capacity of the atmosphere is weak. The theoretical work performed within IBOOT provides a first detailed explanation as to how this regeneration takes place. This finding is essential for policy-making, since it will strongly impact the model estimates of how anthropogenic activities (i.e. pollutants emissions and land-use changes) influence the abundance of key pollutants like ozone and the climate gas methane. A recent global modeling study has demonstrated the impact of the new chemistry on the expected future evolution of the oxidizing capacity of the atmosphere.

How much do BVOCs contribute to atmospheric aerosol concentrations?

Secondary organic aerosol (SOA) is a major component of fine aerosols over continents. Work within IBOOT provided new insights allowing improved estimations for the role of BVOCs as a source of secondary organic aerosols. Our model calculations show that biogenic SOA is by far the largest component of organic aerosol, although a large fraction of it is due to poorly characterized oligomerization processes in clouds and in aerosols. The presence of nitrogen oxides appears to partially inhibit the formation of SOA from α -pinene, in agreement with experimental data.

In conclusion, our work shows that BVOC emissions have only little impact on the oxidizing capacity, in particular at remote locations (e.g. rainforests). It appears therefore that, contrary to previous model estimations, deforestation is not expected to increase the self-cleansing property of the atmosphere and to mitigate pollutant build-up. However, BVOCs are a substantial source of organic aerosol having far-reaching effects on climate and air quality. The complex interaction of these emissions with anthropogenic emissions (e.g. NO_x and sulfur compounds) warrants further investigation.

IV. DISSEMINATION AND VALORISATION

- The IBOOT project results were primarily disseminated through publications and presentations at international conferences, with 26 articles in international peer-reviewed journals. The recent paper on HO_x regeneration in isoprene oxidation (Peeters *et al.*, 2009), published as a "hot article" in *Phys. Chem. Chem. Phys.*, was accessed on the PCCP website 170 times during July. This IBOOT research of the KULeuven team was promoted in *Highlights in CHEMICAL SCIENCE* magazine. Jozef Peeters has been invited to give a plenary lecture on this topic at the 21st International Gas Kinetics Symposium in 2010. J.-F. Müller has given invited talks on global modeling and BVOCs at Harvard Univ. (2007), Univ. Edinburgh (2008), NCAR (2007) and at the AGU Conference in San Francisco (Dec. 2007).

- Luc Vereecken is member of the MCM Data Panel, having the mission to discuss the future improvements in the MCM (Master Chemical Mechanism) which is increasingly being acknowledged as the premier link between laboratory data and modeling. During recent meetings of this Data Panel, virtually every aspect of the IBOOT program was touched. Databases of available data were compiled by members of the Data Panel and transferred to KULeuven, significantly helping further extension of the Structure-Activity Relationships (SARs). Several of our SARs (OH-addition; alkoxy decomposition) are now being used in the MCM for the further development of degradation mechanisms of large VOC. Certain new reaction types introduced by the KULeuven team, e.g. peroxy radical isomerization, will also be incorporated in the MCM, in line with the new chemistry in the updated α -pinene + OH mechanism. Given the excellent results of the α -pinene modeling (IASB-BIRA), sections of the BOREAM mechanism should also migrate to the MCM. Luc Vereecken has spent six months (1 Oct 2009 - 31 March 2010) with the group of Prof. M. Pilling – originator of the MCM – at the University of Leeds, where he continued the development of the β -pinene oxidation mechanism and further implemented IBOOT output data in MCM.

- A website detailing the H-abstraction SAR is accessible at:

http://arrhenius.chem.kuleuven.be/~luc/sar_habstr/header.html

- A website detailing the α -pinene mechanism and BOREAM model is accessible at:

<http://tropo.aeronomie.be/boream/index.html>

- IBOOT web page:

<http://tropo.aeronomie.be.iboot/index.htm>

V. PUBLICATIONS

- Capouet, M., and J.-F. Müller, A group contribution method for estimating the vapour pressures of alpha-pinene oxidation products, *Atmos. Chem. Phys.*, **6**, 1455-1467, 2006.
- Carl, S.A., L. Vereecken, and J. Peeters, Kinetic parameters for gas-phase reactions: Experimental and theoretical challenges, *Phys. Chem. Chem. Phys.*, doi:10.1039/b705505f, 2007.
- Dillon, T.J., A. Horowitz, D. Hölscher, J.N. Crowley, L. Vereecken, and J. Peeters, Reaction of HO with hydroxyacetone (HOCH₂C(O)CH₃): Rate coefficients (233 - 363 K) and mechanism, *Phys. Chem. Chem. Phys.*, **8**, 236-246, 2006.
- Khamaganov, V.G., V. Xuan Bui, S.A. Carl, and J. Peeters, Absolute rate coefficient of the OH + CH₃C(O)OH reaction at T = 287-802 K. The two faces of pre-reactive H-bonding, *J. Phys. Chem. A*, **110**, 12852-12859, 2006.
- Römpp, A., R. Winterhalter, and G. K. Moortgat, Oxodicarboxylic acids in atmospheric aerosol particle, *Atmos. Environ.*, **40**, 6848-6862, 2006.
- Sadezky, A., P. Chaimbault, A. Mellouki, A. Römpp, R. Winterhalter, G. Le Bras, and G. K. Moortgat, Formation of secondary organic aerosol and oligomers from the ozonolysis of enol ethers, *Atmos. Chem. Phys.*, **6**, 5009-5024, 2006.
- Kanawati, B., S. Joniec, R. Winterhalter, and G. K. Moortgat, Mass spectrometric characterisation of small oxocarboxylic acids and gas phase ion fragmentation mechanisms studied by Electrospray Triple Quadrupole-MS/MS-TOF system and DFT Theory, *Int. J. Mass Spectrom.*, **266**, 97-113, 2007.
- Karunanandan, R., D. Hölscher, T.J. Dillon, A. Horowitz, J.N. Crowley, L. Vereecken, and J. Peeters, Reaction of HO with glycolaldehyde, HOCH₂CHO: rate coefficients (240 - 362 K) and mechanism, *J. Phys. Chem. A*, **111**, 897-908, 2007.
- Nguyen, M.T., T.L. Nguyen, V.T. Ngan, H.M.T. Nguyen, Heats of formation of the Criegee formaldehyde-oxide and dioxirane, *Chem. Phys. Lett.*, **448**, 183-188, 2007.
- Peeters, J., W. Boullart, V. Pultau, and S. Vandenberg, L. Vereecken, Structure-Activity Relationship for the addition of OH to (poly)alkenes : Site-specific and total rate constants, *J. Phys. Chem. A*, **111**, 1618-1631, 2007.
- Vereecken, L., J.-F. Müller, and J. Peeters, Low-volatility poly-oxygenates in the OH-initiated atmospheric oxidation of α -pinene: Impact of non-traditional peroxy radical chemistry, *Phys. Chem. Chem. Phys.*, doi:10.1039/b708023a, 2007.
- Capouet, M., J.-F. Müller, K. Ceulemans, S. Compennolle, L. Vereecken, and J. Peeters, Modeling aerosol formation in alpha-pinene photooxidation experiments, *J. Geophys. Res.*, **113**, D02308, doi:10.1029/2007JD008995, 2008
- Kanawati, B., F. Herrmann, S. Joniec, R. Winterhalter, and G. K. Moortgat, Mass spectrometric characterisation of β -caryophyllene ozonolysis products in the aerosol

- studied by an electrospray triple quadrupole and time-of-flight analyzer hybrid system and density functional theory, *Rapid Comm. Mass Spectrom.*, 22, 185-186, 2008.
- Kanawati, B., S. Joniec, R. Winterhalter, and G. K. Moortgat, Mass spectrometric characterisation of 4-oxopentanoic acid and gas-phase ion fragmentation mechanisms studied using a triple quadrupole and time-of-flight analyzer hybrid system and density functional theory, *Rapid Comm. Mass Spectrom.*, 22, 2269-2279, 2008.
- Sadezky, A., R. Winterhalter, B. Kanawati, A. Mellouki, G. Le Bras, A. Römpf, B. Sprengler, P. Chaimbault, and G. K. Moortgat, Oligomer formation during gas-phase ozonolysis of small alkenes and enol ethers: new evidence for the central role of the Criegee Intermediate as oligomer chain unit, *Atmos. Chem. Phys.*, 8, 2667-2699, 2008.
- Vereecken, L., Computational study of the stability of α -nitroxy-substituted alkyl radicals, *Chem. Phys. Lett.*, 466, 127-130, DOI: 10.1016/j.cplett.2008.10.042, 2008.
- Compernelle, S., K. Ceulemans, and J.-F. Müller, Influence of non-ideality on condensation to aerosol, *Atmos. Chem. Phys.*, 9, 1325-1338, 2009.
- Nguyen, T.L., J. Peeters, and L. Vereecken, Theoretical study of the gas-phase ozonolysis of β -pinene, *Phys. Chem. Chem. Phys.*, 11, 5643-5656, DOI: 10.1039/B822984H, 2009a.
- Nguyen, T.L., R. Winterhalter, G. Moortgat, B. Kanawati, J. Peeters, and L. Vereecken, The gas-phase ozonolysis of β -caryophyllene (C₁₅H₂₄); Part II: A theoretical study, *Phys. Chem. Chem. Phys.*, 11, 4173-4183, doi:10.1039/B817913A, 2009b.
- Peeters, J., T.L. Nguyen, and L. Vereecken, HO_x radical regeneration in the oxidation of isoprene, *Phys. Chem. Chem. Phys.*, doi:10.1039/b908511d, 2009.
- Stavrakou, T., J.-F. Müller, I. De Smedt, M. Van Roozendael, M. Kanakidou, M. Vrekoussis, F. Wittrock, A. Richter, and J. Burrows, The continental source of glyoxal estimated by the synergistic use of spaceborne measurements and modelling, *Atmos. Chem. Phys. Discuss.*, 9, 13593-13628, 2009a.
- Stavrakou, T., J.-F. Müller, I. De Smedt, M. Van Roozendael, G. van der Werf, L. Giglio, and A. Guenther, Evaluating the performance of pyrogenic and biogenic emission inventories against one decade of space-based formaldehyde columns, *Atmos. Chem. Phys.*, 9, 1037-1060, 2009b.
- Stavrakou, T., J.-F. Müller, I. De Smedt, M. Van Roozendael, G. van der Werf, L. Giglio, and A. Guenther, Global emissions of non-methane hydrocarbons deduced from SCIAMACHY formaldehyde columns through 2003-2005, *Atmos. Chem. Phys.*, 9, 3663-3679, 2009c.

- Vereecken, L., and J. Peeters, Decomposition of substituted alkoxy radicals – part I: a generalized structure-activity relationship for reaction barrier heights, *Phys. Chem. Chem. Phys.*, doi:10.1039/b909712k, 2009.
- von Hessberg, C., P. von Hessberg, U. Pöschl, M. Bilde, O.J. Nielsen, and G.K. Moortgat, Temperature and humidity dependence of secondary organic aerosol yield from the ozonolysis of β -pinene, *Atmos. Chem. Phys.*, 9, 3583-3599, 2009.
- Winterhalter, R., F. Herrmann, B. Kanawati, T.L. Nguyen, J. Peeters, L. Vereecken, and G. Moortgat, The gas-phase ozonolysis of β -caryophyllene (C₁₅H₂₄): Part I: An experimental study, *Phys. Chem. Chem. Phys.*, 11, 4152-4172, doi:10.1039/B817824K, 2009.
- Ceulemans, K., S. Compennolle, J. Peeters, and J.-F. Müller, Evaluation of a detailed model of secondary aerosol formation from α -pinene against dark ozonolysis experiments, *Atmos. Environ.*, 40, 5434-5442, 2010.
- Compennolle, S., K. Ceulemans, and J.-F. Müller, Technical note: Vapor pressure estimation methods applied to secondary aerosol constituents from alpha-pinene oxidation: an intercomparison study, *Atmos. Chem. Phys.*, 10, 6271-6282, 2010.
- Vereecken, L., and J. Peeters, A Structure-Activity Relationship for the rate coefficient of H-migration in substituted alkoxy radicals, *Phys. Chem. Chem. Phys.*, 12, 12608-12620, doi: 10.1039/C0CP00387E, 2010.
- Nguyen, T.L., L. Vereecken and J. Peeters, Theoretical study of the HOCH₂OO + HO₂ reaction: detailed molecular mechanisms of the three reaction channels, *Z. Phys. Chem.*, 224, 1081-1093, DOI: [10.1524/zpch.2010.6142](https://doi.org/10.1524/zpch.2010.6142), 2010a.
- J. Peeters, J.-F. Müller, Radical regeneration in isoprene oxidation via peroxy radical isomerisations. II: experimental evidence and global impact, *Phys. Chem. Chem. Phys.*, 12, 14227-14235, DOI: [10.1039/C0CP00811G](https://doi.org/10.1039/C0CP00811G), 2010.
- Nguyen, T.L., L. Vereecken and J. Peeters, HO_x Regeneration in the Oxidation of Isoprene. III: Theoretical Study of the key Isomerization of the Z- β -hydroxy-peroxy Isoprene Radicals, *ChemPhysChem*, 11, 3996-4001, DOI: [10.1002/cphc.201000480](https://doi.org/10.1002/cphc.201000480), 2010b.
- Stavrakou, T, J. Peeters and J.-F. Müller, Improved global modelling of HO_x recycling in isoprene oxidation: evaluation against the GABRIEL and INTEX-A aircraft campaign measurements, *Atmos. Chem. Phys.*, 10, 9863-9878, 2010.
- Herrmann, F., R. Winterhalter, G. K. Moortgat and J. Williams. Hydroxyl radical (OH) yields from the ozonolysis of both double bonds for five monoterpenes, *Atmos. Environ.*, 44, 3458-3464, 2010.

Submitted papers:

Compernelle, S., K. Ceulemans, and J.-F. Müller, Technical note: Estimating fusion properties of polyacids, submitted to *Atmos. Chem. Phys.*, 2010.

Beck, M., R. Winterhalter, F. Herrmann and G. K. Moortgat, The gas-phase ozonolysis of α -humulene, *Phys. Chem. Chem. Phys.*, submitted 2010.

Others (non peer-reviewed):

Capouet, M., Modeling the oxidation of α -pinene and the related aerosol formation in laboratory and atmospheric conditions, PhD Thesis, Université Libre de Bruxelles, 2006.

Herrmann, F., Produkte und Reaktionsmechanismen des Sesquiterpeneozonolyse, Diplom Thesis (Master) at Johannes-Gutenberg University Mainz, Dec. 2006.

Bui, V. X., Kinetic and product distribution study of the tropospheric reaction of OH radicals with acetic acid over an extended temperature range, PhD Thesis (supervisors: J. Peeters and S. Carl), KULeuven, 2008.

Beck, M., Bestimmung der Abbauprodukte der Ozonolyse von α -Humulene, Diplom Thesis (Master) at Johannes-Gutenberg University Mainz, September 2009.

VI. ACKNOWLEDGEMENTS

T. Stavrou has been supported by a Belspo PRODEX grant (SECPEA, 2008-2010). K. Ceulemans was supported also by Belspo (Action 1 grant) since 2009. Thanh Lam Nguyen was supported by a doctoral grant (DB, 2006) and by a postdoctoral mandate (PDM, 2007-2008) from the KULeuven Research Council.

VII. REFERENCES

- Antonovskii, V. L., and V. A. Terentev (1967), *Zh.Org.Khim.*, 3, 1011-1013
- Archibald (2010), A.T., M. C. Cooke, S. R. Utembe, D. E. Shallcross, R. G. Derwent and M. E. Jenkin, *Atmos. Chem. Phys.*, 10, 8097–8118.
- Asa-Awuku, A., G. J. Engelhart, B. H. Lee, S. N. Pandis, and A. Nenes (2008), *Atmos. Chem. Phys. Discuss.*, 8, 10105-10151.
- Atkinson, R., A. M. Winer, and J. N. Pitts Jr., (1982), *Atmos. Environ.* 16, 1017-1020.
- Atkinson, R. (2007), *Atmos. Environ.* 41, 8468-8485
- Aumont, B., S. Szopa, and S. Madronich (2005), *Atmos. Chem. Phys.*, 5, 2497-2517.
- Bariseviciute, R., J. Ceponkus, A. Gruodis, and V. Sablinskas (2006), *Cent. Eur. J Chem.*, 4, 578-591.
- Beck, M. (2009), Master Thesis at the Johannes-Gutenberg University Mainz.
- Bond, T., D. G. Streets, K. F. Yarber, S. M. Nelson, J.-H. Woo, and Z. J. Klimont, *Geophys. Res. Lett.* (2004), 109, D14203, doi:10.1029/2003JD003697.
- Bonn, B., G. Schuster, and G. K. Moortgat (2002), *J. Phys. Chem. A*, 106, 2869-2881.
- Booth, A. M., M. H. Barley, D. O. Topping, G. McFiggans, A. Garforth, and C. J. Percival, *Atmos. Chem. Phys.*, 10, 4879-4892.
- Calvert, J. G., R. Atkinson, J. A. Kerr, S. Madronich, G. K. Moortgat, T. J. Wallington, and G. Yarwood (2000), Oxford University Press, Inc., New York, pp. 552.
- Capouet, M., J. Peeters, B. Nozière, and J.-F. Müller (2004), *Atmos. Chem. Phys.*, 4, 2285-2311.
- Capouet, M. and J.-F. Müller (2006), *Atmos. Chem. Phys.*, 6, 1455-1467.
- Capouet, M., J.-F. Muller, K. Ceulemans, S. Compernelle, L. Vereecken, J. Peeters (2008), *J. Geophys. Res.*, 113, D02308, doi:10.1029,2007JD008995.
- Caralp, F., W. Forst, E. Hénon, A. Bergeat, and F. Bohr (2006), *Phys. Chem. Chem. Phys.*, 8, 1072-1078.
- Ceulemans, K. , S. Compernelle, J. Peeters, and J.-F. Müller (2009), *Atmos. Environ.* (submitted).
- Chang, E.I., and J.F. Pankow (2008), *Atmos. Chem. Phys. Discuss.*, 8, 995-1039.
- Chung, S., and J. Seinfeld (2002), *J. Geophys. Res.*, 107(19), 4407, doi:10.1029/2001JD001397.
- Cocker III, D. R., S. L. Clegg, R. C. Flagan, and J.H. Seinfeld (2001), *Atmos. Environ.* 35, 6049-6072
- Compernelle, S., K. Ceulemans, and J.-F. Muller (2009), *Atmos. Chem. Phys.*, 9, 1325-1338.
- Compernelle, S., K. Ceulemans, and J.-F. Müller, Technical note: **Estimating fusion properties for polyacids**, *Atmos. Chem. Phys. Discuss.*, submitted.
- Dallwigk, E., B. Susz and E. Briner (1952), *Helv. Chim. Acta*, 35, 353-362.

- Dillon, T. J., and J. N. Crowley (2008), *Atmos. Chem. Phys.*, 8, 4877-4889. (see also Dillon et al., *Gas Kinetics Symposium*, 2010)
- Fredenslund, A., R. L. Jones and J. M. Prausnitz (1975), *AIChE J.*, 21, 1086-1099.
- Fu, T.-M., D. J. Jacob, F. Wittrock, J. Burrows, M. Vrekoussis, and D. K. Henze (2008), *J. Geophys. Res.*, 113, D15303, doi:10.1029/2007JD009505.
- Griffin, R.J., R. C. Flagan and J. H. Seinfeld (1999), *J. Geophys. Res.*, 104, 3555-3567.
- Grosjean, D., E. L. Williams, E. Grosjean, J. M. Andino and J. H. Seinfeld (1993), *Environ. Sci. Technol.*, 27, 2754-2758.
- Guenther, A., C. Hewitt, D. Erickson, et al. (1995), *J. Geophys. Res.*, 100, 8873-8892.
- Hansen, H.K., P. Rasmussen, A. Fredenslund, M. Schiller, and J. Gmehling (1991), *Ind. Eng. Chem. Res.*, 30, 2352-2355.
- Heaton, K. J., M. A. Dreyfus, S. Wang, and M.V. Johnston (2007), *Environ. Sci. Technol.*, 41, 6129-6136
- Henze, D., and J. Seinfeld (2006), *Geophys. Res. Lett.*, 33, L09812, doi:10.1029/2006GL025976.
- Henze, D., J. Seinfeld, N. Ng, J.H. Kroll, T.-M. Fu, D.J. Jacob, and C. Heald (2008), *Atmos. Chem. Phys.*, 8, 2405-2421.
- Hermans, I., T.L. Nguyen, P.J. Jacobs, and J. Peeters, (2004), *J. Am. Chem. Soc.*, 126, 9908-9909
- Hermans, I, J.-F. Müller, T.L. Nguyen, P.A. Jacobs, and J. Peeters, (2005), *J. Phys. Chem. A*, 109, 4303-4311
- Herrmann, F. (2006), Master Thesis at the Johannes-Gutenberg University Mainz.
- Hilal, S.H., S.W. Karickhoff, and L.A. Carreira (2003), *QSAR & Comb. Sci.*, 22, 565-574.
- Hilal, S.H., S.W. Karickhoff, and L.A. Carreira (2004), *QSAR & Comb. Sci.*, 23, 709-720.
- Hoffmann, T., J. R. Odum, F. Bowman, D. Collins, D. Klockow, R. C. Flagan, and J. Seinfeld (1997), *J. Atmos. Chem.*, 26, 189-222
- Huff Hartz, K. E., T. Rosenorn, S. R. Ferchak, T. M. Raymond, M. Bilde, N. M Donahue and S. N. Pandis (2005), *J. Geophys. Res.*, 110, doi:10.1029/2004JD005754.
- Iinuma, Y., O. Böge, T. Gnauk, and H. Herrmann (2004), *Atmos. Environ.* 38, 761-773
- Jaoui, M., S. Leungsakul and R. M. Kamens (2003), *J. Atmos. Chem.*, 45, 261-287.
- Jenkin, M., *Atmos. Chem. Phys.* (2004), 4, 1741-1757.
- Jenkin, M. E., M.D. Hurley and T. J. Wallington (2007), *Phys. Chem. Chem. Phys.*, 9, 3149-3162
- Joback, K.G. and R.C. Reid (1987), *Chem. Eng. Commun.*, 57, 233-243.
- Kamens, R.M., M. Jang, C. Chien, and K. Leach (1999), *Environ. Sci. Technol.*, 33, 1430-1438.
- Kamens, R.M., and R. M. Jaoui (2001), *Environ. Sci. Technol.*, 35, 1394-1405.
- Kanakidou, M., K. Tsigaridis, F. Dentener, and P.J. Crutzen (2000), *J. Geophys. Res.*, 105, 9243-9254.

- Kanawati, B., F. Herrmann, S. Joniec, R. Winterhalter and G. K. Moortgat (2008), *Rapid Commun. Mass Spectrom.*, 22, 165-186.
- Karunanandan, R., D. Hölscher, T.J. Dillon, A. Horowitz, J.N. Crowley, L. Vereecken, and J. Peeters (2007), *J. Phys. Chem. A*, 111, 897-908
- Khamaganov, V.G., and R. A. Hites (2001), *J. Phys. Chem. A*, 105, 815-822.
- Khamaganov, V. G., V. Xuan Bui, S.A. Carl, and J. Peeters (2006), *J. Phys. Chem. A*, 110, 12852-12859.
- Kroll, J. H., J. S. Clarke, N. M. Donahue, and J. G. Anderson (2001) *J. Phys. Chem. A*, 105, 1554-1560.
- Larsen, B. R., M. Lahaniati, A. Calogirou and D. Kotzias (1998), *Chemosphere*, 37, 1207-1220.
- Lelieveld, J., T.M. Butler, J.N. Crowley, T.J. Dillon, H. Fischer, L. Ganzeveld, H. Harder, M.G. Lawrence, M. Martinez, D. Taraborelli, and J. Williams (2008), *Nature*, 452, 737-740.
- Liggio, J., S.-M. Li, and R. McLaren (2005), *J. Geophys. Res.*, 110(D10304), doi:10.1029/2004JD005113.
- Ma, Y., T.R. Willcox, A.T. Russell and G. Marston (2007), *Chem. Commun.* 1 , 1328-1330.
- Ma, Y. and G. Marston (2008), *Phys. Chem. Chem. Phys.*, 10, 6115-6126.
- Magnussen, T., P. Rasmussen, and A. Fredenslund (1981), *Ind. Eng. Chem. Proc. Des. Dev.*, 20, 331-339.
- Martin, R. V., D. J. Jacob, R. M. Yantosca, M. Chin, and P. Ginoux (2003), *J. Geophys. Res.*, 108(D3), 4097, doi:10.1029/JD2002JD002622.
- Metzger, S. M., F. J. Dentener, A. Jeuken, M. Krol, and J. Lelieveld (2002), *J. Geophys. Res.*, 107, 4312, doi:10.1029/2001JD001102.
- Ming, Y. and L.M. Russell (2002), *AIChE J.*, 48, 1331-1348.
- Moller, B., J. Rarey, and D. Ramjugernath (2008), *J. Mol. Liq.*, 143, 52-63.
- Müller, J.-F., T. Stavrou, S. Wallens, I. De Smedt, M. Van Roozendaal, M. Potosnak, J. Rinne, B. Munger, A. Goldstein, and A. Guenther (2008), *Atmos. Chem. Phys.*, 8, 1329-1341.
- Myrdal, P.B., and S.H. Yalkowsky (1997), *Ind. Eng. Chem. Res.*, 36, 2494-2499.
- Nannoolal, Y., J. Rarey, and D. Ramjugernath, and W. Cordes (2004), *Fluid Phase Eq.*, 226, 45-63.
- Nannoolal, Y., J. Rarey, and D. Ramjugernath (2008), *Fluid Phase Eq.*, 269, 117-133.
- Neeb, P., O. Horie and G. K. Moortgat (1996), *Tetrahedron Lett.*, 37, 9297-9300.
- Ng, N.L., J.H. Kroll, M.D. Keywood, R. Bahreini, V. Varutbangkul, R.C. Flagan, and J. Seinfeld (2006), *Environ. Sci. Technol.*, 40, 2283-2297.
- Nguyen, T.L., J. Peeters, and L. Vereecken (2009a), *Phys. Chem. Chem. Phys.*, 11, 5643-5656.

- Nguyen, T. L., R. Winterhalter, G. K. Moortgat, B. Kanawati, J. Peeters and L. Vereecken (2009b), *Phys. Chem. Chem. Phys.*, 11, 4173-4183.
- Nguyen, T.L., L. Vereecken and J. Peeters (2010a), *Z. Phys. Chem.*, 224, 1081-1093.
- Nguyen, T.L., L. Vereecken and J. Peeters (2010b), *ChemPhysChem*, 11, 3996-4001.
- Nozière, B., I. Barnes and K. H. Becker (1999), *J. Geophys. Res.*, 104, 23645-23656.
- Offenberg, J.H., T. Kleindienst, M. Jaoui, M. Lewandowski, and E.O. Edney (2006), *Geophys. Res. Lett.*, 33, L03816, doi:10.1029/2005GL024623.
- Pankow, J. F. (1994), *Atmos. Environ.*, 28, 185-188.
- Pankow J.F., and W.E. Asher (2008), *Atmos. Chem. Phys.*, 8, 2773-2796.
- Pathak, R. K., C. O. Stanier, N. M. Donahue and S. N. Pandis (2007), *J. Geophys. Res.*, 112, D03201.
- Paulot, F., J.D. Crouse, H.G. Kjaergaard, A. Kürten, J. M. St. Clair, J. H. Seinfeld, and P.O. Wennberg (2009), *Science*, 325, 730-733.
- Peeters, J., W. Boullart, and J. Van Hoeymissen (1994), *Proceedings of EUROTRAC Symposium '94*, P.M. Borrell et al., eds., pp. 110-114, Academic Publishing, The Hague.
- Peeters, J., W. Boullart, V. Pultau, and S. Vandenberg (1996) *Proceedings of EUROTRAC Symposium '96*, P.M. Borrell et al. eds., Computational Mechanics Publications, Southampton.
- Peeters, J., L. Vereecken, and G. Fantechi (2001), *Phys. Chem. Chem. Phys.*, 3, 5489-5504.
- Peeters, J., G. Fantechi, and L. Vereecken (2004), *J. Atmos. Chem.*, 48, 59-80.
- Peeters, J., and L. Vereecken (2006), Poster presentation at 19th International Symposium on Gas Kinetics, Orléans, July 2006.
- Peeters, J., W. Boullart, V. Pultau, S. Vandenberg, and L. Vereecken (2007), *J. Phys. Chem. A*, 111, 1618-1631
- Peeters, J., T. L. Nguyen, and L. Vereecken (2009), *Phys. Chem. Chem. Phys.*, 11, 5935-5939.
- Peeters, J. and J.-F. Müller (2010), *Phys. Chem. Chem. Phys.*, 12, 14227-14235.
- Peng, C., M.N. Chan, and C.K. Chan (2001), *Environ. Sci. Technol.*, 35, 4495-4501.
- Presto, A.A., K. E. H. Huff Hartz and N. M. Donahue (2005), *Environ. Sci. Technol.*, 39, 7046-7054.
- Presto, A. A., and N. M. Donahue (2006), *Environ. Sci. Technol.* 40, 3536-3543.
- Raatikainen, T. and A. Laaksonen (2005), *Atmos. Chem. Phys.* 5, 2475-2496.
- Sadezky, A., P. Chaimbault, A. Mellouki, A. Römpp, R. Winterhalter, G. K. Moortgat and G. Le Bras (2006), *Atmos. Chem. Phys.*, 6, 5009-5024.
- Sadezky, A., R. Winterhalter, B. Kanawari, A. Mellouki, G. Le Bras, A. Römpp, P. Spengler, P. Chaimbault and G. K. Moortgat (2008), *Atmos. Chem. Phys.*, 8, 2667-2699.
- Sauer, F., J. Beck, G. Schuster and G. K. Moortgat (2001), *Chemosphere - Global Change Sci.*, 3, 295-307.

- Shilling, J. E., Q. Chen, S. King, T. Rosenoern, J. H. Kroll, D. R. Worsnop, K. A. McKinney, and S. T. Martin (2008), *Atmos. Chem. Phys.*, **8**, 2073-2088
- Song, C., R. A. Zaveri, M. L. Alexander, J. A. Thornton, S. Madronich, J. V. Ortega, A. Zelenyuk, and X. Y. Yu (2007), *Geophys. Res. Lett.* **34**, L20803
- Soonsin, V., A. A. Zardini, C. Marcolli, A. Zuend, and U. K. Krieger, *Atmos. Chem. Phys.* **10**, 11753-11767.
- Staffelbach, T.A., J.J. Orlando, G.S. Tyndall, and J.G. Calvert (1995), *J. Geophys. Res.*, **100**, 14189-14198.
- Stavrakou, T., and J.-F. Müller (2006), *J. Geophys. Res.*, **111**, D15304, doi:10.1029/2005JD006896.
- Stavrakou, T., J.-F. Müller, I. De Smedt, M. Van Roozendaal, M. Kanakidou, M. Vrekoussis, F. Wittrock, A. Richter, and J. Burrows (2009a), *Atmos. Chem. Phys. Discuss.*, **9**, 13593-13628.
- Stavrakou, T., J.-F. Müller, I. De Smedt, M. Van Roozendaal, G. van der Werf, L. Giglio, and A. Guenther (2009b), *Atmos. Chem. Phys.*, **9**, 1037-1060.
- Stavrakou, T., J.-F. Müller, I. De Smedt, M. Van Roozendaal, G. van der Werf, L. Giglio, and A. Guenther (2009c), *Atmos. Chem. Phys.*, **9**, 3663-3679.
- Stavrakou, T, J. Peeters and J.-F. Müller (2010), *Atmos. Chem. Phys.*, **10**, 9863-9878.
- Takekawa, H., H. Minoura and S. Yamazaki (2003), *Atmos. Environ.*, **37**, 3413-3424.
- Taraborelli, D., M. G. Lawrence, T. M. Butler, R. Sander, and J. Lelieveld, *Atmos. Chem. Phys.*, **9**, 2751-2777, 2009.
- Tobias, H. J. and P.J. Ziemann (2000), *Environ. Sci. Technol.*, **34**, 2105-2115
- Tobias, H. J. and P. J. Ziemann (2001), *J. Phys. Chem. A*, **105**, 6129-6135.
- Tsigaridis, K., and M. Kanakidou, Secondary organic aerosol importance in the future atmosphere (2007), *Atmos. Environ.*, **41**, 4682-4692.
- Tyndall, G. S., T. A. Staffelbach, J. J. Orlando, et al., 1995, *Int. J. Chem. Kinet.*, **27**, 1009-1020.
- Valverde-Canossa, J., L. Ganzeveld, B. Rappenglück, R. Steinbrecher, O. Klemm, G. Schuster and G. K. Moortgat (2006), *Atmos. Environ.*, BEWA 2000 special issue, S55-S67.
- van der Werf, G., J. Randerson, L. Giglio, G. Collatz, P. Kasibhatla, and A. Arellano (2006), *Atmos. Chem. Phys.*, **6**, 3423-3441.
- Vereecken, L., and J. Peeters (2004), *J. Phys. Chem. A*, **108**, 5197-5204
- Vereecken, L., J.-F. Müller and J. Peeters (2007), *Phys. Chem. Chem. Phys.*, **9**, 5241-5248.
- Vereecken, L., *Chem. Phys. Lett.* (2008), **466**, 127-130.
- Vereecken, L., and J. Peeters (2009), *Phys. Chem. Chem. Phys* **11**, 9062-9074.
- Vereecken, L., and J. Peeters (2010), *Phys. Chem. Chem. Phys.*, **12**, 12608-12620.
- von Hessberg, C., P. von Hessberg, U. Pöschl, M. Bilde, O. J. Nielsen and G. K. Moortgat (2009), *Atmos. Chem. Phys.*, **9**, 3583-3599.

- Warneke, C., J.A. de Gouw, L. Del Negro, J. Briouse, S. McKeen, H. Stark, W.C. Kuster, P.D. Goldan, M. Trainer, F.C. Fehsenfeld, C. Wiedinmyer, A. Guenther, A. Hansel, A. Wisthaler, and A. Atlas (2008), *J. Geophys. Res.*, submitted.
- Winterhalter, R., F. Herrmann, B. Kanawati, T. L. Nguyen, J. Peeters, L. Vereecken and G. K. Moortgat (2009), *Phys. Chem. Chem. Phys.*, 11, 4152-4172.
- Winterhalter, R., P. Neeb, D. Grossmann, A. Kolloff, O. Horie and G. K. Moortgat (2000), *J. Atmos. Chem.*, 35, 165-197.
- Wisthaler, A., N. R. Jensen, R. Winterhalter, W. Lindinger and J. Hjorth (2001), *J. Atmos. Chem.*, 35, 6181-6191.
- Xia, A. G., D. V. Michelangeli, and P. A. Makar (2008) *J. Geophys. Res.* 113, D10301
- Yu, J., D. R. Cocker, R. J. Griffin, and R. Flagan (1999), *J. Atmos. Chem.*, 34, 207-258.
- Zhang, D. and R. Zhang (2005), *J. Chem. Phys.*, 122, 114308.